Earth-Science Reviews 226 (2022) 103947

Contents lists available at ScienceDirect

Earth-Science Reviews

journal homepage: www.elsevier.com/locate/earscirev

Shoreline evolution in the Late Cretaceous North American Cordilleran foreland basin: An exemplar of the combined influence of tectonics, sea level, and sediment supply through time

Zhiyang Li [a,b,*], Jennifer Aschoff [a]

[a] Department of Geological Sciences, University of Alaska, Anchorage, AK 99508, USA
[b] Department of Geology, Colorado College, Colorado Springs, CO 80903, USA

A B S T R A C T

The stratigraphic record from the North American Cordilleran foreland basin (CFB) serves as a critical archive of how tectonics, sea level, and sediment supply interacted throughout the geologic past, providing valuable insights into the formation and filling of foreland basins. By integrating a range of stratigraphic, sedimentologic, and geochronological datasets, the roles of various geological processes within the CFB are better constrained, especially more enigmatic subcrustal processes probably related to large-scale mantle flows. This study summarizes the complex shoreline evolution of the central part of the CFB (Wyoming, Utah, Colorado, and New Mexico) in 25 temporally constrained paleogeographic maps illustrating high-resolution shoreline history (location and migration trend) and distribution of gross depositional environments through the Late Cretaceous. Detailed stratigraphic synthesis indicates that sediment fill of the CFB was subject to complex interactions of tectonics (both local and regional scale and both crustal and subcrustal processes), eustasy, and sediment supply because stratigraphic stacking patterns and shoreline migration trends varied along the coeval shoreline during most of the Late Cretaceous. The spatial variability in the shoreline migration trend, as well as changes in the sediment dispersal pattern help to disentangle the effects of subsidence caused by crustal and/or subcrustal processes, and provide constraints on the spatial and temporal scales these processes operate on. Subcrustal processes such as mantle flow, possibly associated with enhanced coupling by subduction of an oceanic plateau (i.e., the conjugate Shatsky rise) attached to the Farallon plate, were documented as an important mechanism influencing the subsidence/uplift and sediment dispersal patterns in the CFB since at least ~85 Ma. The along-strike variation in shoreline migration trend along the coeval shoreline is likely the norm, rather than the exception, due to the spatial variation in topographic load, lithospheric strength, mantle-induced dynamic topography, and sediment supply across the CFB. Although quantifying the relative roles of different allogenic factors on the architecture of the CFB strata remains a challenging task, the chronostratigraphic framework, shoreline trends, and paleogeographic maps compiled herein could provide critical boundary conditions for forward modeling, such as geodynamic and landscape models, to better understand the paleogeographic and tectonic evolution of the CFB and other basins worldwide, in a more comprehensive way that considers the effect of the mantle on basin-formation. Eventually, high-resolution reconstruction of the geohistory of the CFB through holistic approaches will greatly advance our understanding of the roles of different allogenic factors in sediment filling of the CFB and enable us to better use the stratigraphic record of foreland basins as important archives of paleoenvironmental evolutions and the interaction between surficial and deep Earth processes through geological time.

1. Introduction

One of the grand challenges in earth sciences is deciphering how various geological processes (e.g., tectonics, sea level, and sediment supply) have shaped the Earth's surface. Although these processes can be recorded in the stratigraphic record of sedimentary basins, interpreting the interaction of tectonics, sea level, and sediment supply from the sedimentary basin fill remains a challenging task because it requires a comprehensive suite of datasets including a high-resolution chronological framework, stratigraphic architecture, sediment dispersal pattern, sediment provenance data, and the distribution of sediment accumulation and depositional environments. These different datasets are not always available in sedimentary basins worldwide except for a few exceptions. One such exception is the Cretaceous Cordilleran foreland basin (CFB), probably the best-preserved, best-dated, and most intensively studied sedimentary basins in the world (Miall et al., 2008). With an extensive subsurface database and excellent outcrops, studies of the CFB have significantly contributed to the development of many aspects of geology and serves as an exemplar for retroarc foreland basins (Miall et al., 2008). For instance, geodynamic models for foreland basins recognizing the genetic association between crustal loading and basin formation were first developed here (Jordan, 1981). The important role

* Corresponding author at: Department of Geological Sciences, University of Alaska, Anchorage, AK 99508, USA.
E-mail address: zli20@alaska.edu (Z. Li).

https://doi.org/10.1016/j.earscirev.2022.103947
Received 28 August 2021; Received in revised form 18 January 2022; Accepted 24 January 2022
Available online 3 February 2022

of subcrustal loading on the foreland basin subsidence (i.e., dynamic subsidence) was also first recognized in the CFB (Bond, 1976; Cross and Pilger, 1978; Mitrovica et al., 1989; Gurnis, 1992). Moreover, studies of the CFB have greatly enhanced our understanding of the relationship between tectonics and sedimentation. The general linkage between the active timing and locations of tectonic structures and depocenters within the CFB is well constrained by abundantly available stratigraphic sections, sediment composition data, paleocurrent data, isopach maps, and geochronological data (Armstrong, 1968; Dyman et al., 1994; DeCelles et al., 1995; Pang and Nummedal, 1995; Roberts and Kirschbaum, 1995; White et al., 2002; DeCelles, 2004; Horton et al., 2004; Liu et al., 2005; DeCelles and Coogan, 2006; Dickinson and Gehrels, 2008; Laskowski et al., 2013; Painter and Carrapa, 2013; Painter et al., 2014; Yonkee and Weil, 2015; Bush et al., 2016; Heller and Liu, 2016; Quinn et al., 2016; Bartschi et al., 2018). High-resolution invertebrate biozones and closely spaced datable bentonites within the sediment fill of the CFB, occupied by a large epicontinental seaway known as the Western Interior Seaway during the Late Cretaceous, significantly contributed to the development of the Cretaceous time scale (Obradovich, 1993; Cobban et al., 2006; Ogg et al., 2012). Extensive subsurface and surface datasets with excellent chronostratigraphic constraints allow much refined stratigraphic analysis, providing critical insights into the roles of allogenic controls (e.g., tectonics, sea level, and climate) on sedimentation (Hale and Van De Graaff, 1964; Fouch et al., 1983; Lawton et al., 1986; Merewether and Cobban, 1986; Van Wagoner et al., 1990; Devlin et al., 1993; Kauffman and Caldwell, 1993; Gardner, 1995; Krystinik and DeJarnett, 1995; Catuneanu et al., 1997; Sageman et al., 1997; Varban and Guy Plint, 2008; Hampson, 2010; Aschoff and Steel, 2011; Fielding, 2011; Zhu et al., 2012; Liu et al., 2014; Rudolph et al., 2015; Van Cappelle et al., 2018; Lin et al., 2019; Minor et al., 2021; Li and Aschoff, 2022).

Early regional studies of the CFB stratigraphy emphasized the roles of long-term (several to tens of million years first- to second-order; Fig. 2) tectonic and eustatic cycles on the development of stratigraphic cyclicity and regional unconformities (Hale and Van De Graaff, 1964; Armstrong, 1968; McGookey et al., 1972; Kauffman, 1977; Weimer, 1984). Detailed lithostratigraphic studies constrained by ammonite biozones allowed the reconstruction of paleogeography and shoreline history within the CFB throughout the Late Cretaceous, revealing the widespread presence of shorter-term (less than a few million years third- to higher-order; Fig. 2) depositional sequences (Franczyk et al., 1992; Cobban et al., 1994; Elder and Kirkland, 1994; Gardner, 1995; Krystinik and DeJarnett, 1995; Roberts and Kirschbaum, 1995; Minor et al., 2021). The presence of third- to fourth-order depositional sequences was further strengthened by the growing application of high-frequency stratigraphic analysis (e.g., sequence stratigraphy, cyclostratigraphy, and chemostratigraphy), revealing the critical roles of high-frequency sea level and climate cycles on sedimentation within the CFB (Van Wagoner et al., 1990; Sageman et al., 1997; Plint and Kreitner, 2007; Zhu et al., 2012; Joo and Sageman, 2014; Eldrett et al., 2015; Ma et al., 2017; Lin et al., 2019; Li and Schieber, 2020; Minor et al., 2021).

Despite the various stratigraphic studies that have been conducted in numerous areas within the CFB, a comprehensive and detailed understanding of the relationship between tectonics, sea level, and sedimentation within the foreland basin has not been completed. One of the most important questions that remains unanswered is how the combined effects of tectonics and sea level generated the apparent synchroneity of stratigraphic cycles observed over multiple time scales in the CFB strata. Although the ten long-term (first- to second-order) eustatic transgressive-regressive cycles (T-R cycles) proposed by Kauffman (1977) provided a useful general framework to correlate Cretaceous strata over great distances (hundreds to thousands of kilometers) across the CFB, careful examinations of the stratigraphic stacking pattern at different areas indicate these T-R cycles are not synchronous everywhere across the CFB (Molenaar et al., 1988; Schröder-Adams, 2014). By integrating stratigraphic stacking patterns with biostratigraphic controls (ammonite biozones), Krystinik and DeJarnett (1995) demonstrated that most, if not all, observed second- to third-order depositional sequences in the Campanian to Maastrichtian strata from New Mexico to Alberta are not synchronous. The largely asynchronous first- to third-order depositional sequences across the CFB strongly indicate the interactions between tectonics (regional and local scale) and sea-level changes, and their effects on sedimentation are much more complex and shorter-duration than generally considered (Krystinik and DeJarnett, 1995; Hampson, 2010; Gani et al., 2015; Schultz et al., 2020).

Understanding of the relationship between tectonics, sea level, and sedimentation within the CFB has been limited by the lack of a comprehensive and regional geologic context at high temporal resolution. Out of necessity, many previous studies tended to focus on only a limited temporal or spatial scale and emphasize one dominant type of allogenic control rather than the combined effects of multiple processes. Although these studies employed robust stratigraphic analyses, depositional sequences were correlated either in a more general way over vast areas, or in a very detailed way in smaller subareas. Integrating previous local studies into a regional stratigraphic framework is problematic because of differences in correlation methods and chronostratigraphic constraints of depositional sequences between different subbasins within the CFB. Without putting the stratigraphic stacking pattern and shoreline trend revealed by a local depositional sequence into a regional context with robust chronostratigraphic controls, it is impossible to unequivocally determine whether the apparent base-level rise/fall inferred from a restricted area was due to tectonic activities, sea-level changes, sediment supply or any combination of the above. General compilations of the distribution and evolution of depositional environments, stratigraphic stacking patterns, and shoreline history do exist in the form of a series of paleogeographic maps at different times or biozones (McGookey et al., 1972; Cobban et al., 1994; Roberts and Kirschbaum, 1995). These maps, however, typically depict the average long-term trend of shoreline history and stratigraphic stacking patterns and are not high-resolution enough to allow the discrimination between tectonic and sea-level changes over relatively short-term (e.g., third- to higher-order) periods, let alone that the combined effects of tectonic uplift/subsidence, sea-level changes, and sediment supply tend to vary laterally (Krystinik and DeJarnett, 1995; Chang and Liu, 2020; Schultz et al., 2020).

Another factor that may have complicated our understanding of the linkage between tectonics, sea level, and sedimentation within the CFB is flexural subsidence and uplift related to thrust sheet has been considered as the overriding cause of CFB development (Jordan, 1981). Although dynamic topography (including subsidence and uplift) associated with large-scale sublithosphere mantle flows has been increasingly recognized as another important mechanism influencing the development of retroarc foreland basins, including the CFB (Jones et al., 2011; Painter and Carrapa, 2013; Liu et al., 2014; Heller and Liu, 2016; Li and Aschoff, 2022), the processes of mantle flows and effects (e.g., extent and magnitude) of dynamic topography remains relatively poorly understood. Consequently, the subsidence/uplift induced by dynamic topography has not yet been taken into consideration to explain short-term sedimentation and stratigraphic patterns of the strata in the CFB.

To resolve the complex interactions between tectonics, sea level, and sediment supply and their effects on sedimentation within the CFB, this review integrates a range of stratigraphic, sedimentologic, and geochronological datasets from research over the past more than half a century. The main objective of this synthesis is to incorporate the timing and locations of active tectonic features (including both thin-skinned and thick-skinned structures), stratigraphic stacking patterns, sediment dispersal pattern, sediment provenance data, and the distribution of sediment accumulation and depositional environments within the CFB into a high-resolution and robust chronostratigraphic framework. This study specifically focused on Upper Cretaceous strata in the central part of the CFB (i.e., Wyoming, Utah, Colorado, and northern New

Mexico) because 1) Upper Cretaceous strata of these areas provide an excellent archive of shoreline history (i.e., location and migration trend), 2) the Late Cretaceous ammonite biozones in these areas are high-resolution (50,000–100,000 yr. scale) and widespread (thousands of km) enough to serve as excellent time markers when examining the spatial variability in the stratigraphic architecture (Cobban et al., 2006; Ogg et al., 2012), and 3) dynamic topography was documented to have played a significant role influencing the development of CFB in these areas during the Late Cretaceous (Liu and Nummedal, 2004; Liu et al., 2010; Aschoff and Steel, 2011; Liu et al., 2011; Liu et al., 2014; Heller and Liu, 2016; Li and Aschoff, 2022). Based on the reconstructed paleogeographic and tectonic evolution of the CFB during the Late Cretaceous, this review provides 1) a chronostratigraphically-constrained framework that records the relationship between tectonics, sea level, and sedimentation within the CFB through the Late Cretaceous, 2) a better understanding of the spatial variability in the combined effects of allogenic factors on sedimentation and development of stratigraphy, 3) additional evidence indicative of the role of dynamic topography in sedimentation within the CFB. The much-refined geohistory of the CFB during the Late Cretaceous can also aid in future geodynamic and landscape models examining the relationship between tectonics (e.g., thrust-load-induced flexural subsidence and dynamic topography), sea level, and sedimentation in the CFB and other retroarc foreland basins (Liu et al., 2008; Spasojevic et al., 2009; Chang and Liu, 2020).

2. Geologic context

As one of the type examples of retroarc foreland basin developed along an ocean-continent convergent plate boundary, the CFB is genetically related to the Jurassic-Paleogene subduction of the oceanic lithosphere of the Farallon Plate beneath the continental lithosphere of western North America. The forces associated with plate convergence, combined with conductive heating and slab dehydration associated with subduction, led to the formation of a volcanic arc along the western margin of the North American continent and thin-skinned Sevier fold-thrust belt of the North American Cordillera (Fig. 1) (Livaccari, 1991; DeCelles, 2004). In response to crustal loading by the Sevier fold-thrust belt, the CFB developed coeval with the folding and thrusting on the eastern margin of the Sevier fold-thrust belt (Kauffman, 1985; Kauffman and Caldwell, 1993). Throughout the Late Cretaceous, the Sevier fold-thrust belt propagated irregularly eastward, as did the CFB (DeCelles, 2004; Liu et al., 2005). In addition to short-wavelength (< 300 km) flexural subsidence, dynamic subsidence induced by large-scale mantle downwelling associated with the flat subduction of the Farallon slab has been increasingly recognized to play an important role in producing long-wavelength (e.g., > 500 km away from the Sevier thrust belt), regional-scale subsidence in the CFB (Liu and Nummedal, 2004; Jones et al., 2011; Liu et al., 2011; Painter and Carrapa, 2013; Liu et al., 2014; Heller and Liu, 2016; Li and Aschoff, 2022). Previous studies have linked the development of the flat subduction of the Farallon Plate to the subduction of a buoyant oceanic plateau—the Conjugate Shatsky Rise (Livaccari et al., 1981; Saleeby, 2003; Liu et al., 2010; Humphreys et al., 2015; Liu and Currie, 2016). The plateau is thought to have collided with North America near what is now southern California between 90 and 85 Ma, and generally moved in a northeast arcuate path across the Colorado Plateau, Colorado Rocky Mountains, and the Great Plains between 85 and 65 Ma (Fig. 1) (Liu et al., 2010; Humphreys et al., 2015). During the Campanian to Paleogene, deformation within the CFB became dominated by thick-skinned in style (i.e., Laramide Orogeny), and the CFB became locally segmented by intraforeland Laramide-style basement-cored uplifts (Fig. 1) (Dickinson et al., 1988; Lawton, 2008).

The development of CFB during the Late Cretaceous was accompanied by a global eustatic highstand (Miller et al., 2005), leading to the inundation of more than one-third of North America by an epicontinental seaway known as the Western Interior Seaway (WIS) at its maximum extent during the early Turonian (Fig. 1) (Kauffman, 1985). During the early Late Cretaceous, deposition within the CFB was

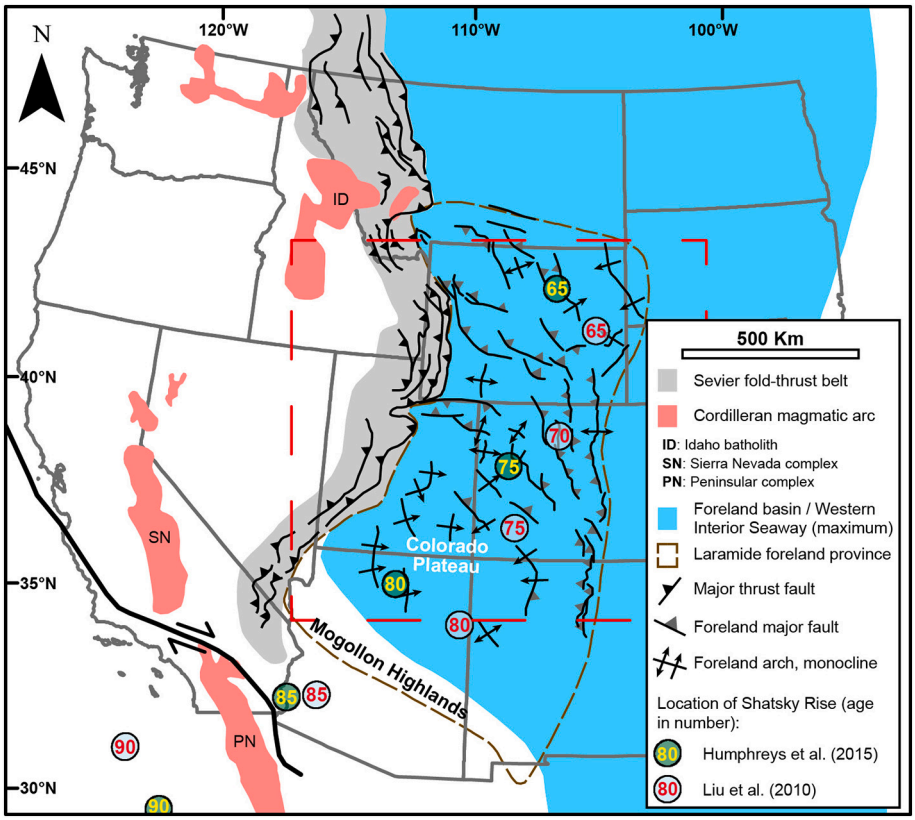

Fig. 1. Regional index map of the western U.S. including the Sevier fold-thrust belt, Laramide province, and Cordilleran magmatic arc (modified from DeCelles, 2004; Yonkee and Weil, 2015). Areas focused in this study are indicated by the red dashed box. Approximate locations of the conjugate Shatsky Rise during 90–65 Ma from Liu et al. (2010) and Humphreys et al. (2015) are shown. The migration direction of the conjugate Shatsky Rise generally parallels to the direction of relative motion between the Farallon and North American plates during the Late Cretaceous. (For interpretation of the references to colour in this figure legend, the reader is referred to the web version of this article.)

characterized by widespread marine mudstone, chalk and minor marginal marine and coastal-plain siliciclastic deposits. After the peak transgression during the early Turonian, the WIS gradually retreated from the continental interior but was interrupted by several second-order eustatic transgressive-regressive cycles (Kauffman, 1977). The first-order withdrawal of the WIS led to the east- to northeast-directed progradation of shorelines and more widespread nonmarine alluvial-plain to coastal-plain sedimentation in the foreland basin as nonmarine depositional systems fed these prograding shorelines.

During the Late Cretaceous, sediments derived from erosion of the rising Sevier fold-thrust belt were generally transported eastward into the WIS as a series of wedges of alluvial-plain, coastal-plain, and shallow marine siliciclastic deposits (Armstrong, 1968; McGookey et al., 1972; Kauffman and Caldwell, 1993; Roberts and Kirschbaum, 1995). Additional sources of sediment supply to the CFB were located to the southwest of the CFB, where the rift shoulder of the northwest-southeast trending Bisbee rift basin formed the Mogollon Highlands (Fig. 1) (Bilodeau, 1986). Sediments derived from the Cordilleran magmatic arc and Mogollon Highlands were transported in a dominant northeast (axially) direction, approximately orthogonal to the eastward-directed (transverse) sediment supply from the Sevier fold-thrust belt (Bilodeau, 1986; Lawton and Bradford, 2011; Lawton et al., 2014; Szwarc et al., 2015). During most of the Late Cretaceous, the circulation within the seaway was largely controlled by storms and waves that produced dominant southward-directed longshore currents and net sediment drift along its western margin, as indicated by paleoenvironmental reconstructions (Barron, 1989; Ericksen and Slingerland, 1990; Slingerland and Keen, 1999). The general sediment dispersal pattern within the CFB became more complex in response to local Laramide-style basement-cored uplifts, which served as additional sediment sources for newly-formed intermontane basins (Lawton, 2008).

3. Data and methods

This paper integrates data including age-control, biostratigraphic control, stratigraphic surfaces for correlation, depositional environments, provenance data, sediment dispersal data, outcrop sections, and well-logs compiled from research in the CFB over the past more than half a century (Fig. 3). A total of 25 paleogeographic maps illustrating approximate shoreline locations, sediment dispersal, shoreline migration trends, and distribution of gross depositional environments (GDE) through the Late Cretaceous were constructed. Each paleogeographic map was developed to depict the paleogeography in the study area at the top of selected ammonite biozones. The selection of ammonite biozones for paleogeographic reconstructions was largely based on the widespread distribution of the ammonite species and the large availability of stratigraphic data tied to these ammonite biozones.

3.1. Paleogeographic reconstructions

To construct each paleogeographic map a chronostratigraphic framework was first constructed based on the robust ammonite biostratigraphy and geochronological data (Fig. 4 and Fig. 5). Using this framework, previous paleogeographic maps developed for different time-intervals based on ammonite biozones were first georeferenced in ArcGIS (McGookey et al., 1972; Franczyk et al., 1992; Cobban et al., 1994; Elder and Kirkland, 1994; Blakey, 2014). Stratigraphic data used to construct these previous paleogeographic maps, when available, were verified, georeferenced, and incorporated as control points for our paleogeographic maps. Additional control points were compiled from many other sources, where published detailed stratigraphic sections could be tied to ammonite biozones. For a given paleogeographic map, each control point includes information such as the Formation/Member name, type of gross depositional environment (or hiatus), and reference source. To avoid line-interference, control points are not displayed in the paleogeographic maps, but all datapoints are available in the Supplementary Data section of this paper.

The paleoshoreline location and distribution of gross depositional environments and regional scale unconformities at different times (i.e., tops of different ammonite biozones) were constrained and depicted on each paleogeographic map based on all control points. Spatial variations in the paleoshoreline location and distribution of gross depositional environments within the CFB can thus be illustrated on the scale of less than one to a few million years through the Late Cretaceous, depending on the duration of ammonite biozones. Additionally, the local shoreline migration trend (i.e., landward vs. seaward) was illustrated on each paleogeographic map based on the stratigraphic stacking pattern (i.e., retrogradational vs. progradational) documented in the compiled stratigraphic sections.

Paleocurrent data were also compiled from many previous studies and depicted on certain paleogeographic maps. The depicted paleocurrent data should be considered as the average dominant paleoflow directions (bimodal paleoflow directions were recorded) during the geologic stage/substage. Similarly, long-term (substage to stage scale) sediment dispersal directions inferred based on petrography and detrital zircon provenance data were also compiled and shown on paleogeographic maps of relevant ages. Sources of all paleocurrent data and sediment dispersal patterns compiled in this study can be found in Supplementary Data.

Tectonic features, including Sevier thrusts, thrust-sheets, and Laramide-style structures, were compiled from multiple sources (Dickinson et al., 1988; DeCelles, 2004; Yonkee and Weil, 2015; Heller and Liu, 2016). The presumed positions of Sevier thrust-sheet segments, forebulge, Laramide-style structures that are presumed to have been active, and the reconstructed locations of the conjugate Shatsky Rise during different times through the Late Cretaceous were overlain on each paleogeographic map to show the correspondence of age-equivalent geologic features. Similarly, tectonic features were also depicted over relatively long-term periods (e.g., on the scale of geologic stage or occasionally substage). Legend for structural features, distribution of gross depositional environment, sediment dispersal, and stratigraphic stacking pattern depicted in all reconstructed paleogeographic maps were summarized in Fig. 6.

3.2. Resolving the roles of tectonics, eustasy, and sediment supply

This study discriminated the relative influence of tectonics, eustasy, and sediment supply on the third-order (i.e., 0.5–3 Ma; Fig. 2) stratigraphic stacking pattern (i.e., progradation vs. retrogradation) and shoreline migration trend, which can be resolved based on the high-resolution ammonite biozones within the WIS. On this time scale, the stratigraphic stacking pattern of coastal to nearshore deposits is largely controlled by allogenic factors such as subsidence, sea level (influenced by climate), and sediment supply (influenced by climate) rather than autogenic factors (Paola et al., 2018) and can be considered as governed by the rate of change of accommodation (i.e., the space available for sediment) versus the rate of change of sediment supply; the ratio of these is the A/S ratio, which provides a framework to interpret stratigraphic

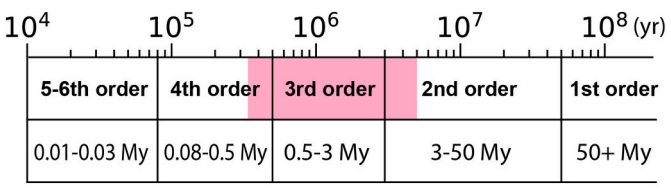

Fig. 2. Hierarchy system based on the duration of stratigraphic cycles (Vail et al., 1977; Mitchum and Van Wagoner, 1991). The cycle duration focused in this study is indicated in red. For reference, the average duration of ammonite biozones in the Late Cretaceous WIS is ~0.5 Ma. (For interpretation of the references to colour in this figure legend, the reader is referred to the web version of this article.)

architecture (Schlager, 1993; Muto and Steel, 1997). Accommodation is controlled by both tectonics and eustasy. If one of these three allogenic factors (i.e., tectonics, eustasy, and sediment supply) can be fairly well constrained, the relative roles of the other two factors can then be inferred based on the observed stratigraphic stacking pattern at the shoreline and the A/S concept: shoreline shifts seaward when A/S < 1 (progradational), landward when A/S > 1 (retrogradational), and remains stationary when A/S = 1 (aggradational).

Several studies have attempted to reconstruct the Late Cretaceous eustasy (Haq et al., 1987; Sahagian et al., 1996; Miller et al., 2005; Kominz et al., 2008; Haq, 2014). Despite disparities among various eustatic reconstructions, the second- to third-order sea-level changes (i.e., rise or fall) through the Late Cretaceous are typically much better constrained and correlated globally (Kominz et al., 2008; Ray et al., 2019). To compile eustatic changes reconstructed by the above previous studies (Sahagian et al., 1996; Miller et al., 2005; Kominz et al., 2008; Haq, 2014), the time-scale used in these studies was first converted to the same time-scale used here (i.e., GTS 2012 *sensu* Gradstein et al., 2012; Ogg et al., 2012). The sea-level trend (i.e., rise or fall) at the top of selected ammonite biozones was then considered as the sea-level trend suggested by the majority of sources at this time (Fig. 7). Using the agreed sea level trend as an input, the relative influence of tectonics, eustasy, and sediment supply on the observed stratigraphic stacking pattern during different time intervals can be determined based on the stratigraphic stacking pattern at the shoreline and the A/S concept, the workflow of which is summarized in Fig. 8.

3.3. Discriminating flexural and dynamic subsidence

In retroarc foreland basins, flexural and dynamic subsidence produce very different spatial footprints in terms of their geographic extent, shape (i.e., distribution of basin-fill), and relationship to key tectonic features such as the fold-thrust belt (Burgess and Moresi, 1999; Liu and Nummedal, 2004; Liu et al., 2005; Spasojevic et al., 2009; Chang and Liu, 2019; Chang and Liu, 2020). Based on the spatial variability in the stratigraphic stacking pattern, reconstructed eustatic changes, and the A/S ratio concept, the lateral variability in the effects of tectonics and sediment supply on the stratigraphic architecture and shoreline migration history across the CFB through the Late Cretaceous can be determined. These can provide insight into spatial variability in tectonically-generated topography (i.e., subsidence and uplift), and sediment dispersal patterns. Based on the inferred distribution of topographic high and low areas, flexural subsidence caused by loading of the Sevier fold-thrust belt can be discriminated from dynamic topography associated with the flat subduction of the Farallon plate beneath the North American plate. Specifically, lexural loading of the thrust belt typically creates short-wavelength (< 200 km) subsidence adjacent and subparallel to the orogenic belt. In contrast, dynamic subsidence is usually invoked to account for the long-wavelength (up to ~1000 km) subsidence because stresses induced by mantle flows can translate over much

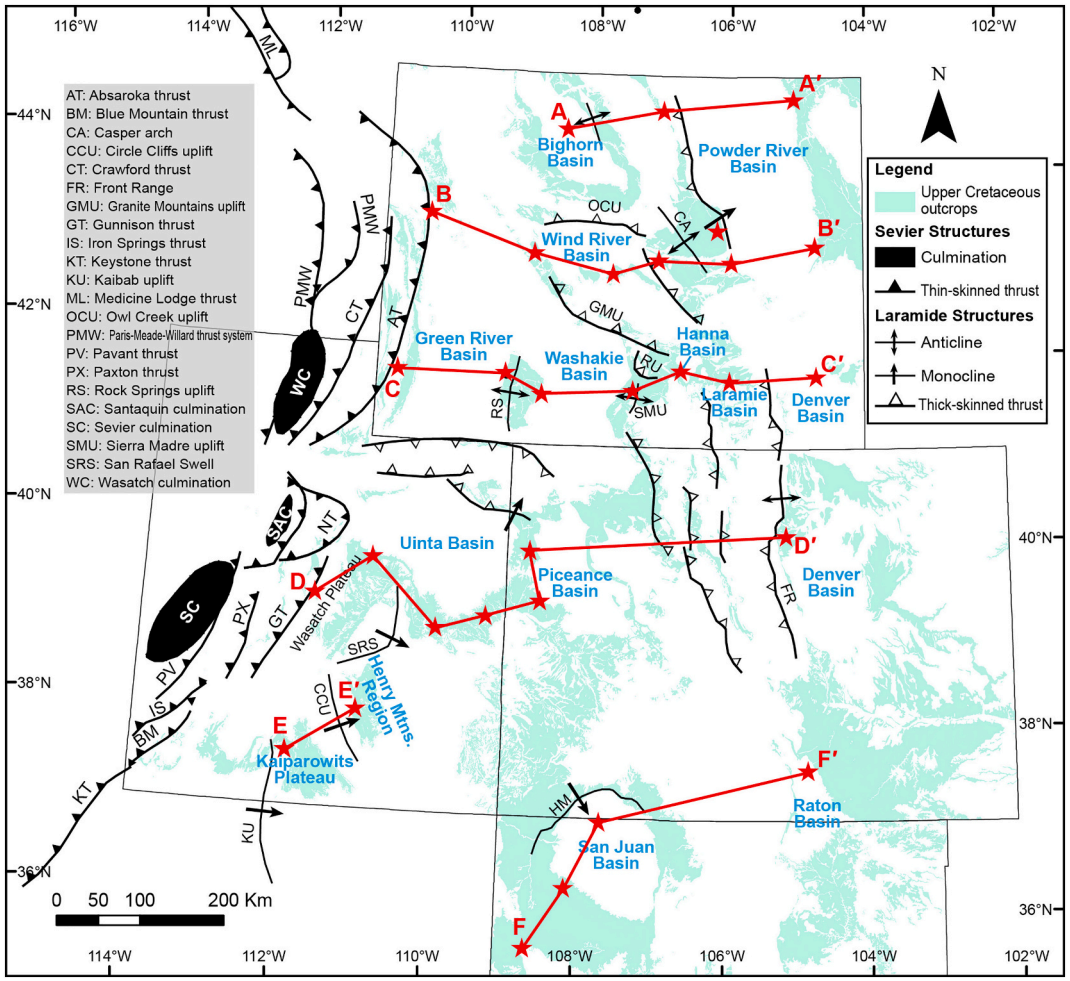

Fig. 3. Map of the study area showing the outcrops of Upper Cretaceous strata and multiple basins and regions from where stratigraphic sections were incorporated to reconstruct paleogeography through the Late Cretaceous. Areas covered by this map is indicated by the red dashed box in Fig. 1. The map also shows Sevier (thin-skinned) thrusts (DeCelles, 2004) and Laramide (thick-skinned) structures (Dickinson et al., 1988; Yonkee and Weil, 2015) that were active at different times through the Late Cretaceous. (For interpretation of the references to colour in this figure legend, the reader is referred to the web version of this article.)

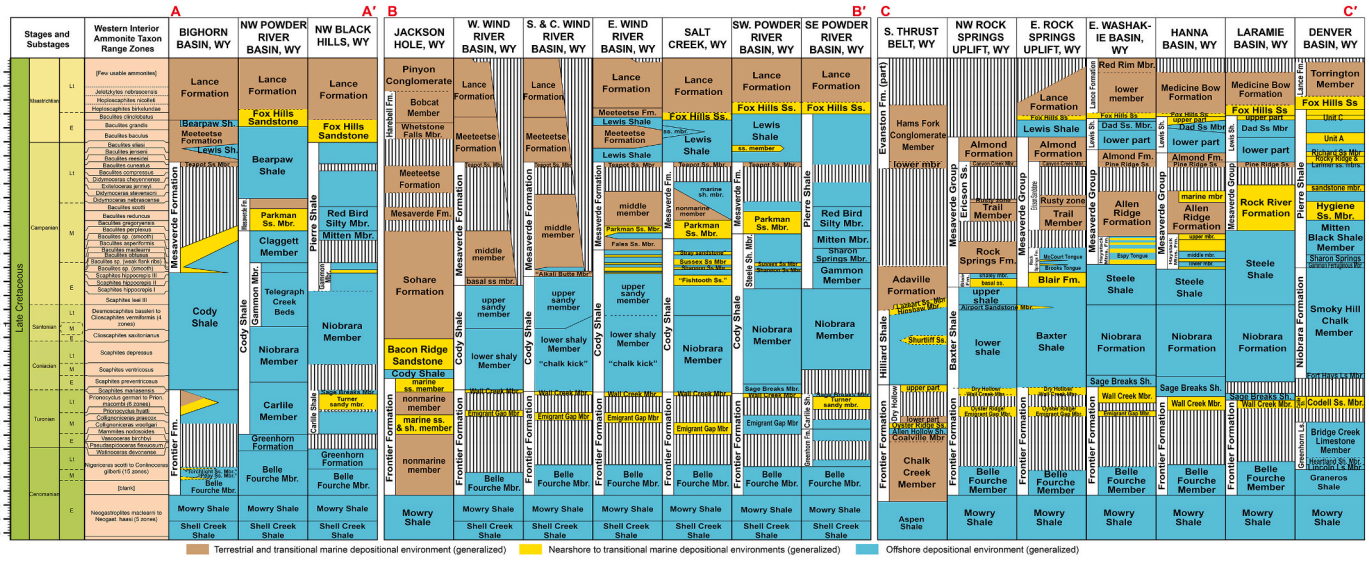

Fig. 4. Chronostratigraphic and biostratigraphic framework of Upper Cretaceous strata in Wyoming along cross sections AA′, BB′, and CC′. See Fig. 3 for cross section locations.

larger distances (Mitrovica et al., 1989; Gurnis, 1992; Catuneanu et al., 1997; Burgess and Moresi, 1999).

Most models predicted a broad zone of dynamic subsidence above the leading part of the subducting oceanic plateau—the conjugate Shatsky Rise, where both the negative buoyancy of the flat slab (due to older age or eclogitization of the basaltic crust) and the magnitude of dynamic coupling between the mantle and the lithosphere would be the greatest (Mitrovica et al., 1989; Liu et al., 2010; Heller and Liu, 2016). The lithosphere above the trailing part of the conjugate Shatsky Rise, however, would experience much less dynamic subsidence (or possibly uplift) due to reduced negative buoyancy of the younger crust and decreased dynamic coupling (Liu et al., 2010; Dávila and Lithgow-Bertelloni, 2015; Heller and Liu, 2016). The associated dynamic uplift and subsidence along the migration trajectory of the conjugate Shatsky Rise, therefore, would potentially create more complex topography overprinting the simple, four-depozone foreland basin profile (i.e., wedge-top, foredeep, forebulge, and backbulge) produced by dominant flexural subsidence (DeCelles and Giles, 1996). With a comprehensive understanding of the relative roles of tectonics (both regional and local scales, flexural and dynamic subsidence/uplift) and sediment supply within the CFB inferred from the observed stratigraphic stacking pattern during different time intervals, the footprints of dynamic topography during the development of the CFB can be better constrained in terms of the subduction and migration of the conjugate Shatsky Rise throughout the Late Cretaceous.

4. Evolution of paleogeography within the CFB

This section focuses on describing the paleogeography, with an emphasis on marine shorelines and their positions within the study area at different times. Shorelines were a primary focus in this study because they are sensitive to paleotopography, and are more easily dated with ammonite assemblages. Each paleogeographic map represents a snapshot in time illustrating the distribution of different gross depositional environments (GDE) at the top of a given ammonite biozone. Additionally, the lateral variability in the stratigraphic stacking pattern and the shoreline change trend will be discussed over different time intervals (i.e., during an ammonite biozone or between two ammonite biozones). For clarification, the term "ammonite biozone time" in the following sections refers to the instant at the top of the given ammonite biozone, while the "ammonite biozone" refers to the duration of time recorded in the specific ammonite biozone.

4.1. Cenomanian (100.5 Ma - 93.9 Ma)

During Cenomanian time, the frontal part of the Sevier fold-thrust belt began to take shape. Active thrust systems on the margin of the CFB included the Willard-Meade thrust in the Idaho-Wyoming-Utah salient, the Nebo thrust in the Charleston-Nebo salient in north-central Utah, the Pavant thrust in central Utah, and the Keystone thrust system in southern Nevada (Fig. 7) (DeCelles, 2004; DeCelles and Coogan, 2006). The Cenomanian was characterized by a long-term warming trend and overall eustatic rise (Sahagian et al., 1996; Kominz et al., 2008; Haq, 2014; Joo et al., 2020), during which the Rocky Mountain and Great Plains regions became increasingly inundated by the WIS from the north. Cenomanian deposits within the CFB were considered largely controlled by the second-order Greenhorn transgressive sea level cycle (Kauffman, 1977).

4.1.1. Early cenomanian: top of Neogastroplites americanus zone (~97.8 Ma)

The early Cenomanian records the incursion of a shallow, epicontinental sea into the map area (Fig. 9A). At the *Neogastroplites americanus* time (97.8 Ma), the study area was generally divided into a marine environment to the north and a nonmarine environment to the south by a dominantly northwesterly trending shoreline across the Utah-Colorado boundary (Fig. 9A) (Franczyk et al., 1992; Cobban et al., 1994). Marine mudstones (non-calcareous) of the Mowry Shale and Graneros Shale were deposited in Wyoming, a small part of northeastern Utah, and northern to central Colorado, which grade southward into the nearshore marine deposits of the Dakota Sandstone (Fig. 9A). A coastal-plain environment was probably present landward of the shoreline (Fig. 9A; the Chalk Creek Member of the Frontier Formation at the Coalville area, Utah). Braided fluvial sandstones of the Dakota Sandstone (early Cenomanian in age) were deposited further landward in south-central and southern Utah (Henry Mountains and Kaiparowits Plateau regions; Fig. 9A) (Peterson et al., 1980; Uličný, 1999; Antia and Fielding, 2011), although the age of the Dakota Sandstone (in terms of ammonite biozone) cannot be well constrained because of the absence, or scarcity, of age-diagnostic fossils (Peterson et al., 1980; Gustason, 1989; Uličný, 1999).

Paleocurrent directions measured from the Dakota Sandstone of the early Cenomanian age in southern Utah (Kaiparowits Plateau region) show a southeast mean flow direction, perpendicular to the northeast-southwest trending part of the Sevier belt (Gustason, 1989; Uličný,

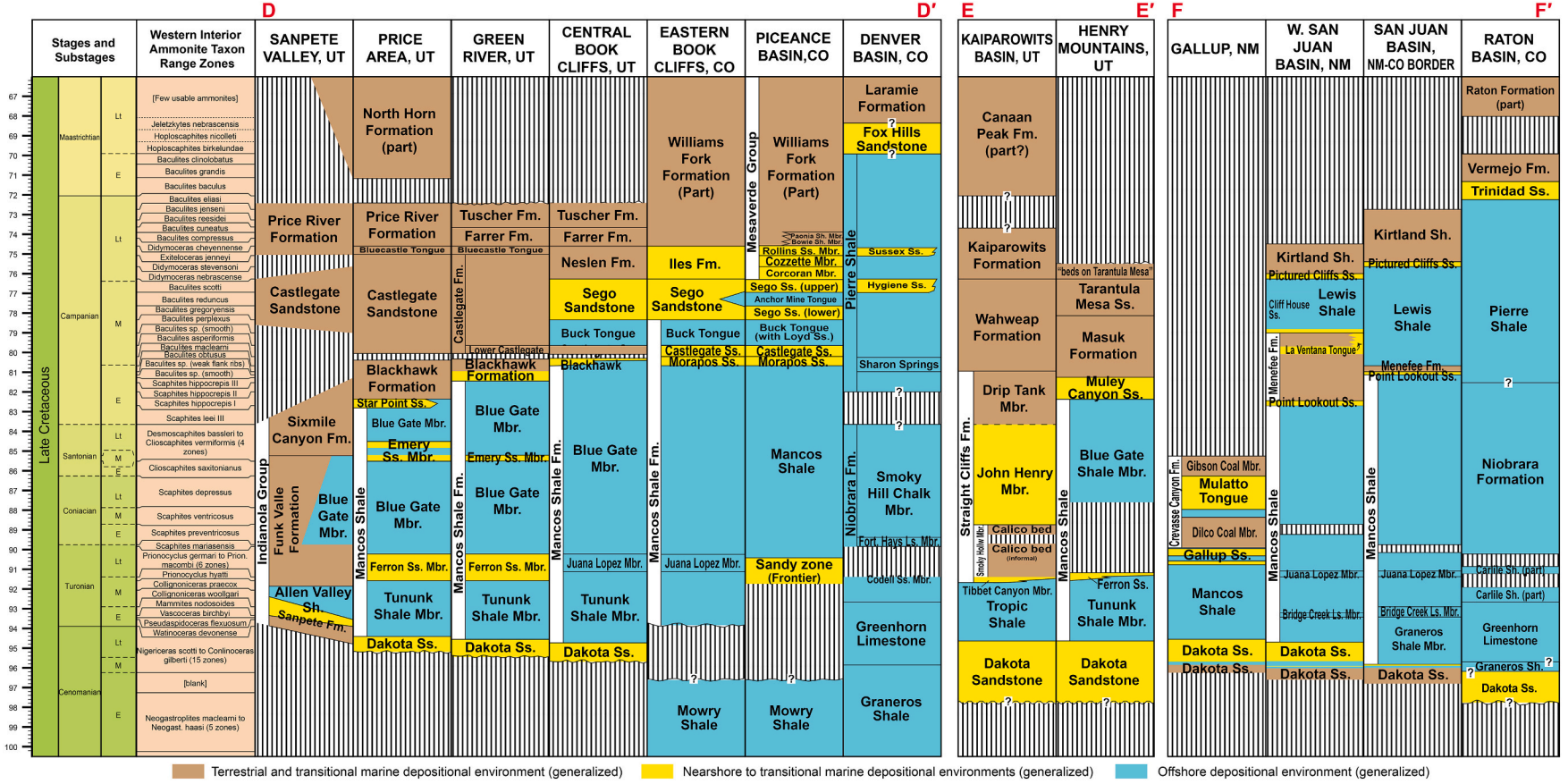

Fig. 5. Chronostratigraphic and biostratigraphic framework of Upper Cretaceous strata in Utah, Colorado, and New Mexico along cross sections DD′, EE′, and FF′. See Fig. 3 for cross section locations. Sources for each stratigraphic column shown in Fig. 4 and Fig. 5 can be found in the Supplementary Data file.

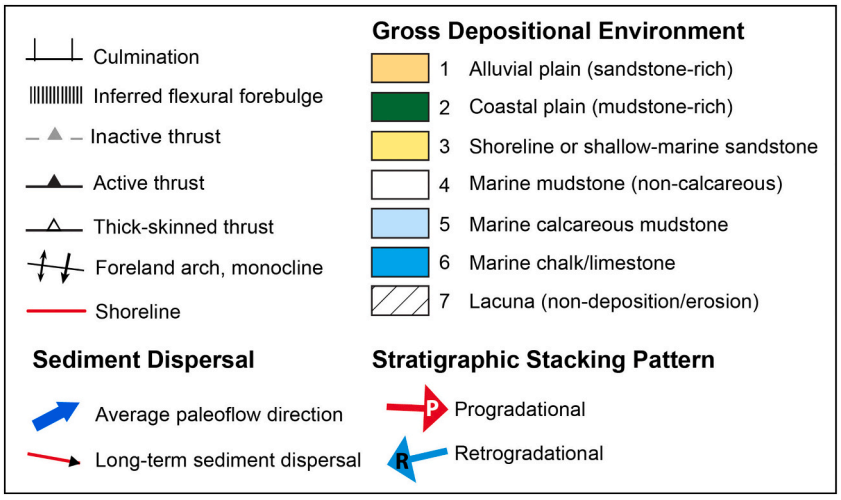

Fig. 6. Legend for structural features, distribution of gross depositional environment, sediment dispersal, and stratigraphic stacking pattern depicted in paleogeographic maps. For all paleogeographic maps, active vs. inactive Sevier thrusts were mainly from Fig. 4 and DeCelles (2004). Information on the control points for different gross depositional environments for each paleogeographic maps was provided in the Supplementary Data file. Average paleoflow direction was from measured paleocurrent data, while long-term sediment dispersal pattern was based on detrital zircon and sandstone provenance data. Sources for sediment dispersal were also provided in the Supplementary Data file.

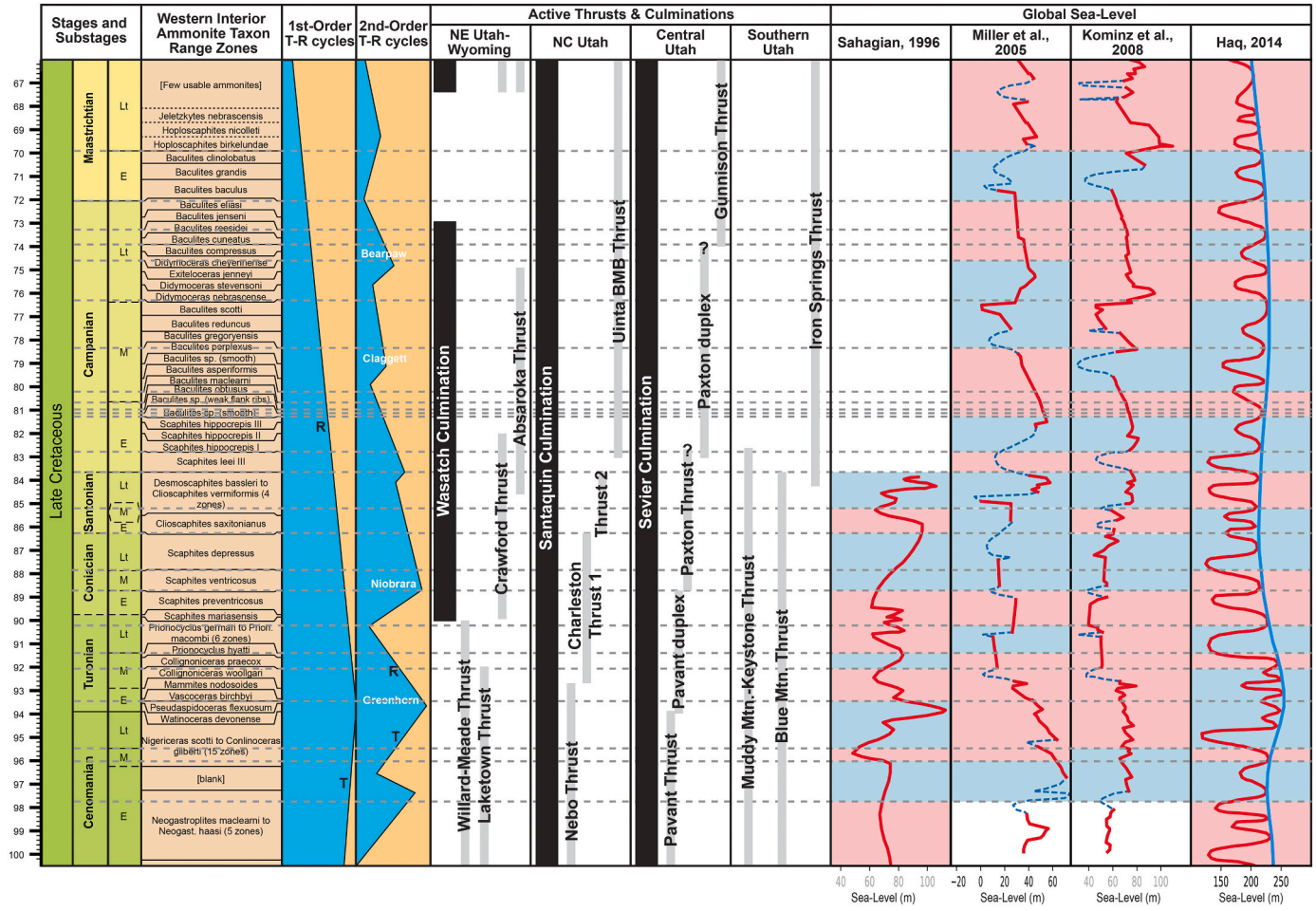

Fig. 7. Diagram showing the Late Cretaceous time scale and ammonite zonations used in this study (Ogg et al., 2012), with the second-order transgressive-regressive cycles from Kauffman (1977), the kinematic history in five selected segments of the frontal (Sevier belt) part of the Cordilleran thrust belt (DeCelles, 2004), and the comparison of Late Cretaceous eustatic changes of Sahagian et al. (1996), Miller et al. (2005), Kominz et al. (2008), and Haq (2014). The second-order transgressive-regressive cycles are not tied to ammoniate zonations. The ages of paleogeographic maps reconstructed in this study are indicated by dashed gray lines across the figure. The dashed segments in the eustatic curves of Miller et al. (2005) and Kominz et al. (2008) represent inferred eustatic changes during hiatuses.

1999). Further (~ 200 km) away from the thrust front, the Dakota Sandstone in south-central Utah (Henry Mountains region) shows east to northeast directions (Fig. 9A) (Antia and Fielding, 2011). At the *Neogastroplites americanus* time, areas of erosion or nondeposition (lacuna) were at least located at central to eastern Utah and the San Juan Basin in southwestern Colorado and northwestern New Mexico (Fig. 9A).

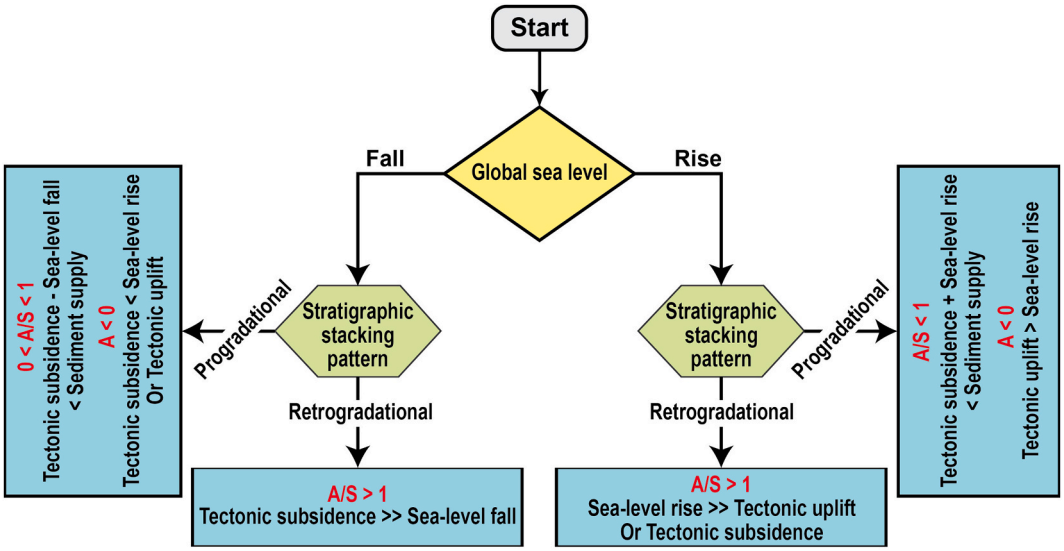

Fig. 8. The workflow to determine the relative influence of tectonics and sediment supply based on eustatic changes and the stratigraphic stacking pattern (retrogradational vs progradational) at the shoreline. The eustatic change at a given time was determined by the agreed trend suggested by the majority of eustatic reconstructions (the intersection between dashed gray lines and different eustatic curves in Fig. 4). The stratigraphic stacking pattern of deposits around the shoreline at the same time was either directly documented from previous stratigraphic studies or based on shoreline migration trend reflected by successive paleogeographic maps. A: rate of change of accommodation; S: rate of change of sediment supply.

4.1.2. Middle Cenomanian: top of Conlinoceras tarrantense zone (~96.1 Ma)

The seaway from the north (Boreal Sea) connected with a seaway from the south (Tethys Sea) during the earliest middle Cenomanian. The shoreline along the western margin of the WIS established a general north-south orientation at the *Conlinoceras tarrantense* time (96.1 Ma). Marine mudstones had increased in extent in the study area, including the Belle Fourche Member of the Frontier Formation in central and eastern Wyoming and the Graneros Shale in most of Colorado (Fig. 9B). The Peay Sandstone within the Belle Fourche Member located at northcentral Wyoming represents delta-front deposits deflected by the southward-directed geostrophic current along the western margin of the WIS (Fig. 9B) (Merewether et al., 1979; Bhattacharya and Willis, 2001; Hutsky et al., 2012; Hurd et al., 2014). Nonmarine deposits of this age include coastal-plain deposits of the Chalk Creek Member of the Frontier Formation in western Wyoming and the Dakota Sandstone in the Henry Mountains and Kaiparowits Plateau regions in Utah, and the San Juan Basin (Peterson et al., 1980; Uličný, 1999; Antia and Fielding, 2011; Kirschbaum and Mercier, 2013).

Paleocurrent measurements from delta-front deposits of the Peay Sandstone show a dominant south-southeast sediment dispersal, reflecting deflection by southward-directed geostrophic currents (Hutsky et al., 2012). Fluvial sandstones of the Dakota Sandstone in the Henry Mountains and Kaiparowits Plateau regions show a dominant east-southeast and northeast paleoflow direction, respectively (Fig. 9B) (Uličný, 1999; Antia and Fielding, 2011). The Dakota Sandstone deposited in the San Juan Basin at this time exhibits a retrogradational stacking pattern (Fig. 9B). One lacuna was located at northeastern Utah, the northwestern corner of Colorado, and southern Rock Springs uplift in Wyoming (Fig. 9B).

4.1.3. Earliest Late Cenomanian: top of Plesiacanthoceras wyomingsense zone (~95.5 Ma)

The WIS continued to expand through the late Cenomanian. At the *Plesiacanthoceras wyomingsense* time (95.5 Ma), marine mudstones deposited in the study area include the Belle Fourche Member in most Wyoming, the Mancos Shale in western Colorado, and the Graneros Shale in northern New Mexico (Fig. 9C). Calcareous mudstone and skeletal limestone of the Lincoln Limestone Member of the Greenhorn Formation were deposited in eastern Colorado (Sageman and Johnson, 1985). The Torchlight Sandstone within the Belle Fourche Member was deposited as a deflected delta-front sandstone in northern Wyoming (Fig. 9C), similar to the middle Cenomanian Peay Sandstone (Hutsky et al., 2012). Preserved marine shoreline deposits of this age include the Dakota Sandstone around the Utah-Colorado boundary and northwestern New Mexico (Fig. 9C). Coeval nonmarine deposits include coastal-plain deposits in western Wyoming and south-central to southern Utah (Uličný, 1999; Antia and Fielding, 2011; Kirschbaum and Mercier, 2013). The lacuna located at northwestern Utah, the northwestern corner of Colorado, and southwestern Wyoming (southern Rock Springs uplift) persisted (Fig. 9C).

4.1.4. Shoreline migration trend and sediment dispersal pattern during Cenomanian time

Due to the common hiatus and poor preservation of shoreline deposits in the study area during the Cenomanian, the lateral variability in third-order stratigraphic stacking pattern through this time is not well constrained. Nevertheless, since the seaways from the north and south connected by the *Conlinoceras tarrantense* time (earliest middle Cenomanian), the north-south oriented western shoreline of the WIS had generally shifted westward (landward). From the earliest middle Cenomanian to the earliest late Cenomanian (96.1–95.5 Ma), the western shoreline in the southern study area (e.g., southwestern Colorado and northeastern New Mexico) migrated landward by ~200 km, distinctly longer distance compared to the landward migration distance of its northern counterpart in western Wyoming (Fig. 9B and Fig. 9C). Littoral deposits of the Dakota Sandstone through the Cenomanian have therefore been considered to record the first westward expansion of the WIS across the Colorado Plateau region during the Late Cretaceous (Peterson et al., 1980; Uličný, 1999; Dickinson and Gehrels, 2008; Antia and Fielding, 2011).

During Cenomanian time, sediments deposited within the study area were largely derived from the Phanerozoic sedimentary cover strata exposed in the growing Sevier fold-thrust belt and the magmatic arc to the west (DeCelles, 2004; Laskowski et al., 2013; Bush et al., 2016; Lawton et al., 2020). An additional sediment source, particularly for the southern study area (Arizona-New Mexico border), was from the Mogollon Highlands (Figs. 1 and 9B) (Wolfe, 1989; Dickinson and Gehrels,

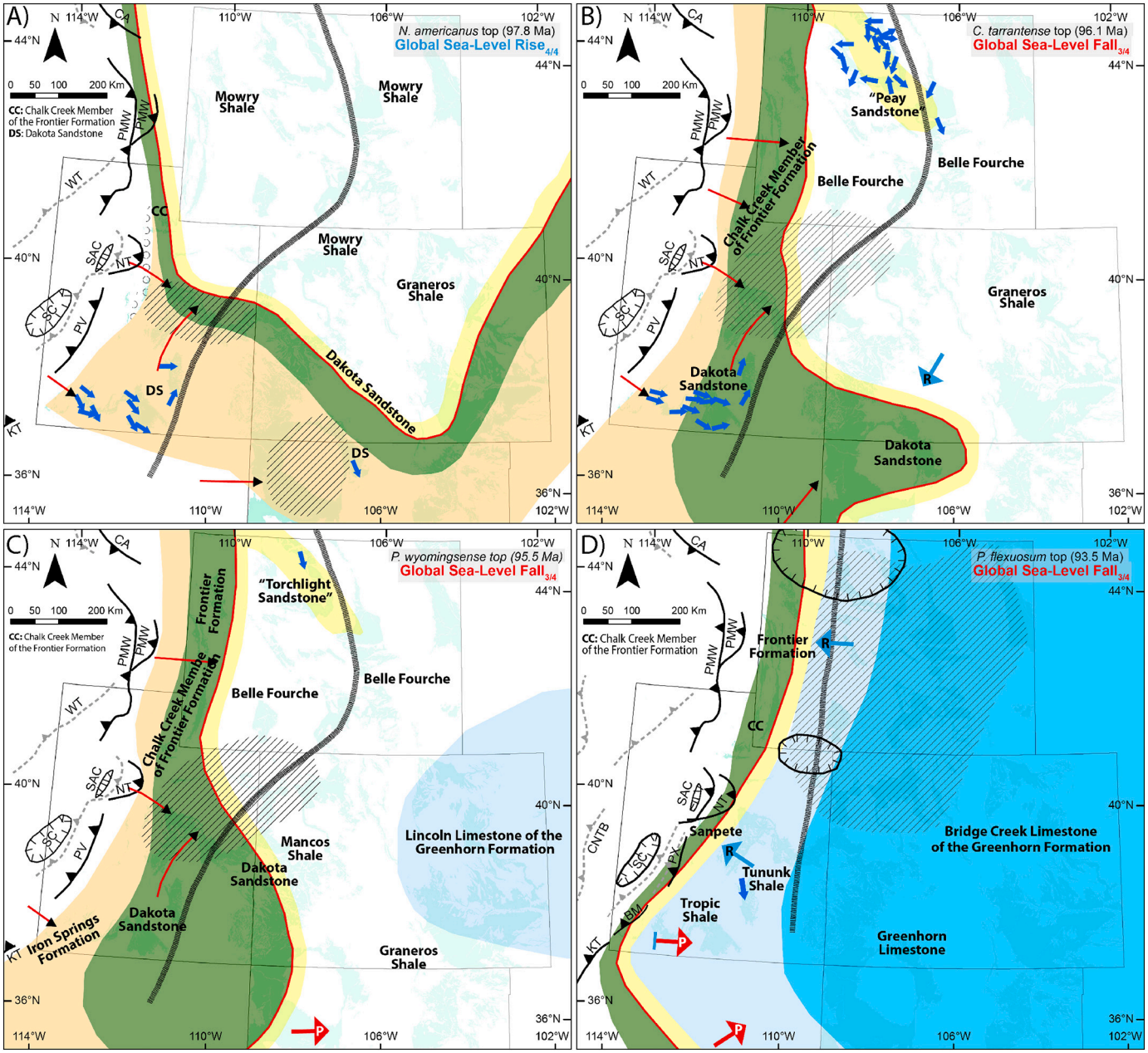

Fig. 9. A) Paleogeographic map at the early Cenomanian *Neogastroplites americanus* time (97.8 Ma). The global sea-level trend suggested by the majority of various eustatic reconstructions, is indicated by the text in the upper right corner. For instance, 4/4 represents that four out of four eustatic reconstructions (Fig. 7) suggest global sea-level was rising at the *Neogastroplites americanus* time. Refer to Fig. 3 for abbreviations of major structures of the Cordilleran thrust belt. B) Paleogeographic map at the middle Cenomanian *Conlinoceras tarrantense* time (96.1 Ma). One lacuna was located at northeastern Utah, the northwestern corner of Colorado, and southern Rock Springs uplift in Wyoming. The extent of lacunas (areas of erosion or nondeposition) in all paleogeographic maps are highly conjectural—active deposition might have occurred at the particular time but subsequently eroded or erosion/nondeposition at the particular time. C) Paleogeographic map at the late Cenomanian *Plesiacanthoceras wyomingsense* time (95.5 Ma). The lacuna located at northwestern Utah, the northwestern corner of Colorado, and southwestern Wyoming (southern Rick Springs uplift) persisted. D) Paleogeographic map at the early Turonian *Pseudaspidoceras flexuosum* time (93.5 Ma). An extensive marine lacuna was present throughout much of Wyoming, the northeastern corner of Utah, and the northwestern corner of Colorado. The stratigraphic stacking pattern differs along the western shoreline. The approximate location of forebulge during this time is from DeCelles (2004).

2008; Laskowski et al., 2013). The predominantly northeast-directed paleoflow in the Henry Mountains region, parallel to the interpreted orientation of the forebulge in that region (Fig. 9B), suggests some structural control on the distribution of fluvial drainage of the Dakota Sandstone (forebulge uplift) (Antia and Fielding, 2011).

4.2. Turonian (93.9 Ma - 89.8 Ma)

During Turonian time, the Willard-Meade thrust in the Idaho-Wyoming-Utah salient remained active (Liu et al., 2005). In north-central Utah, the Nebo thrust in the Charleston-Nebo salient was active during the early Turonian, replaced by the Charleston thrust during the middle to late Turonian (Fig. 7). The Pavant thrust sheet began to imbricate internally and form the Pavant duplex (DeCelles and Coogan, 2006). The Keystone thrust in southern Nevada and the Blue Mountain thrust in southwestern Utah remained active through the Turonian (Fig. 7).

More than one-third of North America was inundated by the WIS

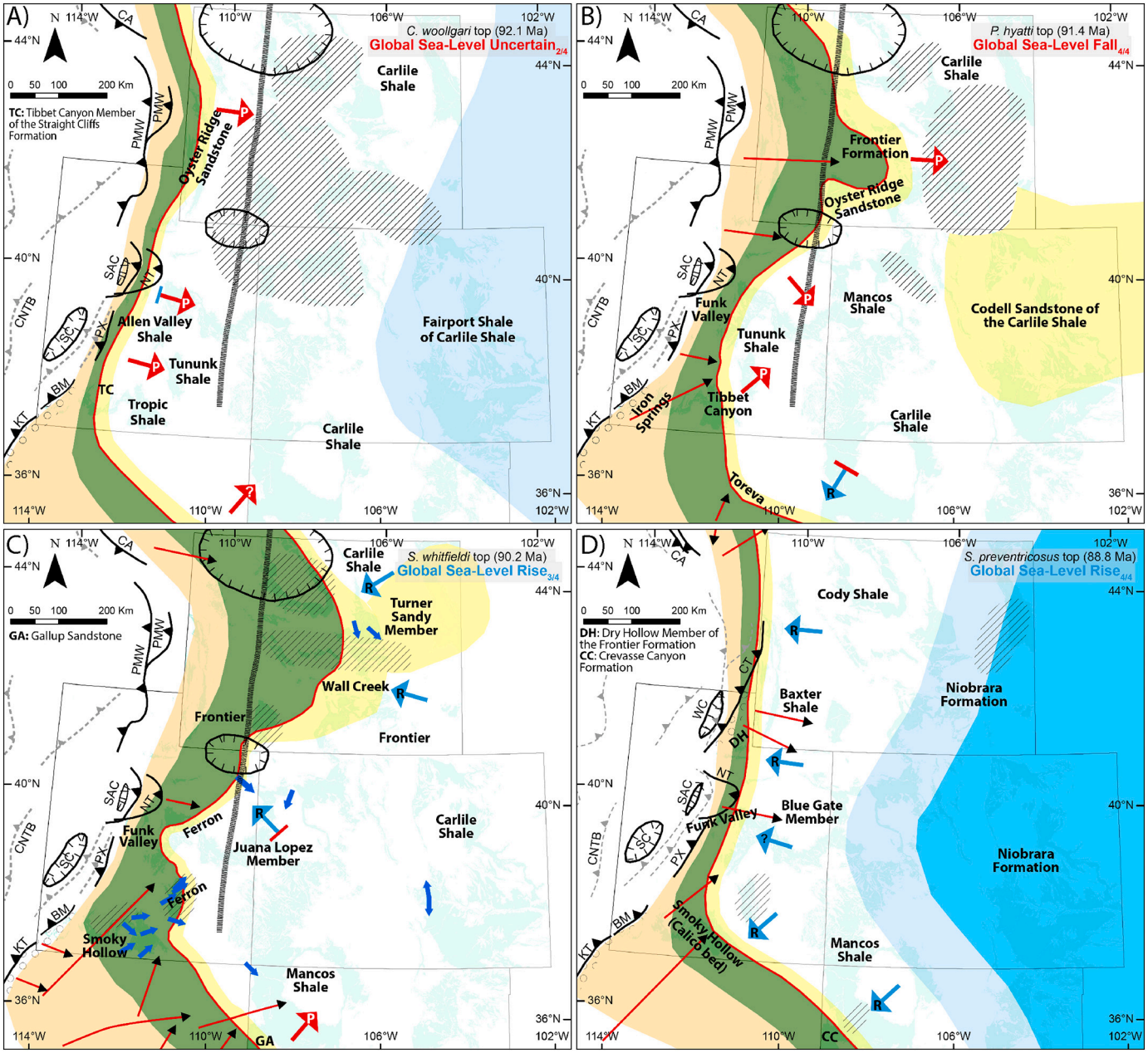

Fig. 10. A) Paleogeographic map at the middle Turonian *Collignoniceras woollgari* time (92.1 Ma). The marine lacuna became irregular in shape, locating at north-central Wyoming, central to southern Wyoming, northeastern Utah, and northwestern Colorado. Deposits along the western shoreline of the WIS show a uniform but not completely synchronous progradational stacking pattern. The shoreline at central Utah (west of the Wasatch Plateau) had just reached its landward limit and started to migrate seaward/eastward, whereas the seaward migration of shoreline in other areas had taken place for some time. B) Paleogeographic map at the late Turonian *Prionocyclus hyatti* time (91.4 Ma). Several areas of erosion/nondeposition were present at southeastern Wyoming, northern Wyoming, and northwestern Colorado. The stratal stacking patterns of shoreline deposits vary along the western margin of the WIS. C) Paleogeographic map at the late Turonian *Scaphites whitfieldi* time (90.2 Ma). The Henry Mountains region at this time was occupied by a lacuna. The paleoflow directions are from the Ferron Sandstone which is slightly older than the *Scaphites whitfieldi* zone and are shown here only to illustrate the overall sediment dispersal pattern in southern Utah. Several lacunas were located at up-dip and subparallel to the shoreline in Wyoming and around and landward of the shoreline in southern Utah. Shoreline deposits show along-strike variations in stratal stacking pattern between the northern and southern parts of the study area. D) Paleogeographic map at the early Coniacian *Scaphites preventricosus* time (88.8 Ma). Only a few local lacunas (those confined to a few thousands of square kilometers) were present in lower Coniacian strata in eastern Wyoming, the Henry Mountains region in Utah, and southwest of the San Juan Basin. Nearshore deposits uniformly show a retrogradational stacking pattern along the western shoreline. The approximate location of forebulge shown in A) to C) is from DeCelles (2004).

during the early Turonian (Sageman and Arthur, 1994). The timing of the maximum transgression corresponds to the highest global sea level during the Late Cretaceous indicated by Sahagian et al. (1996) and Haq (2014) and overall high global sea level suggested by Miller et al. (2005) and Kominz et al. (2008) (Fig. 7). From the early to late Turonian, global sea level gradually fell (Fig. 7). Turonian strata within the CFB are largely considered as deposited across the maximum Greenhorn transgression and from the subsequent Greenhorn regression (Kauffman, 1985).

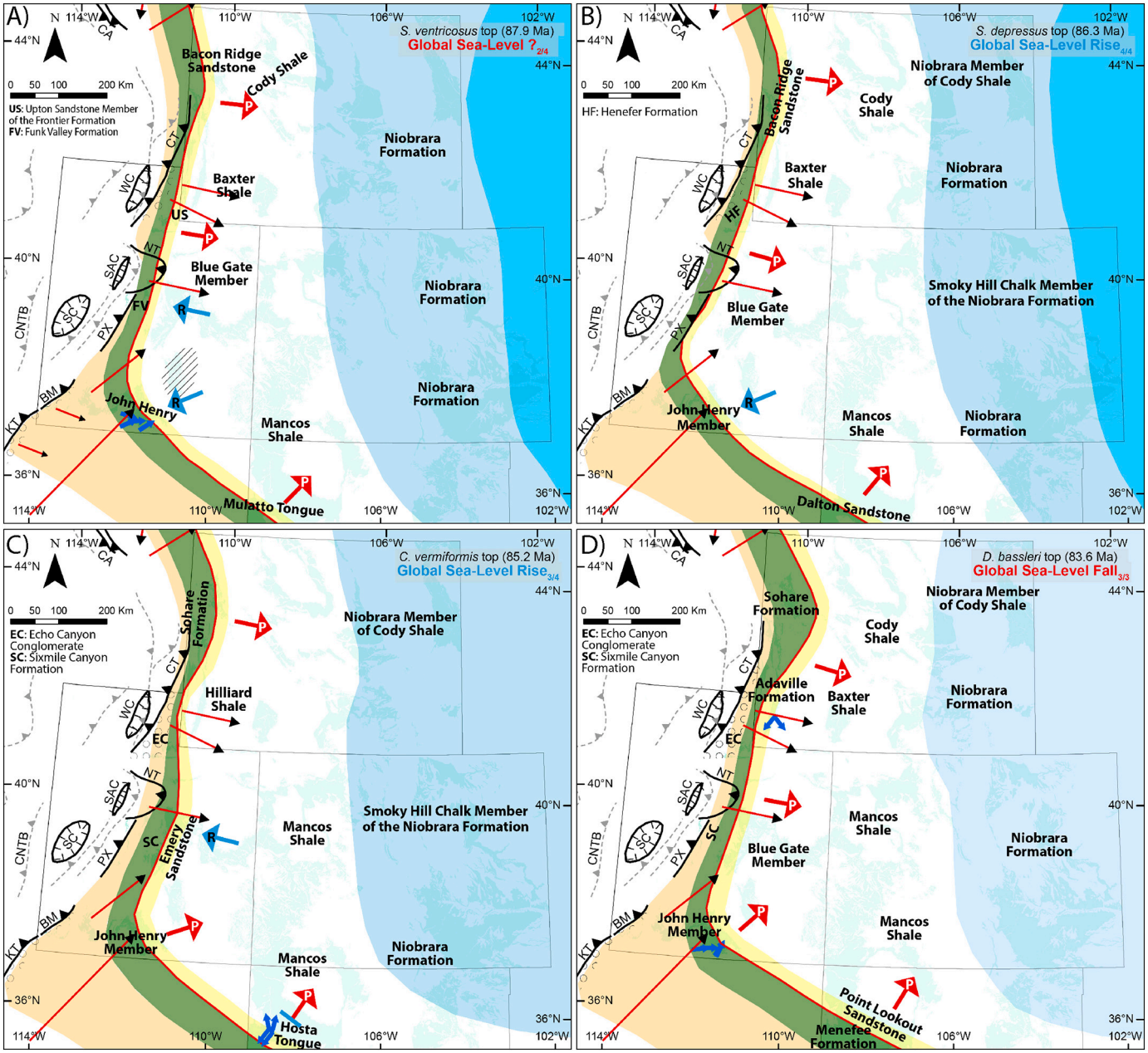

Fig. 11. A) Paleogeographic map at the middle Coniacian *Scaphites ventricosus* time (87.9 Ma). Only the local lacuna in the Henry Mountains region persisted. Deposits along the western shoreline show along-strike variability in stratigraphic stacking patterns. B) Paleogeographic map at the late Coniacian *Scaphites depressus* time (86.3 Ma). Deposits along the western shoreline show laterally variable stratigraphic stacking pattern. The stacking pattern of nearshore deposits in central Utah (west of the Wasatch Plateau) changed from retrogradational to progradational, becoming the same as those in western Wyoming and northwestern New Mexico. The retrogradational stacking pattern in the John Henry Formation in southern Utah persisted. C) Paleogeographic map at the middle Santonian *Clioscaphites vermiformis* time (85.2 Ma). Deposits along the shoreline show laterally variable stratigraphic stacking patterns. The progradation of the Hosta Tongue just began, whereas the progradation of the Sohare Formation and John Henry Formation had initiated for some time. The Emery Sandstone in central Utah shows a retrogradational stacking pattern. D) Paleogeographic map at the late Santonian *Desmoscaphites bassleri* time (83.6 Ma). The stratigraphic stacking pattern in central Utah changed from retrogradational to progradational, becoming the same as the shoreline deposits in other shoreline segments.

4.2.1. Early Turonian: top of Pseudaspidoceras flexuosum zone (~93.5 Ma)

The maximum Greenhorn transgression occurred around the *Pseudaspidoceras flexuosum* zone (93.5 Ma), when the WIS reached its maximum spatial extent (Fig. 9D). The study area at this time comprised widespread marine calcareous mudstones in central and southern Utah (e.g., the Tununk Shale Member of the Mancos Shale Formation and the Tropic Shale) and marine chalks/limestones of the Greenhorn Formation in eastern Wyoming, most of Colorado, and northern New Mexico (Fig. 9D). The westward migration of shoreline during the Greenhorn transgression is reflected by the westward-younging of the Mancos-Dakota boundary from western Colorado toward central/southern Utah (Fouch et al., 1983). The Sanpete Formation, west of the Wasatch Plateau, is probably the only preserved shoreline deposits of this age in the study area (Fouch et al., 1983). Preserved nonmarine deposits include the Frontier Formation in the westernmost part of Wyoming and the Coalville area in Utah (Fig. 9D).

Due to the extensive deposition of marine mudstones during the maximum Greenhorn transgression, few paleoflow data were reported in the literature. One distinct feature revealed by the paleogeographic

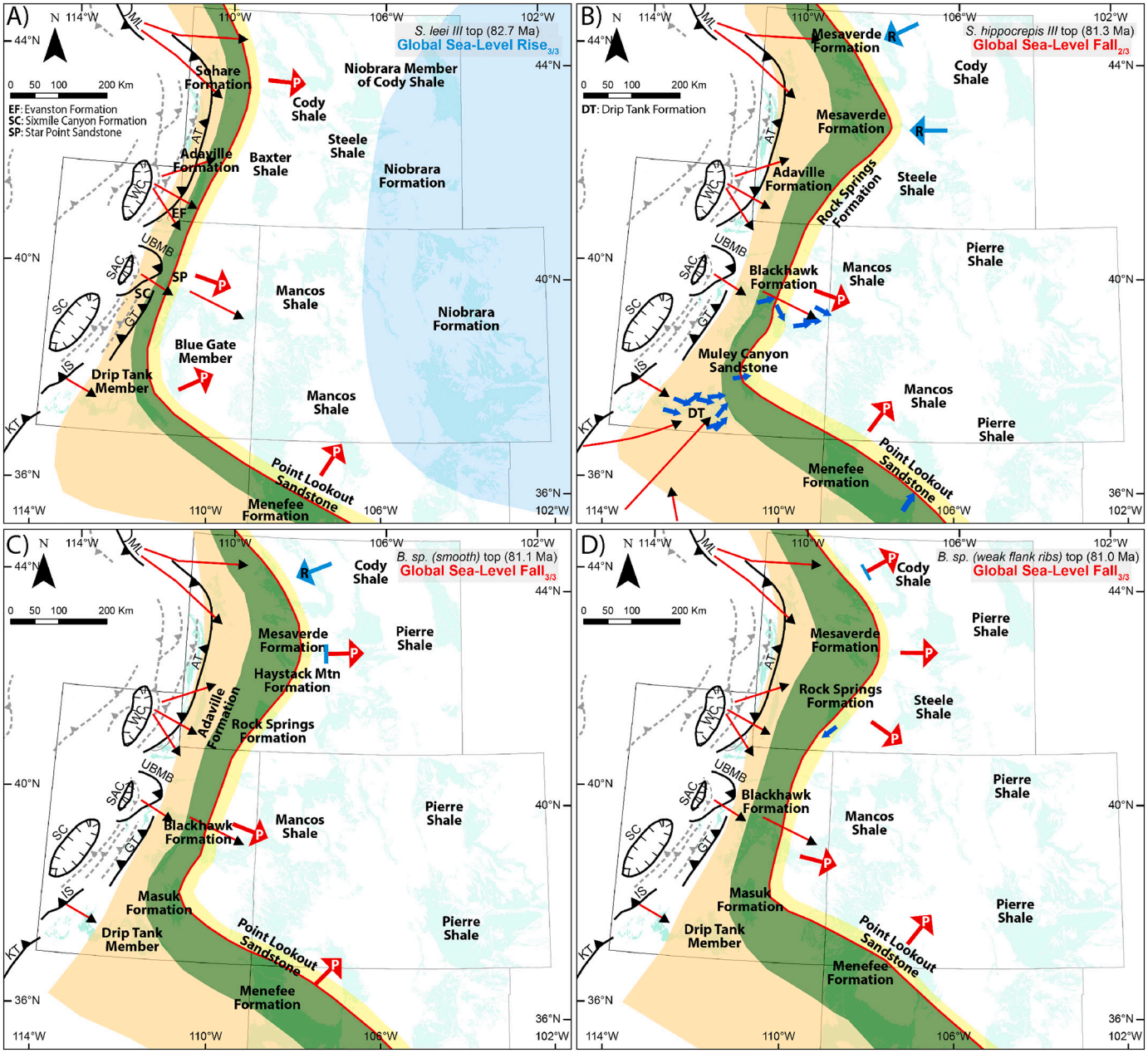

Fig. 12. A) Paleogeographic map at the early Campanian *Scaphites leei III* time (82.7 Ma). Deposits along the western shoreline of the WIS continue to uniformly show a progradational stacking pattern. B) Paleogeographic map at the early Campanian *Scaphites hippocrepis III* time (81.3 Ma). Deposits along the western shoreline show different stratigraphic stacking patterns between the northern and southern study area. C) Paleogeographic map at the early Campanian *Baculites* sp. *(smooth)* time (81.1 Ma). The stratigraphic stacking pattern in shoreline deposits in central Wyoming (Wind River Basin) changed to progradational and became the same as the shoreline deposits further south in the study area. The retrogradational stacking pattern in shoreline deposits persisted only in northern Wyoming (Bighorn Basin). D) Paleogeographic map at the early Campanian *Baculites* sp. *(weak flank ribs)* time (81.0 Ma). The stacking pattern of shoreline deposits in northern Wyoming changed from retrogradational to progradation, and therefore deposits along the entire shoreline in the study area show a progradational stacking pattern.

map at the *Pseudaspidoceras flexuosum* time is the extensive marine lacuna present throughout much of Wyoming, the northeastern corner of Utah, and the northwestern corner of Colorado (Fig. 9D). The stratigraphic stacking pattern differs along the western shoreline from north to south. The Frontier Formation in western Wyoming and the Sanpete Formation in western to central Utah show a retrogradational stacking pattern, while age-equivalent strata in central to southern Utah (i.e., the Tropic Shale and the Tununk Shale Member) shifts from a retrogradational to a progradational stacking pattern (Leithold, 1994; Li and Schieber, 2018).

4.2.2. *Middle Turonian: top of Collignoniceras woollgari zone (~92.1 Ma)*

Sediments deposited during the middle Turonian were subject to the second-order Greenhorn regressive cycle (Kauffman, 1985). At the *Collignoniceras woollgari* time (92.1 Ma), marine mudstones in the study area include the Allen Valley Shale in central Utah, the Tununk Shale in southcentral Utah, the Tropic Shale in southern Utah, and the Carlile Shale in northeastern Wyoming, western Colorado, and northern New Mexico (Fig. 10A). Calcareous mudstones (the Fairport Shale Member of the Carlile Shale Formation) were deposited in eastern Colorado. Preserved coeval shoreline sandstones include the Oyster Ridge Sandstone of the Frontier Formation in westernmost Wyoming, and the Tibbet Canyon Member of the Straight Cliffs Formation in southern Utah

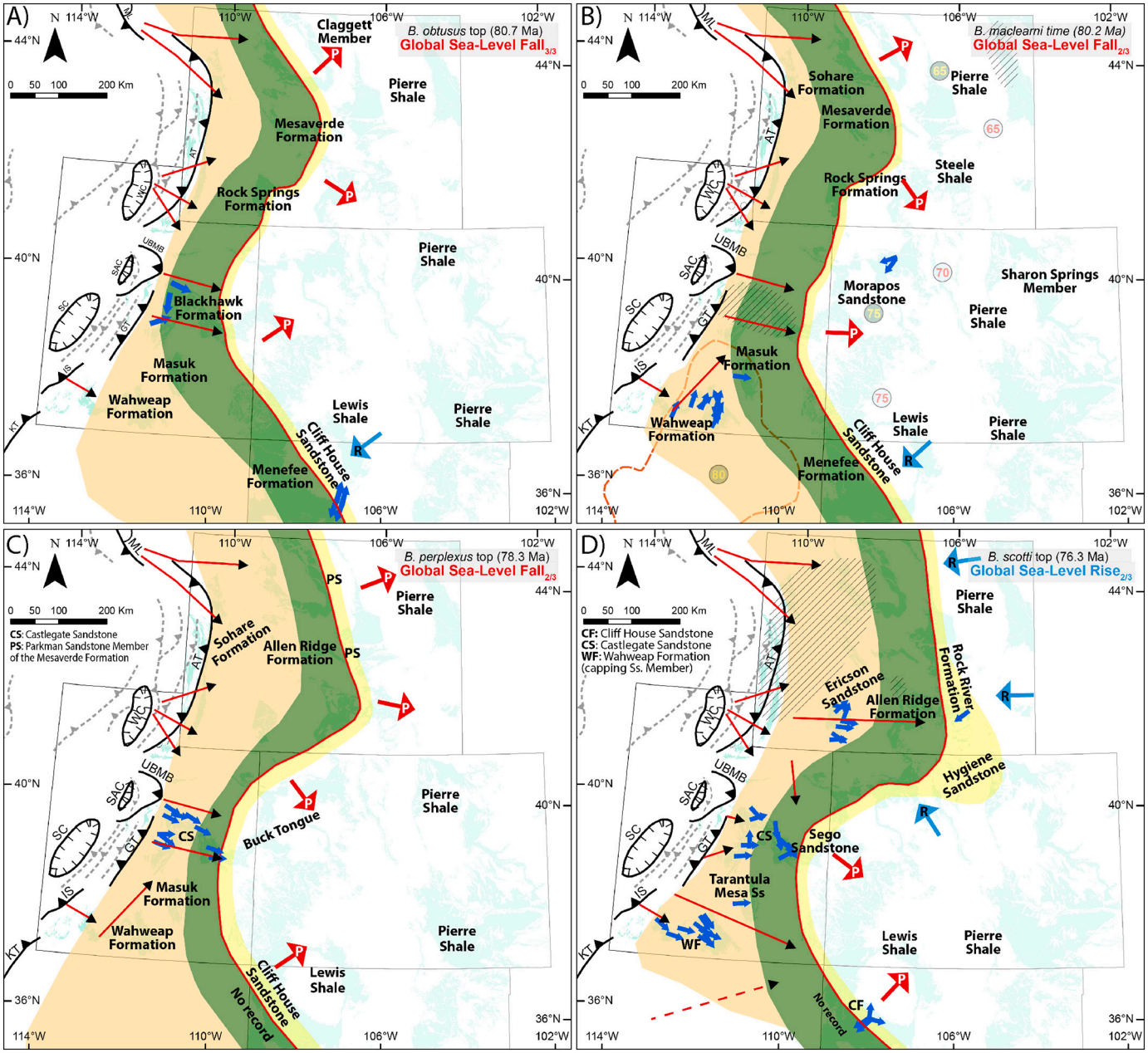

Fig. 13. A) Paleogeographic map at the middle Campanian *Baculites obtusus* time (80.7 Ma). Shoreline deposits from Wyoming to eastern Utah continued to show a progradational stacking pattern, while shoreline deposits of the Point Lookout Sandstone in northwestern New Mexico were replaced by the Cliff House Sandstone, exhibiting a retrogradational stacking pattern. B) Paleogeographic map at the middle Campanian *Baculites maclearni* time (80.2 Ma). The difference in the stratigraphic stacking pattern between the northern area (Wyoming to eastern Utah) and southern area (northwestern New Mexico) persisted. The number in green and gray circles represent the approximate locations of the conjugate Shatsky rise from Liu et al. (2010) and Humphreys et al. (2015). C) Paleogeographic reconstruction at the middle Campanian *Baculites perplexus* time (78.3 Ma). Deposits along the western shoreline uniformly show a progradational stacking pattern. D) Paleogeographic reconstruction at the middle Campanian *Baculites scotti* time (76.3 Ma). An extensive lacuna occupied the western one-quarter of Wyoming and a local lacuna was located at south-central Wyoming. The shoreline migration trend in the northern study area (central Wyoming to northernmost Colorado) decoupled from that in the southern area (western Utah to northwestern New Mexico). (For interpretation of the references to colour in this figure legend, the reader is referred to the web version of this article.)

(Fig. 10A). The marine lacuna became irregular in shape, locating at north-central Wyoming, central to southern Wyoming, northeastern Utah, and northwestern Colorado (Fig. 10A). Deposits along the western shoreline of the WIS show a uniform progradational stacking pattern.

4.2.3. Earliest Late Turonian: top of Prionocyclus hyatti zone (~91.4 Ma)

The Greenhorn regressive cycle continued through the *Prionocyclus hyatti* zone, and the western shoreline migrated seaward/eastward within the study area (Fig. 10B). At this time, marine mudstones (largely non-calcareous), including the Mancos Shale and the Carlile Shale, were deposited in eastern Utah, western Colorado, northeastern Wyoming, and the San Juan Basin (Fig. 10B). Age-equivalent, shallow-marine deposits of the Codell Sandstone Member of the Carlile Shale were deposited in eastern Colorado. Preserved shoreline sandstones of this age include the Frontier Formation (e.g., Oyster Ridge Sandstone) across north-south Wyoming, the Funk Valley Formation in central Utah, and the Tibbet Canyon Member of the Straight Cliffs Formation in southern Utah (Fig. 10B). The promontory of the Frontier Formation located at

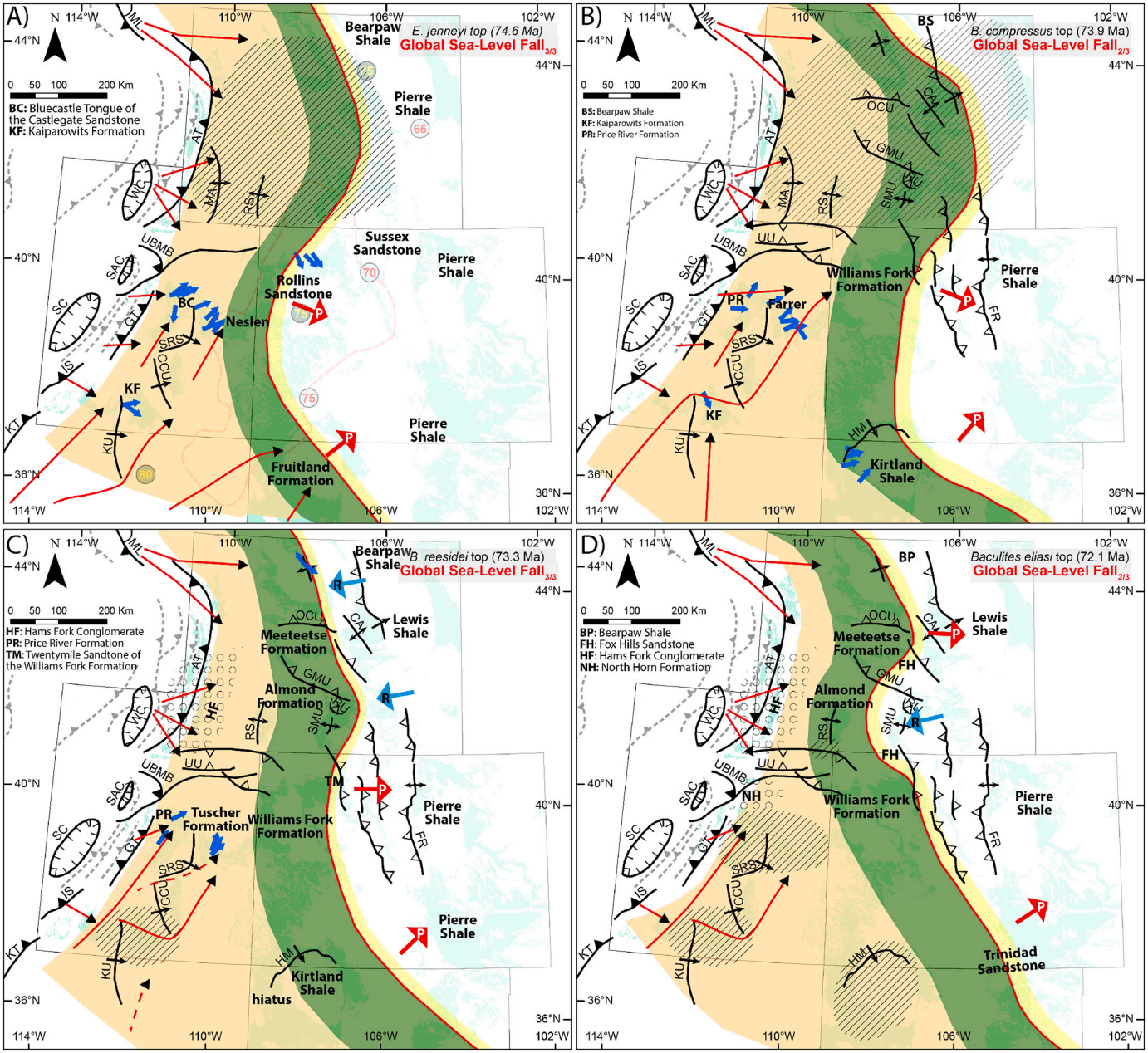

Fig. 14. A) Paleogeographic reconstruction at the late Campanian *Exiteloceras jenneyi* time (74.6 Ma). The lacuna in Wyoming expanded in extent to occupy the western three-quarters of Wyoming. Shoreline deposits from western Colorado to northwestern New Mexico show a progradational stacking pattern. B) Paleogeographic reconstruction at the late Campanian *Baculites compressus* time (73.9 Ma). The lacuna in the northern map area further expanded to occupy almost the entire Wyoming. The coastal-plain deposits in northern Colorado show a progradational stacking pattern, so do those in the San Juan Basin. C) Paleogeographic reconstruction at the late Campanian *Baculites reesidei* time (73.3 Ma). The extensive lacuna in Wyoming disappeared at this time. A local lacuna was located at the Kaiparowits Plateau region in southern Utah. The shoreline migration trend in the northern and southern study area was decoupled again. D) Paleogeographic reconstruction at the late Campanian *Baculites eliasi* time (72.1 Ma). Several lacunas were located at central-eastern Utah, southern Utah, and the San Juan Basin at this time. The shoreline migration trend remained decoupled along the western shoreline.

central Wyoming (Fig. 10B) is also noticed in Kirschbaum and Mercier (2013). Coeval nonmarine deposits include the coastal-plain deposits of the Frontier Formation in western Wyoming and the Funk Valley Formation in central Utah. Preserved alluvial-plain deposits of this age include the Iron Springs Formation in southwestern Utah.

Several areas of erosion/nondeposition were present at southeastern Wyoming, northern Wyoming, and northwestern Colorado at the *Prionocyclus hyatti* time (Fig. 10B). Erosion of sediments off these potential topographic highs represented by the unconformities may have been an important sediment source for the widespread shallow-marine offshore bars and/or shoreface sandstones of the Codell Sandstone Member of the Carlile Shale in northeastern Colorado (Elder and Kirkland, 1994). The stratal stacking patterns of shoreline deposits vary along the western margin of the WIS—progradational stacking pattern from western Wyoming to southern Utah and retrogradational stacking pattern from northeastern Arizona to northwestern New Mexico (Fig. 10B).

4.2.4. *Late Turonian: top of Scaphites whitfieldi zone (~90.2 Ma)*

The Greenhorn regressive cycle culminated approximately during the *Scaphites whitfieldi* zone (ca. 90.2 Ma), and the western shoreline in the study area migrated further seaward/eastward (Fig. 10C). Marine deposits at this time include non-calcareous mudstones of the Juana

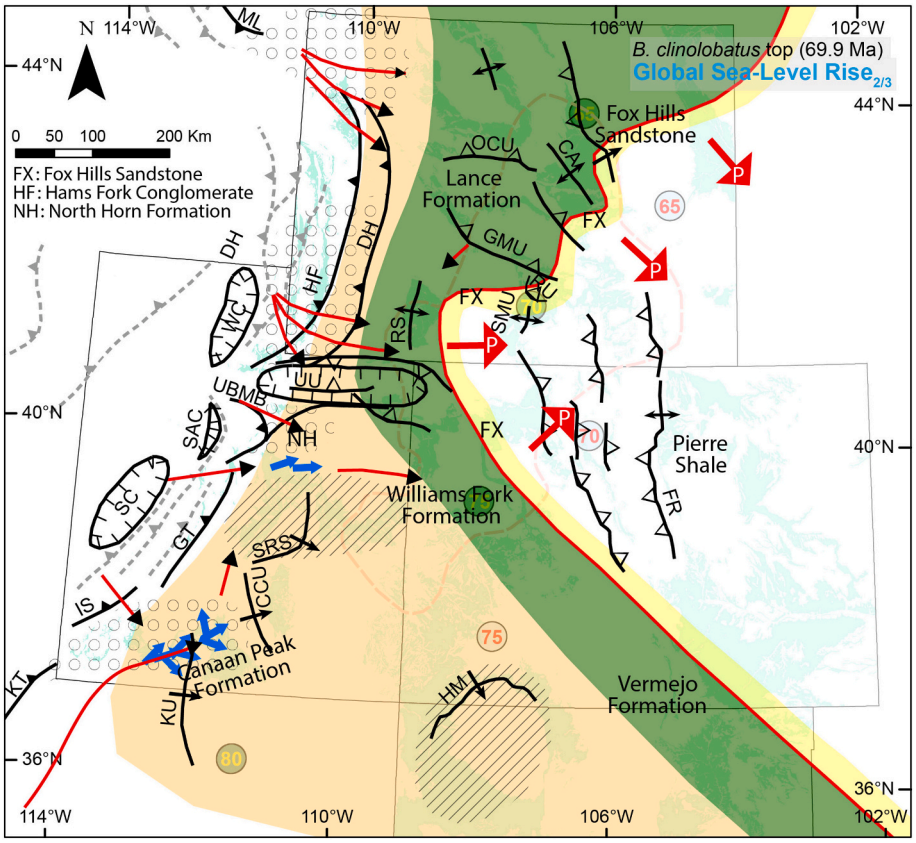

Fig. 15. Paleogeographic reconstruction at the early Maastrichtian *Baculites clinolobatus* time (69.9 Ma). The two lacunas at central-eastern Utah and the San Juan Basin persisted. Shoreline deposits of the Fox Hills Sandstone along the western shoreline consistently show a progradational stacking pattern.

Lopez Member in eastern Utah and western Colorado, the Manco Shale in the San Juan Basin, and the Carlile Shale in eastern Colorado (Fig. 10C). Marine shoreline deposits include the Wall Creek Member of the Frontier Formation and the Ferron Sandstone Member of the Mancos Shale deposited as a series of deltaic complexes along the western margin of the WIS (Fig. 10C). The Turner Sandstone Member of the Carlile Shale in the Powder River Basin probably represents shelf sandstones deposited in a more offshore setting than the Wall Creek Member (Merewether, 1996; Melick, 2013). Nonmarine deposits include coastal-plain deposits of the Frontier Formation in western Wyoming, Funk Valley Formation in central Utah, and the Smoky Hollow Member of the Straight Cliffs Formation in southern Utah (Fig. 10C).

The average paleoflow in the Smoky Hollow Member at the Kaiparowits Plateau region at this time is directed northeast (Primm et al., 2018). The Smoky Hollow Member prograded as the Ferron Notom delta in the Henry Mountains region, the paleocurrent data from which also show a dominant northeast flow direction (Fig. 10C) (Primm et al., 2018). Delta-front sandstones of the Frontier delta in northeastern Utah show an average southeast flow direction, offshore and perpendicular to the local shoreline orientation (Fig. 10C). Paleocurrent data from offshore deposits (0–100 km from the shoreline) are overall oblique to parallel to the proximal shoreline orientation, likely reflecting the influence of longshore currents—the paleocurrents are southeast-directed from central Wyoming (i.e., Wall Creek Member of the Frontier Formation), southwest-directed from northwestern Wyoming (i.e., Frontier Formation), and southeast-directed at the Four Corners area (i.e., Juana Lopez Member) (Fig. 10C).

Several lacunas were located at up-dip and subparallel to the shoreline in Wyoming and around and landward of the shoreline in southern Utah at this time (Fig. 10C). Shoreline deposits, again, show along-strike variations in stratal stacking pattern between the northern and southern parts of the study area. Shoreline deposits from Wyoming to northeastern Utah show a retrogradational stacking pattern, whereas their counterparts in northwestern New Mexico show an overall progradational stacking pattern (Fig. 10C).

4.2.5. *Shoreline migration trend and sediment dispersal pattern during Turonian time*

The lateral variability in third-order stratigraphic stacking pattern of shoreline deposits in the study area can be better constrained during Turonian time. One of the most distinct features revealed by the paleogeographic maps through Turonian is the decoupled (asynchronous) shoreline migration trend along the western shoreline. When the Greenhorn transgression culminated in the southern study area around the *Pseudaspidoceras flexuosum* time (93.5 Ma), coeval shoreline in the northern study area (western Wyoming to central Utah) had not reached the landward limit yet and continued to migrate landward/westward (Fig. 9D). Despite that deposits along the western shoreline of the WIS show a uniformly progradational stacking pattern at the *Collignoniceras woollgari* time (92.1 Ma), the shoreline at central Utah (west of the Wasatch Plateau) had just reached its landward limit and started to migrate seaward/eastward, whereas the seaward migration of shoreline in other areas had taken place for some time (Fig. 10A). At the *Prionocyclus hyatti* time (91.4 Ma), the shoreline migration trend in the southernmost study area decoupled from that in the rest of study area—shifting landward/southwestward at south of the Four Corners area, whereas seaward/eastward in other areas (Fig. 10B). The shoreline migration trend reversed from the *Prionocyclus hyatti* time to the *Scaphites whitfieldi* time (90.2 Ma), but the decoupled shoreline migration trend across the western shoreline persisted (Fig. 10C).

Sediments deposited within the CFB during the early to middle Turonian (i.e., around the maximum Greenhorn transgression) were likely derived from the Sevier fold-thrust belt due to the proximity of the shoreline to the Sevier fold-thrust belt (small transverse transport

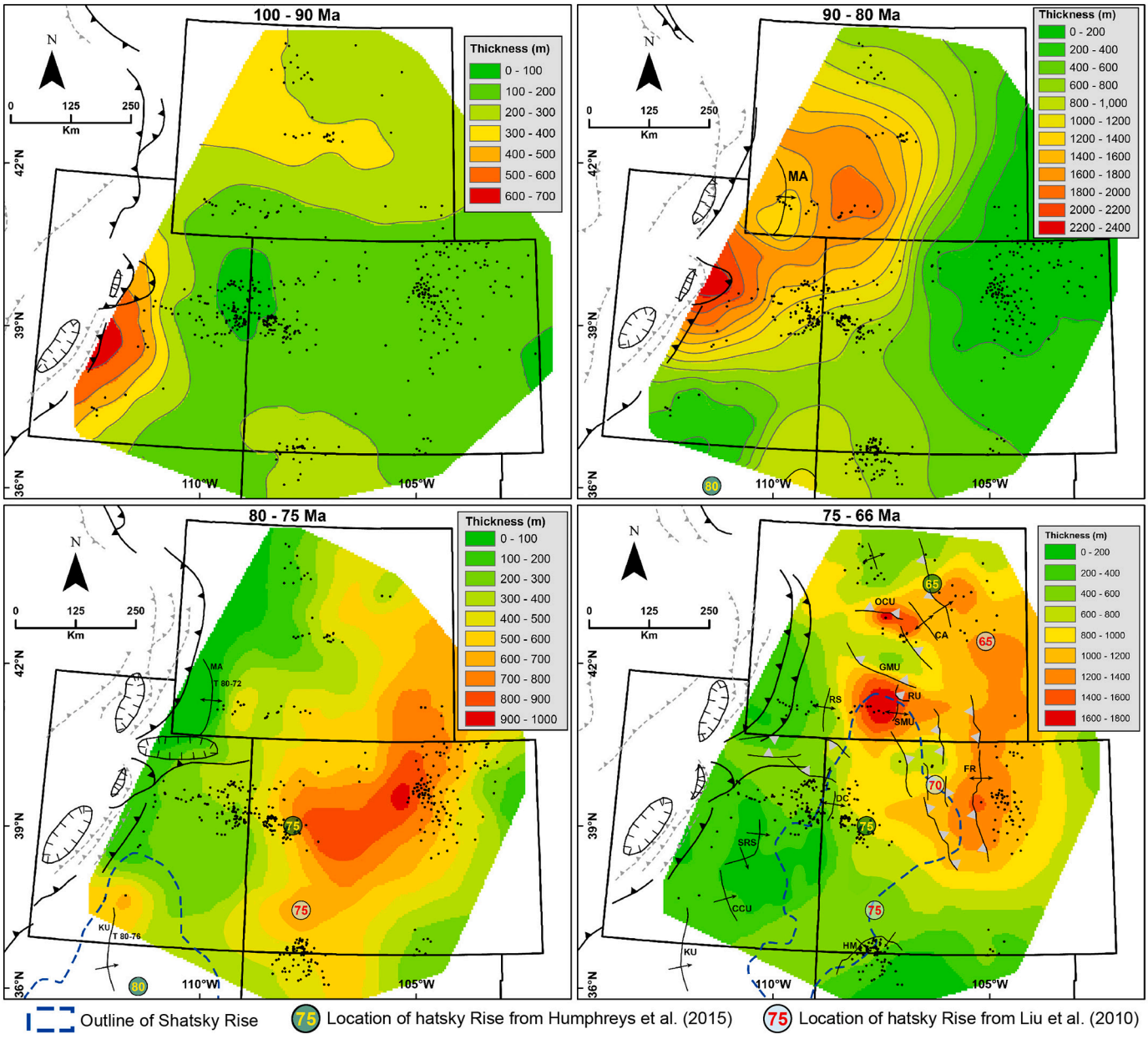

Fig. 16. Isopach maps of Cenomanian to late Turonian (ca. 100–90 Ma) strata (A), late Turonian to early middle Campanian (ca. 90–80 Ma) strata (B), middle Campanian to late Campanian (ca. 80–75 Ma) strata (C), and late Campanian to Maastrichtian (ca. 75–66 Ma) strata (D) in the study area (from Li and Aschoff, 2022). Black dots represent well log control points. The well-developed foredeep, forebulge, and back-bulge depozones suggest that development of the CFB during the Cenomanian to late Turonian was dominated by flexural subsidence (A). Flexural subsidence in response to loading of the Sevier thrust sheet continued to be the dominant mechanism to control the distribution of sediment accumulation during the late Turonian to middle Campanian, although the moderate stratal thickness at the four corners area was likely created due to the dynamic subsidence in front of the conjugate Shatsky Rise (B). The broad depocenter centered in northcentral Colorado during the middle to late Campanian can be distinctly attributed to the long-wavelength dynamic subsidence in front of the conjugate Shatsky Rise (C). The depocenters within the CFB during the late Campanian to Maastrichtian is likely the result of flexural subsidence due to lithospheric loading of adjacent Laramide-style uplifts and some degree of mantle-induced dynamic subsidence (D).

distance) when the WIS was much more expansive (e.g., Fig. 9D and Fig. 10A). During the subsequent Greenhorn regression (middle to late Turonian), marginal-marine deposits associated with regressive progradation of the shoreline in the southern study area record an increasing amount of sediment supply from the Mogollon Highlands through time, as indicated by the detrital zircon populations in samples from the Henry Mountains region (Ferron Sandstone), Kaiparowits Plateau (Smoky Hollow Member), Black Mesa (Toreva Formation), and San Juan Basin (Gallup Sandstone) (Dickinson and Gehrels, 2008; Laskowski et al., 2013; Szwarc et al., 2015; Pecha et al., 2018; Primm et al., 2018; Ferron, 2019). The sediment input from the Mogollon Highlands and paleocurrent data indicate the presence of a northeast-flowing, axial fluvial system (Fig. 10C), fed by rivers draining the Mogollon Highlands and Cordilleran magmatic arc to the south and by transverse drainages from the Sevier fold-thrust belt to the west (Szwarc et al., 2015; Pecha et al., 2018). Particularly for the southern study area during middle to late Turonian, the Sevier fold-thrust belt to the west was probably the main source of sediment supply only for the proximal foreland basin, whereas areas farther east (e.g., Black Mesa and San Juan basins) were largely fed longitudinally from sources along the Mogollon Highlands to the south (Dickinson and Gehrels, 2008; Laskowski et al., 2013). Nevertheless, detrital zircon populations indicate minor admixtures of

sand from the Sevier thrust belt are apparent within the CFB at least 500 km from the thrust belt (e.g., the Four Corners region) (Dickinson and Gehrels, 2008; Pecha et al., 2018), suggesting indicate episodic influx from the Sevier fold-thrust belt via transverse drainage systems (Primm et al., 2018) or redistribution by south-directed longshore currents (Fig. 10C).

4.3. Coniacian to Santonian (89.8 Ma - 83.6 Ma)

In Coniacian-Santonian time, the Sevier fold-thrust Belt in western Utah and eastern Nevada was actively culminating throughout the area with eastward-propagation and internal crustal shortening (DeCelles, 2004). In the Idaho-Wyoming-Utah salient, the Crawford thrust developed during the Coniacian and was active through Santonian (DeCelles, 1988; DeCelles, 1994). In central Utah, the Paxton thrust sheet was initially emplaced during the Santonian (Liu et al., 2005; DeCelles and Coogan, 2006). The Charleston thrust in the Charleston-Nebo salient and the Blue Mountains thrust and the Keystone thrust system in southern Utah and Nevada remained active (Fig. 7) (Goldstrand, 1994; DeCelles, 2004). Global sea level during the Coniacian to Santonian was characterized by a long period of stasis or a subtle long-term rise with some short-term small-magnitude fluctuations (Fig. 7). However, deposition within the CFB during the late Turonian to Santonian was considered subject to the second-order Niobrara transgressive-regressive cycle, which began in the late Turonian and reached maximum transgression during the early Coniacian (Fig. 7) (Kauffman, 1977).

4.3.1. Early Coniacian: top of Scaphites preventricosus zone (~88.8 Ma)

From the *Scaphites whitfieldi* time to the *Scaphites preventricosus* time (90.2–88.8 Ma), the western shoreline of the WIS, especially the shoreline in the northern study area, significantly shifted landward/westward from central to the westernmost Wyoming over ~300 km during the Niobrara transgression (Fig. 10C and Fig. 10D). At the *Scaphites preventricosus* time, deposits within the WIS include non-calcareous mudstones of the Cody Shale in northwestern Wyoming, the Baxter Shale in southwestern Wyoming, and the Mancos Shale in eastern Utah (i.e., the Blue Gate Member) and San Juan Basin (Fig. 10D). Extensive calcareous mudstones and chalks of the Niobrara Formation were deposited in eastern Wyoming, eastern Colorado, and northeastern New Mexico (Fig. 10D). Coeval marine shoreline deposits include the Funk Valley Formation west of the Wasatch Plateau and the John Henry Member of the Straight Cliffs Formation in southern Utah. Coastal-plain deposits were located within a thin belt landward of the shoreline, including the Dry Hollow Member of the Frontier Formation in northern Utah (Coalville area), the Funk Valley Formation in central Utah, the John Henry Member in southern Utah, and the Crevasse Canyon Formation located southwest of the San Juan Basin (Fig. 10D).

The regionally extensive unconformity present in Turonian strata was subsequently annealed during the *Scaphites preventricosus* time interval. In contrast, only a few local lacunas (those confined to a few thousands of square kilometers) were present in lower Coniacian strata in eastern Wyoming, the Henry Mountains region in Utah, and southwest of the San Juan Basin (Merewether and Cobban, 1986; Molenaar et al., 2002). Nearshore deposits uniformly show a retrogradational stacking pattern along the western shoreline at this time (Fig. 10D).

4.3.2. Middle Coniacian: top of Scaphites ventricosus zone (~87.9 Ma)

The western shoreline in the study area had overall migrated landward (westward from western Wyoming to southern Utah and southwestward in northwestern New Mexico during the *Scaphites ventricosus* zone (88.8–87.9 Ma). At the *Scaphites ventricosus* time, the deposition of marine non-calcareous mudstones slightly expanded into western Colorado (Fig. 11A). Marine calcareous mudstones were still mainly deposited in the eastern study area (Fig. 11A). Coeval shoreline deposits include the Bacon Ridge Sandstone in westernmost Wyoming, the Upton Sandstone Member of the Frontier Formation in the Coalville area, the John Henry Member in southern Utah, and the Mulatto Tongue southwest of the San Juan Basin (Fig. 11A). A narrow belt of coastal-plain deposits was located landward of the shoreline (e.g., the Funk Valley Formation west of the Wasatch Plateau and the John Henry Formation in southern Utah) (Fouch et al., 1983; Primm et al., 2018). Only the local lacuna in the Henry Mountains region persisted at this time. Regionally extensive areas of erosion/nondeposition were not present in the study area until middle late Campanian.

The average paleoflow in the John Henry Formation at the Kaiparowits Plateau region at the *Scaphites ventricosus* time was directed east to east-northeast (Fig. 11A) (Gooley et al., 2016; Primm et al., 2018; Koch et al., 2019). Deposits along the western shoreline show along-strike variability in stratigraphic stacking patterns. The Funk Valley Formation in central Utah and the John Henry Formation show a retrogradational stacking pattern (Fouch et al., 1983; Gooley et al., 2016). In contrast, the Bacon Ridge Sandstone in western Wyoming and the Mulatto Tongue in northwestern New Mexico show a progradational stacking pattern (Fig. 11A).

4.3.3. Late Coniacian: top of Scaphites depressus zone (~86.3 Ma)

The shoreline in western Wyoming and northwestern New Mexico migrated seaward, whereas the shoreline in central and southern Utah shifted landward during the *Scaphites depressus* zone (87.9 Ma to 86.3 Ma). During this time, the distribution of different depositional environments in the study area remained roughly the same. The deposition of marine non-calcareous mudstones had slightly expanded in extent at the expense of marine calcareous mudstones/chalks (Fig. 11B).

Deposits along the western shoreline show laterally variable stratigraphic stacking pattern at the *Scaphites depressus* time (Fig. 11B). The stacking pattern of nearshore deposits in central Utah (west of the Wasatch Plateau) changed from retrogradational to progradational, becoming the same as those in western Wyoming and northwestern New Mexico (Fig. 11B). The retrogradational stacking pattern in the John Henry Formation in southern Utah persisted at this time (Fig. 11B) (Gooley et al., 2016).

4.3.4. Middle Santonian: top of Clioscaphites vermiformis zone (~85.2 Ma)

Most segments of the western shoreline in the study area, except for southern Utah, migrated seaward from the *Scaphites depressus* time to the *Clioscaphites vermiformis* time (86.3–85.2 Ma). At the *Clioscaphites vermiformis* time, the western limit of marine non-calcareous mudstones slightly shifted eastward, whereas the distribution of marine calcareous mudstone remained roughly the same, located in eastern Wyoming, eastern Colorado, and northeastern New Mexico (Fig. 11C). Preserved coeval marine shoreline deposits include the Emery Sandstone in central Utah and the Hosta Tongue southwest of the San Juan Basin (Fig. 11C). A narrow belt of coastal-plain deposits was located landward of the shoreline, including the Sohare Formation in western Wyoming, the Sixmile Canyon Formation in central Utah, and the John Henry Member in southern Utah (Fig. 11C). Local alluvial-fan deposits of the Echo Canyon Conglomerate were located in the Coalville area, Utah (Fig. 11C) (Liu et al., 2005; Painter et al., 2014; Haque et al., 2020).

Deposits along the shoreline at the *Clioscaphites vermiformis* time show laterally variable stratigraphic stacking patterns (Fig. 11C). Shoreline deposits in western Wyoming, southern Utah, and northwestern New Mexico show an overall progradational stacking pattern—the progradation of the Hosta Tongue just began, whereas the progradation of the Sohare Formation and John Henry Formation had initiated for some time. In contrast, the Emery Sandstone in central Utah shows a retrogradational stacking pattern (Fouch et al., 1983; Edwards et al., 2005).

4.3.5. Latest Santonian: top of Desmoscaphites bassleri zone (~83.6 Ma)

From the *Clioscaphites vermiformis* time to *Desmoscaphites bassleri* time (85.2–83.6 Ma), the western shoreline in the study area generally

migrated seaward, except for the shoreline in central Utah, which migrated landward (Fig. 11D). The overall distribution of different gross depositional environments in the study area remained roughly the same. Marine non-calcareous mudstones were deposited along a north-south belt in the middle of the study area, bounded by coastal-plain and shoreline deposits to the west and calcareous mudstones to the east (Fig. 11D).

The average paleoflow in the John Henry Formation at the Kaiparowits Plateau region at the *Desmoscaphites bassleri* time remained to be directed east to northeast (Gallin et al., 2010; Gooley et al., 2016). Shoreface deposits of the Lazeart Member of the Adaville Formation show northeast and southeast bimodal paleocurrent directions (Heinzel, 2000). The stratigraphic stacking pattern in central Utah changed from retrogradational to progradational, becoming the same as the shoreline deposits in other shoreline segments (Fig. 11D).

4.3.6. *Shoreline migration trend and sediment dispersal pattern during Coniacian to Santonian*

The third-order shoreline migration trend varied along the western margin of the WIS in the study area during most Coniacian to Santonian. Particularly, the migration trend of shoreline in central or southern Utah almost always decoupled from that in other shoreline segments during this time. Specifically, at the *Scaphites ventricosus* time (87.9 Ma), the shoreline in central to southern Utah was migrating landward/westward, whereas other shoreline segments were migrating seaward (eastward in western Wyoming to northeastern Utah and northwestward in northwestern New Mexico; Fig. 11A). The landward shoreline migration in southern Utah persisted through the *Scaphites depressus* time (86.3 Ma), when the shoreline in central Utah had started to migrate seaward, together with the shoreline in western Wyoming and northwestern New Mexico (Fig. 11B). When the shoreline in southern Utah started to migrate seaward by the *Clioscaphites vermiformis* time (85.2 Ma) along with the shoreline in western Wyoming and northwestern New Mexico, the shoreline in central Utah started to migrate landward (westward) (Fig. 11C). The migration of shoreline in central Utah changed from landward to seaward at the *Desmoscaphites bassleri* time (83.6 Ma), when the western shoreline in the study area was uniformly migrating seaward (Fig. 11D).

Generalized sediment dispersal data suggest an east-directed dispersal in the northern study area (Wyoming) and a mix of east- and north- directed dispersal in the southern study area (the Uinta region and south thereof) (DeCelles, 2004; Laskowski et al., 2013). Detrital-zircon provenance studies and paleocurrent data demonstrate that the John Henry Member in southern Utah and the Crevasse Canyon Formation (Torrivio Member) in the Four Corners region received sediments not only from the Sevier fold–thrust belt to the west but also from additional major source areas to the south (Mogollon Highlands) and southwest (Cordilleran magmatic arc) (Lawton et al., 2014; Szwarc et al., 2015; Ferron, 2019). Sediments derived from the Mogollon Highlands were considered to have transported as far as ~1700 km through a northeast directed axial system based on detrital zircon provenance data from the Mancos Formation in the Uinta region (Laskowski et al., 2013).

4.4. *Campanian (83.6 Ma - 72.1 Ma)*

The Campanian was a period of increased tectonic activity along the Sevier fold-thrust belt, and frontal thrust systems in the Sevier belt were characterized by continued eastward propagation and phases of internal structural culmination (DeCelles, 2004; Miall et al., 2008). In the Idaho-Wyoming-Utah salient, the Absaroka thrust (early) developed during the earliest Campanian and remained active until the latest Campanian (Fig. 7) (DeCelles, 1994; Liu et al., 2005; Yonkee and Weil, 2015). In the Charleston-Nebo Salient, the basal thrust linked with the Uinta Basin-Mountain Boundary (UBMB) thrust (DeCelles, 2004). In central Utah, a large antiformal duplex formed (the Paxton duplex), and the Gunnison thrust developed during the late Campanian (DeCelles et al., 1995; DeCelles and Coogan, 2006). In southwestern Utah, the Iron Springs thrust developed (Fig. 7) (Goldstrand, 1994).

Global sea level during the Campanian was characterized by a long-term fall interrupted by some shorter-term rises (Fig. 7). Within the CFB, the long-term Niobrara regressive cycle ended during the early Campanian. Middle to upper Campanian deposits within the CFB were then subject to two transgressive-regressive sea-level cycles (Fig. 7; the Claggett and Bearpaw cycles of Kauffman, 1977). The maximum transgression during these two cycles was much less extensive than that during the earlier Niobrara and Greenhorn cycles, largely reflecting the first-order regression of the WIS.

During the Campanian, magmatism swept inboard into the central Rocky Mountain region, probably in response to a decrease in the angle of subduction of the Farallon plate, which caused a cooling of the mantle wedge and cessation of melting (Coney and Reynolds, 1977; Liu and Currie, 2016; Copeland et al., 2017). For the first time, Laramide intraforeland basement uplifts began to significantly disrupt the regional subsidence/uplift pattern in the CFB (Dickinson et al., 1988; DeCelles, 2004; Lawton, 2008). The approximate initiation ages of incipient Laramide-style uplifts in the study area during the Late Cretaceous were compiled and summarized in Table 1.

4.4.1. *Early Campanian: top of Scaphites leei III zone (~82.7 Ma)*

The western shoreline in the study area had overall migrated seaward from the *Desmoscaphites bassleri* time to the *Scaphites leei III* time (83.6–82.7 Ma). At the *Scaphites leei III* time, marine non-calcareous mudstones were distributed along a north-south belt in the middle study area (Fig. 12A). Marine calcareous mudstones of the Niobrara Formation were deposited in eastern Wyoming, eastern Colorado, and the northeastern corner of New Mexico. Coeval shoreline deposits include the Star Point Sandstone of the Blackhawk Formation in central Utah and the Point Lookout Sandstone southwest of the San Juan Basin (Fig. 12A). Coastal-plain deposits include the Sohare Formation in western Wyoming, the Adaville Formation in southwestern Wyoming, the Sixmile Canyon Formation in central Utah, the Drip Tank Member of the Straight Cliffs Formation in southern Utah, and the Menefee Formation in northwestern New Mexico. At the *Scaphites leei III* time, deposits along the western shoreline of the WIS continue to uniformly show a progradational stacking pattern (Fig. 12A).

4.4.2. *Early Campanian to early middle Campanian: Top of Scaphites hippocrepis III zone to top of Baculites maclearni zone (~81.3 Ma - 80.2 Ma)*

The entire western shoreline continued to migrate seaward from the *Scaphites leei III* time to the *Scaphites hippocrepis III* time (82.7 Ma - 81.3 Ma). Marine deposits in the study area now comprise mostly non-calcareous mudstones (Fig. 12B). Preserved coeval shoreline deposits include the Rock Springs Formation in southwestern Wyoming, the Blackhawk Formation in northeastern Utah, the Muley Canyon Sandstone in south-central Utah, and the Point Lookout Sandstone in the San Juan Basin (Fig. 12B). Landward of the shoreline sediments were deposited in coastal-plain to alluvial-plain environments in western Wyoming, northeastern-to-southern Utah, and northwestern New Mexico (Fig. 12B). The distribution of gross depositional environments remained overall the same from the *Scaphites hippocrepis III* time to *Baculites maclearni* time (81.3–80.2 Ma) and had only slightly changed in extent in response to changes in shoreline configuration (Fig. 12B to Fig. 13B).

At the *Scaphites hippocrepis III* time, rocks deposited in various environments across Utah record a dominant eastward paleoflow direction, away from the Sevier fold-thrust belt (Fig. 12B). Meanwhile, deposits along the western shoreline show different stratigraphic stacking patterns between the northern and southern study area. Shoreline deposits in northern and central Wyoming exhibit a retrogradational stacking pattern, whereas their counterparts from eastern

Table 1
Sources on the initiation times of Laramide-style uplifts in the study area during the Late Cretaceous.

Laramide Uplifts	Age Range (Ma)	Note	Reference
Casper Arch	75–66	Based on the rapid southward thinning of late Campanian to Maastrichtian strata in the Wind River Basin	Li and Aschoff, 2022
Circle Cliffs uplift	75–66	Occurred in latest Campanian to Maastrichtian	Lawton et al., 1986; Goldstrand, 1994; Lawton and Bradford, 2011
Douglas Creek Arch	74–66	Not active prior to deposition of Castlegate. Unlike the larger Laramide uplifts, the Douglas Creek arch was apparently never a major positive topographic feature	Cross, 1986; Johnson and Flores, 2003; Mederos et al., 2005
Front Range	71–66		Kluth, 1997; Sonnenberg and Bolyard, 1997; Kelley, 2002
Granite Mountains Uplift	75–66	Late Campanian to Maastrichtian strata in the eastern Washakie Basin thins against the Granite Mountains Uplift	Li and Aschoff, 2022
Hogback monocline	74–71	Thickening of the Kirtland Formation indicates the bordering Hogback monocline was active during Kirtland deposition	Lorenz and Cooper, 2003; Cather, 2004; Pecha et al., 2018
Kaibab Uplift	80–76	Based on ages of syntectonic strata	Tindall et al., 2010
Owl Creek uplift	75–66	Based on the rapid southward thinning of late Campanian to Maastrichtian strata in the Wind River Basin	Li and Aschoff, 2022
Rawlins uplift	75–66	Active during deposition of the Canyon Creek Mbr (area of reduced subsidence that probably lacked topographic expression)	Wroblewski, 2003; López and Steel, 2015
Rock Springs uplift	76–72	Unconformities in Ericson Formation, maximum uplift in Maastrichtian	Mederos et al., 2005; Leary et al., 2015
San Rafael Swell	77	Influenced sedimentation as early as ca. 77 Ma based on sediment thinning patterns. Influenced sediment dispersal at ca. 75 Ma	Lawton et al., 1986; DeCelles, 2004; Aschoff and Steel, 2011; Bartschi et al., 2018
Sierra Madre Uplift	75–66	Active during deposition of the Canyon Creek Member (area of reduced subsidence that probably lacked topographic expression)	López and Steel, 2015
Uinta Uplift	75	Based on detrital zircon provenance data	Leary et al., 2015; Bartschi et al., 2018

Utah to northwestern New Mexico show a progradational stacking pattern (Fig. 12B). Consequently, by the next ammonite biozone—*Baculites* sp. *(smooth)*—the shoreline in northern and central Wyoming had shifted slightly landward, whereas its southern counterpart migrated seaward (Fig. 12C). At the *Baculites* sp. *(smooth)* time (81.1 Ma), the retrogradational stacking pattern in shoreline deposits persisted only in northern Wyoming (Bighorn Basin). The stratigraphic stacking pattern in shoreline deposits in central Wyoming (Wind River Basin) changed to progradational and became the same as the shoreline deposits further south in the study area (Fig. 12C).

From the *Baculites* sp. *(smooth)* time to the *Baculites* sp. *(weak flank ribs)* time (81.1–81.0 Ma), the entire western shoreline, other than in northernmost Wyoming, had shifted seaward, and the stacking pattern of shoreline deposits in northern Wyoming changed from retrogradational to progradation (Fig. 12C and Fig. 12D). Consequently, deposits along the entire shoreline in the study area show a progradational stacking pattern at the *Baculites* sp. *(weak flank ribs)* time (Fig. 12D). By the *Baculites obtusus* time (80.7 Ma), the shoreline from Wyoming to eastern Utah continued to migrate seaward (Fig. 13A). Meanwhile, shoreline deposits of the Point Lookout Sandstone in northwestern New Mexico were replaced by the Cliff House Sandstone, which exhibits a retrogradational stacking pattern (Fig. 13A). The difference in the stratigraphic stacking pattern between the northern area (Wyoming to eastern Utah) and southern area (northwestern New Mexico) persisted through the *Baculites maclearni* time (80.2 Ma; Fig. 13B). At this time, the dominant paleoflow direction in eastern Utah remained to be eastward but distinctly shifted to a north-northeast direction in southern Utah (Fig. 13B).

4.4.3. Middle Campanian: top of Baculites perplexus zone (~78.3 Ma)

The shoreline in the northern study area migrated seaward, whereas its southern counterpart migrated landward from the *Baculites maclearni* time to the *Baculites perplexus* time (80.2–78.3 Ma). Marine mudstones in the study area now include the Pierre Shale in eastern Wyoming, eastern Colorado, and northeastern New Mexico, the Buck Tongue of the Mancos Shale around the Utah-Colorado boundary, and the Lewis Shale in the San Juan Basin (Fig. 13C). Preserved shoreline deposits include the Parkman Sandstone of the Mesaverde Formation in northern Wyoming, the Castlegate Sandstone in eastern Utah, and the Cliff House Sandstone southwest of the San Juan Basin. Coeval nonmarine deposits in the study area increased in extent, including alluvial-plain and coastal-plain deposits of the Sohare and Allen Ridge formations in western Wyoming and the Castlegate Sandstone, the Masuk and Wahweap formations in Utah (Fig. 13C). The dominant paleoflow of the Castlegate Sandstone in central Utah at this time was toward east to southeast (Robinson and Slingerland, 1998; Bartschi et al., 2018). At the *Baculites perplexus* time, deposits along the western shoreline uniformly show a progradational stacking pattern (Fig. 13C).

4.4.4. Middle Campanian: top of Baculites scotti zone (~76.3 Ma)

The entire stretch of shoreline in the study area migrated further seaward (over 20–100 km) from the *Baculites perplexus* time to the *Baculites scotti* time (78.3–76.3 Ma). The deposition of marine mudstones in the study area had decreased in extent due to the seaward/eastward migration of the shoreline. Preserved coeval shoreline deposits include the Rock River Formation in southeastern Wyoming, the Sego Sandstone around the Utah-Colorado boundary, and the Cliff House Sandstone southwest of the San Juan Basin (Fig. 13D). Historically interpreted as offshore bars, the Hygiene Sandstone was recently reinterpreted as deposited from tide-dominated deltas during regression and subsequently reworked during transgression (Plink-Bjorklund and Kiteley, 2013). Nonmarine environments further increased in extent in Wyoming, including alluvial-plain deposits of the Ericson Sandstone and coastal-plain deposits of the Allen Ridge Formation (Fig. 13D). Other coeval nonmarine deposits include the Castlegate Sandstone, the Tarantula Mesa Sandstone, and the Wahweap Formation in Utah.

In southern Wyoming, rivers represented by the Ericson Sandstone and the Allen Ridge Formation flowed generally to the east (Martinsen et al., 1993; Leary et al., 2015). Paleoflow directions from the Castlegate Sandstone in central Utah are east- to southeast-directed (Fig. 13D). Aschoff and Steel (2011) proposed that over 200 km of progradation of a clastic wedge (from the Castlegate Sandstone to Sego Sandstone) occurred during this time. Detrital zircon provenance data indicate deposition of the Sego Sandstone at ca. 76 Ma marks the introduction of a northern source (Canadian Paleozoic passive margin) in addition to a

thrust-belt source, consistent with the dominant south–southeast progradational direction of tide-dominated deltas of the Sego Sandstone or the potential supply of northern sediments by southward-directed longshore currents in the marine realm (Bartschi et al., 2018). In south-central to southern Utah, paleoflow directions consistently show a dominant eastward direction (Fig. 13D), consistent with detrital zircons nearly exclusively sourced from the Sevier fold-thrust belt in the capping sandstone Member of the Wahweap Formation (Lawton and Bradford, 2011).

At the *Baculites scotti* time, an extensive lacuna occupied the western one-quarter of Wyoming and a local lacuna was located at south-central Wyoming (Fig. 13D). At the same time, the shoreline migration trend in the northern study area (central Wyoming to northernmost Colorado) decoupled again from that in the southern area (western Utah to northwestern New Mexico). Shoreline deposits in Wyoming and the northwestern corner of Colorado show an overall retrogradational stacking pattern, whereas their counterparts from eastern Utah to northwestern New Mexico show a progradational stacking pattern (Fig. 13D).

4.4.5. Late Campanian: top of Exiteloceras jenneyi zone (~74.6 Ma)

The shoreline in Wyoming and northern Colorado largely shifted landward, whereas its southern counterpart had migrated seaward from the *Baculites scotti* time to the *Exiteloceras jenneyi* time (76.3–74.6 Ma). At the *Exiteloceras jenneyi* time, marine mudstones deposited in the study area include the Bearpaw Shale in northeastern Wyoming and the Pierre Shale in eastern Wyoming, most of Colorado, and northeastern New Mexico. Preserved coeval shoreline deposits include the Rollins Sandstone in the Picenace Basin and Pictured Cliffs Sandstone in northeastern San Juan Basin (Fig. 14A). Coeval nonmarine deposits were preserved only in Utah and New Mexico, including alluvial-plain and coastal-plain deposits of the Bluecastle Tongue of the Castlegate Sandstone, the Kaiparowits Formation, the uppermost Neslen Formation, and the Fruitland Formation (Fig. 14A).

Paleoflow directions from the Rollins Sandstone show a dominant southeast direction, approximately perpendicular to the local shoreline orientation (Kiteley, 1983). The Bluecastle Tongue shows a dominant northeast paleoflow direction (Lawton and Bradford, 2011; Bartschi et al., 2018). The dominant paleoflow direction in southern Utah (from the Kaiparowits Formation) remained generally eastward (Roberts, 2007). The lacuna in Wyoming expanded in extent to occupy the western three-quarters of Wyoming (Fig. 14A). The absence of preserved shoreline deposits does not allow the determination of shoreline migration trend in Wyoming. Shoreline deposits from western Colorado to northwestern New Mexico show a progradational stacking pattern. The Uinta Uplift is considered to initiate at ca. 75 Ma, consistent with the up-section decrease in contribution from a northern source and increase in contribution from a southern source in the Bluecastle Tongue and the Neslen Formation (Leary et al., 2015; Bartschi et al., 2018).

4.4.6. Late Campanian: top of Baculites compressus zone (~73. 9 Ma)

The western shoreline migrated further seaward/eastward from the *Exiteloceras jenneyi* time to *Baculites compressus* time (74.6–73.9 Ma). At the *Baculites compressus* time, marine mudstones in the study area include the Bearpaw Shale in northmost Wyoming, the Pierre Shale in eastern Colorado and northeastern New Mexico (Fig. 14B). Coeval shoreline deposits were probably present but were not preserved in the stratigraphic record. Nonmarine environments continued to expand eastward as the WIS withdrew, resulting in alluvial-plain and coastal-plain deposits of the Price River, Kaiparowits, and Farrer formations in Utah, the Williams Fork Formation in northwestern Colorado, and the Kirtland Shale in the San Juan Basin (Fig. 14B).

The Price River Formation and the laterally equivalent Farrer Formation show a northeast flow direction in fluvial channels (Fouch et al., 1983; Aschoff, 2010), consistent with the distinctly increased proportion of axially transported sediments from a southern source in these two formations (Bartschi et al., 2018). The Kaiparowits Formation in southern Utah received sediment detritus either from the southwestern Cordilleran magmatic arc or from the thrust belt to the west (Jinnah et al., 2009; Larsen et al., 2010). At this time, rivers recorded by the middle and upper units of the Kaiparowits Formation were considered to be connected northward to the fluvial system that deposited the Farrer Formation based on detrital zircon and petrographic provenance analysis (Fig. 14B) (Goldstrand, 1992; Lawton and Bradford, 2011; Dickinson et al., 2012). Paleocurrent data from the Kirtland Formation are directed to northeast to east (Pecha et al., 2018).

At the *Baculites compressus* time, the lacuna in the northern map area further expanded to occupy almost the entire Wyoming. The shoreline migration trend in Wyoming at this time thus cannot be unequivocally determined. Coastal-plain deposits in northern Colorado show a progradational stacking pattern, so do those in the San Juan Basin (Fig. 14B).

4.4.7. Late Campanian: top of Baculites reesidei zone (~73.3 Ma)

The shoreline in the northern and southern study area migrated landward and seaward, respectively, from the *Baculites compressus* to *Baculites reesidei* time (73.9–73.3 Ma). At the *Baculites reesidei* time, marine mudstones deposited in the study area include the Bearpaw Shale and Lewis Shale in northeastern Wyoming and the Pierre Shale in southeastern Wyoming, eastern Colorado, and northeastern New Mexico (Fig. 14C). Preserved coeval shoreline deposits include only the Twentymile Sandstone of the Williams Fork Formation in northwestern Colorado. Coeval alluvial-plain and coastal-plain deposits include the Meeteetse and Almond formations in Wyoming, the Price River and Tuscher formations in Utah, the Williams Fork Formation in northwestern Colorado, and the Kirtland Shale in the San Juan Basin (Fig. 14C). In front of the Absaroka thrust, alluvial-fan deposits of the Hams Fork Conglomerate were deposited (Fig. 14C). In northeastern Utah, the Tuscher Formation records a dominant northeast flow direction.

At the *Baculites reesidei* time, the Price River Formation and the laterally equivalent Tuscher Formation show a northeast flow direction in fluvial channels. The Tuscher Formation likely received sediments derived from erosion of foreland basin strata from nascent Laramide uplifts (e.g., San Rafael Swell, Circle Cliffs Uplift, or East Kaibab Monocline) (Roberts, 2007; Lawton and Bradford, 2011). The angular unconformity between the Kaiparowits and Canaan Peak formations in the Kaiparowits Plateau region serves as another piece of evidence indicative of the initiation of Laramide uplifts in southern Utah (Fig. 14C) (Roberts, 2007).

The extensive lacuna in Wyoming disappeared at the *Baculites reesidei* time. Meanwhile, a local lacuna was located at the Kaiparowits Plateau region in southern Utah (Fig. 14C). The shoreline migration trend in the northern and southern study area was decoupled again. Shoreline deposits in Wyoming show an overall retrogradational stacking pattern, whereas shoreline deposits from western Colorado to northeastern New Mexico show a progradational stacking pattern (Fig. 14C).

4.4.8. Latest Campanian: top of Baculites eliasi zone (~72.1 Ma)

From the *Baculites reesidei* to *Baculites eliasi* time (73.3–72.1 Ma), the shoreline in southern Wyoming had distinctly shifted landward by ~130 km, whereas its counterpart from Colorado to New Mexico migrated further seaward by ~90 km (Fig. 14C and Fig. 14D). At the *Baculites eliasi* time, marine mudstones deposited in the study area include the Bearpaw Shale and Lewis Shale in northeastern Wyoming, the Pierre Shale in the Denver Basin. Preserved coeval shoreline deposits include the Fox Hills Sandstone in central Wyoming and the Trinidad Sandstone in the Raton Basin. Coeval nonmarine deposits were distributed in western Wyoming and northwestern Colorado, including the Meeteetse, Almond, and Williams Fork formations. Alluvial-fan deposits include the Hams Fork Conglomerate in southwestern Wyoming and the

North Horn Formation in north-central Utah (Fig. 14D).

Several lacunas were located at central-eastern Utah, southern Utah, and the San Juan Basin at the *Baculites eliasi* time (Fig. 14D). The uplift of the San Rafael Swell caused erosion of as much as 400 m of Cretaceous rock and produced the lacuna in central and eastern Utah (Fouch et al., 1983). The lacunas present in southern Utah and the San Juan Basin can also be attributed to adjacent Laramide uplifts (Pecha et al., 2018). The shoreline migration trend remained decoupled along the western shoreline. Shoreline deposits in central Wyoming and the Raton Basin show a progradational stacking pattern, whereas those in southern Wyoming show a retrogradational stacking pattern (Fig. 14D).

4.4.9. Shoreline migration trend and sediment dispersal pattern during Campanian time

The third-order shoreline migration trend varied laterally along the western margin of the WIS during most of the Campanian. Although the western shoreline overall migrated seaward (eastward from western Wyoming to southern Utah and northeastward in northwestern New Mexico) from the *Scaphites leei III* time to the *Scaphites hippocrepis III* time (82.7–81.3 Ma), the shoreline in the northern study area had prograded over a distinctly longer distance from western to central Wyoming (~ 150 km) than its southern counterpart (Fig. 12A and Fig. 12B). Starting at the *Scaphites hippocrepis III* time, the shoreline in Wyoming started to shift landward (westward), whereas the shoreline in eastern Utah to northwestern New Mexico continued to migrate seaward (eastward and northeastward) (Fig. 12B).

The landward shoreline migration first reversed in central Wyoming at the *Baculites* sp. *(smooth)* time (81.1 Ma), then in northern Wyoming at the *Baculites* sp. *(weak flank ribs)* time (81.0 Ma). From the *Baculites* sp. *(weak flank ribs)* time to the *Baculites perplexus* time (81.0–78.3 Ma), the western shoreline had undergone a clockwise rotation because the shoreline from Wyoming to eastern Utah had shifted seaward (eastward), whereas the shoreline in northwestern New Mexico migrated landward (southwestward) (Fig. 12D to Fig. 13C). Although the entire western shoreline in the study area started to migrate seaward at the *Baculites perplexus* time, the clockwise rotation of shoreline continued till the *Baculites scotti* time (76.3 Ma) because the shoreline protrusion in central-southern Wyoming migrated ~100 km in a southeast direction, whereas southern counterpart of the shoreline had only prograded <20 km during this time (Fig. 13C and Fig. 13D).

From the *Exiteloceras jenneyi* time to the *Baculites compressus* time (74.6–73.9 Ma), the exact location of shoreline in Wyoming cannot be determined because the extensive lacuna occupied much of Wyoming (Fig. 14A and Fig. 14B). During the same time, the shoreline in the southern study area continued to migrate seaward (eastward to northeastward). Starting at the *Baculites reesidei* time (73.3 Ma), the shoreline trend started to rotate counterclockwise, when the shoreline in Wyoming started to migrate landward (westward), whereas its southern counterpart continued to migrate seaward (eastward and northeastward) (Fig. 14C). The landward migration trend of shoreline in northern Wyoming reversed at the *Baculites eliasi* time (72.1 Ma), while in southern Wyoming the landward shoreline migration persisted (Fig. 14D).

Detrital zircon provenance data indicate Campanian strata in the CFB received sediments from a complex mixture of sources such as the Sevier fold-thrust belt, the Cordilleran magmatic arc, the Mogollon Highlands to the south, recycled Sevier foreland basin strata, and Precambrian basement uplifts (Lawton et al., 2003; DeCelles, 2004; Dickinson and Gehrels, 2008; Laskowski et al., 2013; Leary et al., 2015; Lynds and Xie, 2019). Fluvial deposits in the study area, particularly in southern and central Utah, record interactions of transverse (east-directed) and axial (northeast-directed) river systems (Lawton et al., 2003; Roberts, 2007; Dickinson et al., 2012; Lawton et al., 2014; Bartschi et al., 2018). During the early Campanian, the dominant paleoflow direction in both eastern Utah and southern Utah was directed to the east (Fig. 12B), consistent with a dominant thrust-belt source in the fluvial strata of the Blackhawk Formation and the Drip Tank Member (Lawton et al., 2014; Bartschi et al., 2018).

By the earliest middle Campanian (~ 80 Ma), the Wahweap Formation (lower unit) received mixed thrust belt detritus and an increasing amount of Mogollon Highlands detritus, indicating the presence of an axial drainage system based on both detrital zircon populations and the dominant north-northeast-directed paleoflow direction in southern Utah (Fig. 13B) (Lawton et al., 2014). At the latest middle Campanian (~ 76 Ma), the dominant paleoflow direction of the Wahweap Formation (the capping sandstone) in southern Utah shifted to eastward again (Fig. 13D), indicating the dominant influence of a transverse river system (Lawton et al., 2003). The dominantly east to southeast flow direction in the Castlegate Sandstone and the eastward flow direction in the Ericson Sandstone also indicate the dominant influence of transverse river systems in central and eastern Utah and southern Wyoming (Fig. 13D) (Leary et al., 2015; Bartschi et al., 2018).

By the late Campanian (~ 75 Ma), an axial drainage system was established, connecting the Kaiparowits Plateau to northeastern Utah (Fig. 14A). The Bluecastle Tongue contains detrital zircon grains dominated by a thrust-belt source with minor contribution from a southern source, the proportion of which increases up-section, indicating increasing sediment supply from the axial river system (Lawton and Bradford, 2011; Bartschi et al., 2018). The disappearance of northern-sourced sediments at ca. 75 Ma is consistent with the onset of uplift along the southern Uinta Uplift at this time (Leary et al., 2015; Bartschi et al., 2018). At the *Baculites compressus* time (73.9 Ma), the axial river system was considered to supply sediments to the Farrer and Williams Fork formations (Fig. 14B) (Roberts, 2007; Lawton and Bradford, 2011), whereas the Price River Formation, deposited in more proximal areas, records a high thrust-belt contribution (Bartschi et al., 2018). The shift in paleocurrent data from northeast-directed to east-directed in the Kirtland Formation indicates the bordering Hogback monocline was active during Kirtland deposition (Fig. 14B) (Pecha et al., 2018). At *Baculites reesidei* time (73.3 Ma), detrital zircon and petrographic provenance analyses indicate Laramide-style uplifts in central and southern Utah had become sources of recycled foreland sediments (Fig. 14C) (Lawton and Bradford, 2011). Detrital zircon ages of the Upper Campanian strata from the Greater Green River and Hanna basins in Wyoming also indicate an influx of sediment derived from Precambrian basement exposed by some Laramide uplifts (e.g., Uinta and Sierra Madre Mountains), recycling from multiple preexisting sedimentary rocks, and additional contributions from local sources (Lynds and Xie, 2019).

4.5. Maastrichtian (72.1 Ma - 66 Ma)

Both Cordilleran thrusting and Laramide uplifts continued locally through the Maastrichtian. In the Idaho-Wyoming-Utah salient, the Absaroka thrust remained quiescent through the early Maastrichtian and reactivated before Paleocene (Liu et al., 2005). In the Charleston-Nebo salient, internal back-thrusting and frontal triangle zone developed (DeCelles, 2004). In central and southern Utah, slip on the Gunnison and Iron Springs thrusts continued (DeCelles, 2004; Horton et al., 2004). Maastrichtian (to early Eocene) marked the climax of Laramide intraforeland uplift (Dickinson et al., 1988; DeCelles, 2004; Fan and Carrapa, 2014). These Laramide basement-cored uplifts reorganized the sediment dispersal systems and became important local sediments sources (Lawton, 2008; Heller et al., 2013; Bush et al., 2016; Lynds and Xie, 2019).

Global sea level reconstructed by Haq (2014) shows a gradual fall during the Maastrichtian, whereas studies of New Jersey margin suggest global sea level first rises during the early Maastrichtian and then falls during the late Maastrichtian (Fig. 7) (Miller et al., 2005; Kominz et al., 2008). Within the CFB, Maastrichtian strata record continued first-order regression of the WIS, interrupted by a second-order marine transgression in the earliest late Maastrichtian (Fig. 7) (Kauffman, 1977). The

WIS withdrew from the CFB by late Maastrichtian time. Due to much reduced extent of the WIS and limited distribution of ammonite faunas, only one paleogeographic map was reconstructed at the top of the *Baculites clinolobatus* zone (latest early Maastrichtian).

4.5.1. Latest Early Maastrichtian: top of Baculites clinolobatus zone (~69.9 Ma)

From the *Baculites eliasi* to *Baculites clinolobatus* time (72.1–69.9 Ma), the shoreline in northern Wyoming and southern Colorado had shifted seaward, whereas the shoreline across the Wyoming-Colorado boundary migrated landward (Fig. 14D and Fig. 15). At the *Baculites clinolobatus* time, marine mudstones of the Pierre Shale were deposited in southeastern Wyoming and northeastern Colorado. Preserved coeval shoreline deposits include the Fox Hills Sandstone across Wyoming and at northwestern Colorado. Record of nonmarine deposits are located in western Wyoming, northeastern and southern Utah, northwestern Colorado, and the Raton Basin (Fig. 15). Alluvial-fan deposits of this age include the Hams Fork Conglomerate in western Wyoming, the North Horn Formation in northeastern Utah, and the Canaan Peak Formation in southern Utah.

Paleocurrent data from the North Horn Formation exposed along the southwest flank of the Uinta Basin show a dominant eastward direction (Dickinson et al., 2012). In southern Utah, the Canaan Peak Formation was deposited in an east- to northeast-directed braided fluvial system (Goldstrand, 1990; Schmitt et al., 1991; Goldstrand, 1992). At the *Baculites clinolobatus* time, the two lacunas at central-eastern Utah and the San Juan Basin persisted (Fig. 15). Shoreline deposits of the Fox Hills Sandstone along the western shoreline consistently show a progradational stacking pattern.

4.5.2. Shoreline migration trend and sediment dispersal pattern during Maastrichtian time

From the *Baculites eliasi* to *Baculites clinolobatus* time (72.1–69.9 Ma), the shoreline in the northern and southern study area (Wyoming vs. Colorado and New Mexico) had rotated clockwise and counterclockwise, respectively (Fig. 14D and Fig. 15). This is because the shoreline around the Wyoming-Colorado boundary had distinctly shifted landward by ~90 km, whereas the shoreline in the northernmost and southernmost study area had distinctly migrated seaward by over 100 km. This >200 km westward retreat of shoreline in southern Wyoming from the *Baculites reesidei* time to *Baculites clinolobatus* time (73.3–69.9 Ma) is considered the last major marine transgression of the WIS (Fig. 14C to Fig. 15) (Merletti et al., 2018; Minor et al., 2021).

With the continued Laramide regional crustal shortening, sediment dispersal patterns in the CFB were largely influenced by local Laramide uplifts (Heller et al., 2013). Maastrichtian strata of the CFB also received sediments from a complex mixture of sources (Dickinson et al., 2012; Laskowski et al., 2013). The dominant eastward flow direction in the North Horn Formation is compatible with the fact that the detrital zircons of the North Horn Formation are mostly derived from the Sevier thrust belt to the west (Dickinson et al., 2012). The Canaan Peak Formation in southern Utah received sediment detritus derived from erosion of highlands to the west (e.g., southeastern Nevada, southeastern California, and southwestern Utah). The change in the dominant paleocurrent direction from east to northeast indicates deposition of the Canaan Peak Formation was influenced by the adjacent Circle Cliff uplift (Fig. 15) (Goldstrand, 1992). Detrital zircon data indicate the Vermejo Formation in the Raton basin and the Lance Formation in Wyoming received additional sediment inputs directly from local basement exposures (Bush et al., 2016; Lynds and Xie, 2019).

5. Discussion

5.1. Lateral variability in tectonic activities and sediment supply

The complex lateral variability in the shoreline migration history revealed by the reconstructed paleogeographic maps suggests the effects of tectonics, eustasy, and climate significantly varied along the western margin of WIS (along depositional strike) through the Late Cretaceous. Here we discuss the relative roles of tectonics, eustasy, and sediment supply on the third-order stratigraphic stacking pattern (shoreline migration trend) based on the compiled stratigraphic data. This study focused on shorelines, and their third-order stratigraphic stacking pattern and lateral variability because third-order eustatic changes during the Late Cretaceous have been independently reconstructed and are fairly well-constrained, and shorelines are sensitive to developing topography (Fig. 7). In turn, this allows the relative roles of tectonics and sediment supply to be inferred based on the stratigraphic stacking pattern at the shoreline and the A/S concept (Fig. 8).

Additionally, the lateral variability in the migration trend of the western shoreline will be discussed during four time intervals of the Late Cretaceous—Cenomanian to late Turonian (100.5 Ma – 90.2 Ma), late Turonian to middle Campanian (90.2 Ma – 80.2 Ma), middle to late Campanian (80.2 Ma – 74.6 Ma), and late Campanian to Maastrichtian (74.6 Ma – 66 Ma). These intervals are the same as those studied in Li and Aschoff (2022), in which high-resolution isopach maps of each time interval was developed. The integration of stratigraphic stacking pattern (shoreline migration trend) with the distribution of depocenters allows for a better discrimination of the roles of tectonics and eustasy (and potentially sediment supply) in the study area throughout the Late Cretaceous.

5.1.1. Cenomanian to late Turonian (100.5 Ma – 90.2 Ma)

The shoreline history revealed by the three reconstructed paleogeographic maps during the Cenomanian generally conforms to the long-term Greenhorn transgressive cycle (Fig. 9A to Fig. 9C). Once seaway from the north (Boreal Sea) and the south (Tethys Sea) connected by the *Conlinoceras tarrantense* time (96.1 Ma), the western shoreline of the WIS developed a north-south orientation (Fig. 9B). From the *Conlinoceras tarrantense* time to *Plesiacanthoceras wyomingsense* time (96.1–95.5 Ma), the western shoreline had overall shifted westward. The Dakota shoreline in the southern study area migrated landward over a notably longer distance (~ 200 km) compared to the Frontier shoreline in Wyoming (Fig. 9B and Fig. 9C).

Multiple eustatic reconstructions agree that the global sea level had slightly fallen (< 30 m) from the *Conlinoceras tarrantense* time to *Plesiacanthoceras wyomingsense* time (Fig. 7). Therefore, the ~200 km landward shift of the Dakota shoreline during this time suggests tectonic subsidence in the southern map area significantly outpaced sea-level fall ($A/S \gg 1$). During the same time, the Frontier shoreline in western Wyoming had remained largely static or slightly migrated landward (~ 50 km), indicating accommodation creation by tectonic subsidence in western Wyoming is comparable to or slightly outpaced sea-level fall but sediment supply rate could somewhat keep up with the accommodation creation ($A/S \geq 1$). The distinctly large A/S ratio in the southern study area (southern Utah) is also reflected by the retrogradational stacking pattern of the Dakota Sandstone in the Colorado Plateau region at the *Conlinoceras tarrantense* time when global sea level was falling (Fig. 9B). The much larger A/S ratio in the southern study area can be attributed to the combined effects of rapid tectonic subsidence in the southern area and limited sediment supply to the Dakota shoreline. The forebulge located across eastern Utah at this time (indicated by the lacuna located at northeastern Utah and the predominantly northeast paleoflow direction in the Henry Mountains region) likely prevented the transverse river system to deliver sediments from the fold-thrust belt directly to the Four Corners region (Fig. 9B and Fig. 9C).

From the *Plesiacanthoceras wyomingsense* time to *Pseudaspidoceras flexuosum* time (95.5–93.5 Ma), multiple sources disagree on whether global sea level had risen or fallen (Fig. 7). Nevertheless, regardless of global sea-level changes, the significantly longer-distance landward shift of shoreline in central to southern Utah compared to in western Wyoming (500 km vs. < 50 km; Fig. 9C and 12), again, indicates the

amount of accommodation generated by tectonic subsidence in southern Utah is distinctly larger than that in the northern study area. Considering the proximity to the Sevier thrust sheet, the accommodation in southern Utah is attributed to flexural subsidence caused by loading of the Sevier thrust sheet (e.g., the Pavant thrust/duplex and the Blue Mountain thrust; Fig. 9D). The low accommodation (caused by low tectonic subsidence or uplift) in Wyoming is also hinted by the extensive lacuna across most of Wyoming, the northeastern corner of Utah, and northwestern corner of Colorado during the *Pseudaspidoceras flexuosum* zone (Fig. 9D).

From the *Pseudaspidoceras flexuosum* time to the *Collignoniceras woollgari* time (93.5–92.1 Ma), the western shoreline had undergone a slight counterclockwise rotation (Fig. 9D to Fig. 10A). The seaward shift of shoreline in southern Utah can be attributed to global sea level fall during this time ($A < 0$ or $0 < A/S < 1$), while the landward shoreline migration in western Wyoming and central Utah suggests extra accommodation was still created by tectonic subsidence in these areas ($A/S > 1$). From the *Collignoniceras woollgari* time to the *Scaphites whitfieldi* time (92.1–90.2 Ma), the western shoreline had overall migrated seaward, but the Wyoming segment of the shoreline had prograded significantly longer distance compared to its southern counterpart (300 km vs. 150 km; Fig. 10A to Fig. 10C). This indicates larger amount of sediment supply to the shoreline in Wyoming, or smaller accommodation (even negative) generated in western Wyoming compared to in central Utah to northeastern New Mexico, or the combination of both. Considering the widespread unconformities in the Turonian strata in Wyoming (Fig. 4), low (or negative) accommodation is likely the main cause of the rapid seaward shoreline migration in Wyoming. Slow sediment supply rate can be ruled out as the dominant cause of the slower seaward shoreline progradation in the southern area because exhumation rates of the North American Cordillera was consistently rapid (~ 0.9–1 km/m.y.) throughout the Cretaceous (Painter et al., 2014). Nevertheless, lower amount of sediment supply may still have impeded the seaward shoreline migration in the southern study area to some degree, if the axial drainage system presented in southern Utah at this time was less efficient as a transverse drainage system in delivering sediments to the shoreline (Fig. 10C).

5.1.2. Late Turonian to middle Campanian (90.2 Ma – 80.2 Ma)

Following the Greenhorn regression, the rapid Niobrara transgression within the WIS by early Coniacian was also subject to dominant tectonic subsidence. From the *Scaphites whitfieldi* time to the *Scaphites preventricosus* time (90.2–88.8 Ma), multiple eustatic reconstructions agree that global sea level had fallen slightly (less than a few tens of meters). Therefore, the landward shift of the entire western shoreline during this time (Fig. 10C and Fig. 10D) indicates accommodation created by tectonic subsidence outpaced sea-level fall ($A/S > 1$). The longer-distance landward shoreline migration in western Wyoming compared to its southern counterpart (~ 300 km vs. < 50 km) indicates the amount of tectonic subsidence in western Wyoming was distinctly larger than that in Utah during the Niobrara transgression (Fig. 10C and Fig. 10D). The landward shoreline migration trend during the Niobrara transgression—longer-distance landward migration shoreline in Wyoming compared to the southern study area—is opposite to that during the Greenhorn transgression (longer-distance landward shoreline migration in the southern study area). Considering the proximity to the Sevier thrust sheet (in front of the Idaho-Wyoming-Utah salient) and the newly formed Wasatch Culmination during the early Coniacian (DeCelles, 2004), the dominant subsidence mechanism in western Wyoming during this time can be attributed to flexural subsidence (Fig. 10D).

The landward migration of the western shoreline from the *Scaphites preventricosus* time to the *Scaphites ventricosus* time (88.8–87.9 Ma) is consistent with the slight rise of global sea level (Fig. 10D and Fig. 11A). Starting from the *Scaphites ventricosus* time, deposits along most of the western shoreline, except for in central to southern Utah, began to show a progradational stacking pattern by the *Scaphites depressus* time (Fig. 11A and Fig. 11B; 87.9–86.3 Ma). However, various sources agree that global sea level had risen during this time (Fig. 7), which indicates, other than in central and southern Utah, flexural subsidence caused by loading of the Sevier thrust sheet had subdued, and sediment supply becomes the dominant controlling factor leading to the seaward shoreline migration ($0 < A/S < 1$; foredeep uplift is unlikely because no extensive unconformity occurred) from the *Scaphites ventricosus* time to the *Scaphites depressus* time. The landward shoreline shift in central and southern Utah indicates sediment supply rate in central Utah cannot keep pace with the accommodation created by the combined global sea-level rise and flexural subsidence due to loading of the Nebo/Paxton and Blue Mountain thrusts ($A/S > 1$). If sediment supply was not varying significantly along-strike, the local landward shoreline shift in central and southern Utah indicates flexural subsidence in this area was distinctly more rapid compared to other places in front of the Sevier fold-thrust belt during the late Coniacian.

The entire western shoreline in the study area migrated seaward from the *Scaphites depressus* time to *Clioscaphites vermiformis* time (86.3–85.2 Ma; Fig. 11B and Fig. 11C). However, due to uncertain global sea-level history (Fig. 7), the roles of tectonics and sediment supply cannot be unequivocally determined. From the *Clioscaphites vermiformis* time to *Desmoscaphites bassleri* time (85.2–83.6 Ma), the shoreline in western Wyoming, southern Utah, and northwestern New Mexico migrated seaward, whereas the shoreline in central Utah had shifted landward (Fig. 11C and Fig. 11D). Because most eustatic reconstructions suggest that global sea level had risen during this time (Fig. 7), the seaward shoreline migration in western Wyoming and northwestern New Mexico (Fig. 11C to Fig. 11D) indicates sediment supply outpaced the accommodation creation under the combined influence of global sea-level rise and tectonic subsidence ($0 < A/S < 1$; tectonic uplift is unlikely based on the absence of hiatus in western Wyoming). The concurrent landward shoreline migration in central Utah indicates sediment supply cannot keep pace with the accommodation creation in this area ($A/S > 1$), which, again, indicates significant amount of flexural subsidence caused by loading of the Nebo/Paxton thrusts because limited sediment supply in central Utah is unlikely due to the proximity to the Sevier fold-thrust belt.

From the *Desmoscaphites bassleri* time to the *Scaphites hippocrepis III* time (83.6–81.3 Ma), the entire western shoreline migrated seaward (eastward from western Wyoming to central Utah and northeastward from southern Utah to northwestern New Mexico) (Fig. 11D to Fig. 12B). All three available eustatic reconstructions agree that global sea level had risen during this time (Fig. 7). The seaward/eastward migration distance of the shoreline in western Wyoming was distinctly larger than that in the southern map area (> 150 km vs. < 100 km), indicating a distinctly smaller A/S ratio in western Wyoming compared to the southern area.

From the *Scaphites hippocrepis III* time to *Baculites maclearni* time (81.3–80.2 Ma), all three available eustatic reconstructions reveal a progressively falling global sea level (Fig. 7). From the *Scaphites hippocrepis III* time to *Baculites* sp. *(smooth)* time (81.3–81.1 Ma), the shoreline in northern and central Wyoming migrated landward, whereas its southern counterpart continued to migrate seaward (Fig. 12B and Fig. 12C). The landward migration of northern shoreline in the study area indicates a pulse of accommodation generated by the loading of the Absaroka thrust in western Wyoming ($A/S > 1$). The landward shoreline migration persisted in central Wyoming through the *Scaphites hippocrepis III* zone and persisted in northern Wyoming through the *Baculites* sp. *(smooth)* zone (Fig. 12B and Fig. 12C), indicating the accommodation generation rate had decreased first in central Wyoming and then in northern Wyoming. At the *Baculites* sp. *(weak flank ribs)* time (81.0 Ma), the entire western shoreline was uniformly shifting seaward (Fig. 12D), indicating either tectonic subsidence is smaller than sea-level fall in magnitude ($A < 0$) or $0 < A/S < 1$. By the *Baculites obtusus* time (80.7 Ma), the eastward migration of shoreline persisted in Wyoming and

central Utah, but the shoreline in the San Juan Basin started to shift landward (Fig. 13A). The decoupled shoreline migration trend continued till at least the *Baculites maclearni* time (80.2 Ma; Fig. 13B). During the *Baculites obtusus* time to the *Baculites maclearni* time, the landward migration trend of shoreline in the San Juan Basin indicates tectonic subsidence at the shoreline outpaced the sea-level fall and A/S > 1 because global sea level was falling during based on the majority of existing eustatic reconstructions this time (Fig. 7).

5.1.3. Middle Campanian to late Campanian (80.2 Ma – 74.6 Ma)

From the *Baculites maclearni* time to the *Baculites perplexus* time (80.2–78.3 Ma), two out of three eustatic reconstructions suggest global sea level had risen, whereas Haq (2014) suggests global sea level had fallen (Fig. 7). During this time, the shoreline in Wyoming and northwestern Colorado migrated seaward/eastward, whereas its southern counterpart (northwestern New Mexico) had shifted landward/southwestward (Fig. 13B and Fig. 13C). From the *Baculites perplexus* time to the *Baculites scotti* time (78.3–76.3 Ma), the entire western shoreline migrated seaward (Fig. 13C to Fig. 13D); whether this was driven dominantly by tectonics, eustasy, or sediment supply is difficult to resolve because of the uncertain global sea-level history.

Generally, the western shoreline in the study area underwent a clockwise rotation from the *Baculites* sp. *(weak flank ribs)* time to the *Baculites scotti* time (81.0–76.3 Ma), indicating the A/S ratio is distinctly smaller in the northern study area, regardless of sea-level change (Fig. 12D to Fig. 13D). Meanwhile, the shoreline protrusion migrated in a southeast direction from central Wyoming to the Wyoming-Colorado boundary (Fig. 13B to Fig. 13D). This southeastward migration of the shoreline protrusion may be caused by the southward deflection of large sediment supply from the eastward sediment dispersal system by strong longshore currents in the WIS or the establishment of a southeast-directed sediment dispersal pathway from western Wyoming to northern Colorado (Fig. 13D). The clockwise rotation of shoreline in the study area played a crucial role in producing the pronounced embayed morphology of the Utah Bight, within which tidal range was amplified due to tidal resonance, as reflected by the deposition of tide-dominated deltas represented by the Sego Sandstone (Fig. 13D) (Van Cappelle et al., 2018).

Starting from the *Baculites scotti* time, the shoreline in the southern map area had continued to migrate seaward/northeastward, whereas the lacuna in the northern study area expanded to occupy the western three-quarters of Wyoming by the *Exiteloceras jenneyi* time (Fig. 13D and Fig. 14A). The extensive lacuna can be attributed to foredeep isostatic rebound (i.e., uplift) during the quiescent period of the Absaroka thrust and uplifts of the Moxa Arch and Rock Springs uplift (Fig. 14A) (Liu et al., 2005). The seaward migration of shoreline in the southern map area indicates $0 < A/S < 1$ in these areas ($A < 0$ is unlikely based on the absence of hiatus in the southern study area).

5.1.4. Middle Campanian to Maastrichtian (74.6 Ma – 66 Ma)

From the *Exiteloceras jenneyi* time to the *Baculites compressus* time (74.6–73.9 Ma), global sea level remained overall static or had fallen slightly (Fig. 7). The further expansion of the lacuna in Wyoming can be attributed to the continued foredeep uplift or incipient uplifts of Laramide-style structures (Fig. 14B) (Devlin et al., 1993; Liu et al., 2005; Leary et al., 2015; Rudolph et al., 2015). By the *Baculites reesidei* time (73.3 Ma), the shoreline in the southern study area continued to move seaward (eastward and northeastward), but its northern counterpart began to migrate landward/westward (Fig. 14C). From the *Baculites reesidei* time to the *Baculites eliasi* time (73.3–72.1 Ma), global sea level likely had fallen (Fig. 7). Therefore, the landward shift in the shoreline in the northern map area (across Wyoming) during this time indicates accommodation creation outpaced the sea-level fall ($A/S > 1$). The increased accommodation in Wyoming can be caused by renewed loading of the Wasatch Culmination (Yonkee and Weil, 2015), and the preservation of the Hams Fork Conglomerate also indicates increased accommodation in proximal areas due to flexural subsidence (Fig. 14C and Fig. 14D).

Global sea level had distinctly risen from the *Baculites eliasi* time to *Baculites clinolobatus* time (72.1–69.9 Ma). The seaward migration of shoreline in northern Wyoming (eastward) and southern Colorado (northeastward) indicates $A/S < 1$ in these areas (Fig. 14D to Fig. 15). Meanwhile, the continued landward shift of shoreline in southern Wyoming indicates $A/S > 1$. The much-increased A/S ratio in southern Wyoming is not likely caused by limited sediment supply considering the proximity to the Absaroka thrust, especially lateral equivalent shoreline farther away from the thrust sheet (northern Wyoming and southern Colorado) was able to prograde despite the rising sea level (Fig. 15). Instead, the large A/S ratio in southern Wyoming is interpreted to reflect rapid accommodation creation by tectonic subsidence during this time.

5.2. Flexural subsidence versus dynamic topography in the CFB

The paleogeographic evolution and shoreline history in the study area through the Late Cretaceous provide important insights into the timing and locations of tectonic subsidence/uplift and therefore can help resolve different subsidence mechanisms in the CFB (i.e., flexural subsidence vs. dynamic topography). In this section, high-resolution isopach patterns through the Late Cretaceous recently reconstructed by Li and Aschoff (2022) are incorporated to aid in resolving the relationship between tectonics and sedimentation (Fig. 16). Integrating with the spatial variability in the tectonic topography (i.e., subsidence and uplift) and sediment dispersal patterns revealed by the paleogeographic maps, different tectonic subsidence mechanisms and their effects within the CFB through the Late Cretaceous can be better constrained.

5.2.1. Cenomanian to late Turonian (100.5 Ma – 90.2 Ma): dominant flexural subsidence

The lateral variability in the shoreline migration trend indicates a smaller A/S ratio in the northern map area (sediment supply dominated) than in the southern map area (tectonic subsidence dominated) during the Cenomanian to late Turonian, consistent with the isopach pattern (Fig. 16A). The Cenomanian to late Turonian isopach map reveals a distinct foredeep in west-central Utah in front of the Pavant thrust, a well-developed forebulge around the Utah-Colorado boundary, and a backbulge in southeastern Colorado and northeastern New Mexico (Fig. 16A), conforming to the subsidence profile generated dominantly by flexural loading of the Sevier thrust belt, especially in the southern study area (DeCelles, 2004; Li and Aschoff, 2022). The significant amount of flexural subsidence in central to southern Utah, rather than eustatic rise, played a critical role in producing the large-scale Greenhorn transgression in these areas during the Cenomanian to early Turonian (Fig. 9B to Fig. 9D).

However, the well-developed flexural subsidence profile is absent in Wyoming during the Cenomanian to late Turonian (Fig. 16A). The isopach pattern in Wyoming during this time serves as another piece of evidence supporting the dominant role of sediment supply over tectonic subsidence (probably flexural subsidence). The smaller A/S ratio, as well as the poorly developed flexural subsidence profile in Wyoming, may point to a more rigid lithosphere beneath Wyoming. If the loading of the Paris-Meade-Willard thrust system were comparable to that of the thrust system in Utah in scale, flexural subsidence of the more rigid Wyoming lithosphere would be smaller in magnitude but broader in space (Jordan, 1981; DeCelles, 2012; Painter and Carrapa, 2013; Tufano and Pietras, 2017). In this sense, sediments derived from the Sevier fold-thrust belt would have quickly filled the foredeep in front of the Idaho-Wyoming-Utah salient (in western Wyoming), allowing the Frontier delta to prograde long-distance away from the thrust sheet, across the forebulge and into the backbulge depozone (Fig. 10C and Fig. 16A). The much smaller amount of flexural subsidence in Wyoming probably is also consistent with the widespread unconformity in the Turonian strata of Wyoming

(Fig. 9D to Fig. 10C). The extensive lacuna in Wyoming during the Turonian can also be attributed to the forebulge and local intrabasinal uplifts (Fig. 9D and Fig. 10C) (Merewether and Cobban, 1986; Ryer and Lovekin, 1986), which would have further decreased the accommodation in western Wyoming.

5.2.2. Late Turonian to middle Campanian (90.2 Ma – 80.2 Ma): dominant flexural subsidence and early influence of dynamic subsidence

The locations of tectonic subsidence inferred from the shoreline history during the late Turonian to middle Campanian is well consistent with the depocenter locations revealed in the isopach map of this time interval (Fig. 16B). The isopach pattern indicates flexural subsidence in response to loading of the Sevier fold-thrust belt continued to be the dominant mechanism controlling the distribution of sediment accumulation during this time (Fig. 16B). The southwestern corner of Wyoming (around the current Moxa Arch), characterized by a relatively low stratal thickness than the surrounding area, likely represents the forebulge (Luo and Nummedal, 2012). Flexural subsidence in the foredeep west of the Moxa Arch (in front of the Crawford thrust) probably was responsible for the distinct landward shoreline migration in western Wyoming during the Niobrara transgression (during late Turonian to early Coniacian; Fig. 10C to Fig. 10D). The isopach map also reveals a distinct foredeep in front of the Nebo thrust in northcentral Utah (Fig. 16B). Rapid subsidence in northcentral Utah is reflected by the landward shoreline migration in central Utah during the middle Coniacian and middle Santonian, while the shoreline migration trend in this area decoupled from that in other shoreline segments (Fig. 11C).

It is also critical to point out, the depocenter in Wyoming, revealed by the isopach map (Fig. 16B) is much broader (spanning ~250 km from the Sevier thrust sheet) than that during the Cenomanian to the late Turonian. This broadening of the depocenter in southwestern Wyoming is also noted in DeCelles (2004) and Painter and Carrapa (2013) and can be attributed to changes in the lithospheric rigidity. The broad flexural subsidence depocenter serves as another piece of evidence supporting the greater rigidity of the loaded lithosphere beneath Wyoming (Painter and Carrapa, 2013).

The moderate accommodation at the Four Corners area is likely responsible for the landward shoreline migration at the San Juan basin from the *Baculites obtusus* time to the *Baculites maclearni* time (80.7–80.2; the earliest middle Campanian), when the local shoreline migration trend decoupled from that in the northern study area (Fig. 13A and Fig. 13B). The moderate accommodation at the Four Corners area is attributed to the long-wavelength dynamic subsidence in front of the conjugate Shatsky Rise rather than flexural subsidence, considering the Four Corners area is located >400 km from the thrust front in southwestern Utah (Fig. 16B) (Li and Aschoff, 2022). Another possible effect of dynamic topography associated with the landward shoreline migration at the San Juan basin during the earliest middle Campanian is the decrease in the sediment flux to the San Juan basin area. The dominant paleoflow direction in the Kaiparowits Plateau region had changed from east- to northeast-directed by the *Baculites maclearni* time, when the conjugate Shatsky Rise was located beneath northern Arizona (Fig. 13B). The shift from an east-directed to a northeast-directed paleoflow direction in southern Utah indicates northern Arizona (or south thereof) had become a topographic high (Fig. 13B), consistent with the predicted area of dynamic uplift above a buoyant oceanic plateau and the area of distinctly decreased stratal thickness in southern Utah and northern Arizona as indicated by the isopach map (Fig. 16B). The transition from a transverse to an axial sediment dispersal system could decrease the amount of sediment supply to the San Juan basin area, further increasing the A/S and leading to the landward shoreline migration in the Four Corners area during the earliest middle Campanian (Fig. 13B).

5.2.3. Middle Campanian to Late Campanian (80.2 Ma – 74.6 Ma): dominant dynamic topography

The isopach map of the middle to upper Campanian strata reveals a broad depocenter (~ 500 km × 500 km) centered in northcentral Colorado (Fig. 16C). Other than southern Utah (Kaiparowits Plateau region), areas in front of the Sevier thrust belt (western Wyoming, northeastern to central Utah) are characterized by overall low stratal thickness. Based on the predicted locations of the conjugate Shatsky rise and the large distance (~ 500 km) from the Sevier thrust front (Fig. 16C), the broad depocenter centered in northcentral Colorado is attributed to the long-wavelength dynamic subsidence in front of the conjugate Shatsky Rise (Painter and Carrapa, 2013; Li and Aschoff, 2022).

The increased subsidence, indicated by the moderate stratal thickness, in the northern Kaiparowits Plateau during the middle to late Campanian corresponds to the Kaibab uplift in timing, suggesting a possible causal relationship—flexural subsidence caused by loading of the Kaibab uplift (Heller and Liu, 2016). The overall low stratal thickness in western Wyoming can be attributed to foredeep uplift and the uplift of Moxa Arch, which resulted in erosion of several hundred meters of strata and a major unconformity at the base of the Trail Member of the Ericson Formation (Fig. 13D to Fig. 14B) (Liu et al., 2005; Rudolph et al., 2015). However, the low stratal thickness in central and eastern Utah cannot be explained by foredeep rebound because thrusts in central Utah were active during this time (Fig. 7). Instead, flexural subsidence generated by loading of the thrust sheets in central Utah was probably interfered with dynamic uplift above the relatively buoyant conjugate Shatsky Rise when it migrated across this area during 80 to 75 Ma (Fig. 16C).

Changes in local sediment dispersal systems also suggest increased effects of dynamic topography during this time. Results from paleotidal modeling indicates in order for stratigraphic units including the Sego Sandstone and Hygiene Sandstone to preserve pronounced tidal influence, the WIS need to have a deep center (~ 400 m) and southern entrance (> 100 m) (Dean et al., 2019). The location of the deep center of the WIS (central to northern Colorado, eastern Wyoming) (Dean et al., 2019) well corresponds to the broad depocenter produced by dynamic subsidence revealed by the isopach map (Fig. 16C). The increased dynamic subsidence (and deepening) at north-central Colorado could have increased the sediment transport gradient, leading to the southeastward migration of the shoreline protrusion from western Wyoming to northern Colorado during the middle Campanian (80.2–76.3 Ma; Fig. 13B to Fig. 13D). When the buoyant conjugate Shatsky rise migrated away from southern Utah by the *Baculites scotti* time (76.3 Ma), the paleoflow direction in southern Utah returned to an eastward direction—away from the Sevier fold-thrust belt (Fig. 13D). By ~75 Ma (*Exiteloceras jenneyi* time), the conjugate Shatsky rise was located approximately beneath the shoreline across western Colorado. The decrease in accommodation at the shoreline due to dynamic uplift above the still buoyant oceanic plateau likely promoted the seaward shoreline migration in western Colorado starting at the *Exiteloceras jenneyi* time (Fig. 14A).

5.2.4. Middle Campanian to Maastrichtian (74.6 Ma – 66 Ma): dominant dynamic topography and flexural subsidence produced by Laramide uplifts

The isopach pattern of the late Campanian to Maastrichtian strata shows a more complex depocenter distribution within the CFB (Fig. 16D). The isopach map reveals a broad composite depocenter consisting of at least four "sub-depocenters" (i.e., Wind River Basin, Powder River Basin, Washakie Basin, and western Denver Basin), whereas most other areas show overall low stratal thickness (Fig. 16D). The development of depocenters within the CFB during the late Campanian to Maastrichtian can be largely attributed to the flexural subsidence due to loading of adjacent Laramide-style uplifts because the elongation direction of these sub-depocenters generally follows the trend of adjacent Laramide-style uplifts (Fig. 16D). However, flexural loading of Laramide-style uplifts likely is not the sole cause of the

composite depocenter during the late Campanian to Maastrichtian, considering the rather local scale of these basement-involved uplifts and especially that the amount of accommodation of these sub-depocenters (e.g., the Washakie basin) can be even comparable to the foredeep accommodation generated by loading of the regional-scale Sevier thrust sheet (e.g., foredeep in northcentral Utah in Fig. 16B). In this sense, the broad depocenter extending from northcentral Colorado to eastern central Wyoming reflects some degrees of dynamic subsidence associated with the conjugate Shatsky Rise (Li and Aschoff, 2022). For instance, the significant landward shoreline shift in southern Wyoming from the *Baculites reesidei* time to *Baculites clinolobatus* time (73.3–69.9 Ma), decoupled from all other shoreline segments in the study area, suggests a localized high subsidence rate (Fig. 14C to Fig. 15). The abnormally thick stratal thickness in the eastern Washakie basin is likely the result of combined dynamic subsidence and flexural loading of the Rock Springs, Granite Mountains, Rawlins, and Sierra Madre uplifts (Carvajal and Steel, 2011; López and Steel, 2015; Merletti et al., 2018; Li and Aschoff, 2022; Minor et al., 2021).

The combined effects of dynamic subsidence and flexural subsidence caused by loading of local Laramide-style uplifts during the late Campanian to Maastrichtian may have controlled the retreat of the WIS. It is interesting to note, the shoreline at the *Baculites clinolobatus* time (69.9 Ma) seems to enclose the broad depocenter during the late Campanian to Maastrichtian (Fig. 15 and Fig. 16D). The additional accommodation created by flexural loading of local Laramide uplifts and dynamic subsidence directly in front of and above the conjugate Shatsky rise when the oceanic plateau started to lose its buoyancy since 75 Ma (Liu et al., 2010; Humphreys et al., 2015; Li and Aschoff, 2022), in some senses, delayed the retreat of the WIS (controlled where the WIS receded from).

5.3. Reconstructing eustatic changes from the stratigraphic record

Because the observed stratigraphic architecture is produced by the complex interaction of several interdependent controls, including tectonic movements (both local and regional scale), eustatic changes, and sediment flux, the magnitude, rate, and duration of each control are challenging to isolate. Taking the interpretation of eustatic changes as an example, strata of the CFB have long been considered a critical archive of Cretaceous global sea level. However, the complex lateral variability in the stratigraphic stacking pattern along the coeval shoreline through the Late Cretaceous revealed in this synthesis indicates extracting the global sea-level history from the stratigraphic record is anything but straightforward.

Considering the 22 paleographic maps from the Turonian to Maastrichtian, the stratigraphic stacking pattern along the western shoreline is consistent along strike in just seven maps. The times that show relatively consistent along-strike shoreline migration throughout the CFB are: the *Collignoniceras woollgari* (92.1 Ma; Fig. 10A), *Scaphites preventricosus* (88.8 Ma; Fig. 10D), *Desmoscaphites bassleri* (83.6 Ma, Fig. 11D), *Scaphites leei III* (82.7 Ma, Fig. 12A), *Baculites* sp. *(weak flank ribs)* (81.0 Ma, Fig. 12D), *Baculites perplexus* (78.3 Ma; Fig. 13C), *Baculites clinolobatus* (69.9 Ma; Fig. 15) times. The *Exiteloceras jenneyi* and *Baculites compressus* times could not be considered because strata of this age were missing in Wyoming. Even for these seven times with relatively consistent stratigraphic stacking pattern along strike, the stratigraphic stacking pattern at the *Collignoniceras woollgari*, and *Baculites* sp. *(weak flank ribs)* times is not completely synchronous along the shoreline (Fig. 10A and Fig. 12D); the stratigraphic stacking pattern at the *Scaphites leei III*, and *Baculites clinolobatus* times cannot be solely attributed to a dominant eustatic control (Fig. 12A and Fig. 15). For instance, at the *Collignoniceras woollgari* time, the progradation along the shoreline is not perfectly in phase—the shoreline in central Utah had just reached its landward limit and began to prograde eastward, whereas progradation at other shoreline locations had been ongoing for some time (Fig. 10A). Despite the fact that global sea level was likely rising at the *Scaphites leei III*, and *Baculites clinolobatus* times (Fig. 7), the stratigraphic stacking pattern along the western shoreline shows a progradational stacking pattern, indicating at these times the rate of rising sea level (increase in accommodation) is smaller than that of tectonic uplift (decrease in accommodation) or sediment supply (filling of accommodation), or due to the combination of the two above factors (Fig. 8).

Careful evaluation of the regional shoreline migration trends highlighted in this paper show that along-strike variability in the stratigraphic stacking patterns is likely the norm, rather than the exception in retroarc foreland basins. The "global" sea-level rises or falls were not the overarching factor controlling shoreline migration, rather a complex interplay of many factors. This along-strike variability in shoreline stacking pattern is especially true when very large (>1000's km) areas of a basin, or entire basins, are considered such as the entire western shoreline of the WIS (Molenaar et al., 1988; Krystinik and DeJarnett, 1995). The largely asynchronous stratigraphic stacking patterns along the coeval shoreline indicate, at least for the third-order depositional cycles, the stratigraphic stacking pattern observed from any local area (~100 s km) record the interactions of tectonics, eustasy, and sediment supply rather than a sole or dominant eustatic change. To complicate matter even further, different tectonic subsidence mechanisms can lead to spatial variability in subsidence/uplift. Taking CFB as an example, the spatial variability in the loading scale (e.g., width and height) and lithospheric strength (i.e., effective elastic thickness) would result in lateral variability in the magnitude and scale of flexural subsidence (Jordan, 1981; Painter and Carrapa, 2013; Tufano and Pietras, 2017). Dynamic subsidence and uplift in front of, and above, a relatively buoyant oceanic plateau would cause spatial variability in the vertical crustal movement (Dávila and Lithgow-Bertelloni, 2015; Heller and Liu, 2016). Flexural subsidence caused by local uplifts of Laramide-style uplifts would alter local sediment dispersal pattern and affect the development of local accommodation. The complex spatial variability in tectonic subsidence and uplift, combined with eustatic changes (and sediment supply), would therefore almost always result in spatially variable stratigraphic stacking patterns along the coeval shoreline, unless changes in the accommodation caused by eustatic change significantly outpace those caused by the combined tectonics processes and sediment supply. Even under such conditions, the stratigraphic stacking pattern along the coeval shoreline may be only apparently consistent (i.e., the stacking pattern is not perfectly in phase), considering that the combined effects of tectonic processes and sediment supply are likely to vary spatially.

High-frequency sea-level and climate changes driven by Milankovitch cycles were also commonly invoked to explain the fourth-order to fifth-order (tens to hundreds of thousands of years; Fig. 2) cyclicity, particularly in the Late Cretaceous stratigraphic record of the CFB (Laferriere et al., 1987; Elder et al., 1994; Sethi and Leithold, 1994; Sageman et al., 1997; Laurin and Sageman, 2007; Plint and Kreitner, 2007; Zhu et al., 2012; Lin et al., 2019; Li and Schieber, 2020). Tectonic processes were generally ruled out as a possible cause of such high-frequency stratigraphic cyclicity because they were largely thought to be long-term processes and thus unable to produce fourth-order base-level changes. Nevertheless, shorter-term sea level or climate changes can be modulated by long-term base-level rise or fall (Martinson et al., 1998; Varban and Guy Plint, 2008). If the second- to third- depositional sequences across the CFB were not even synchronous, the timing and duration of shorter-term stratigraphic stacking patterns were likely to vary to some degree (at least in phase) across the CFB, not to mention that such high-frequency depositional cyclicity is likely to subject to additional autogenic controls (Muto and Steel, 1997). Although high-frequency (fourth- to fifth-order) depositional sequences documented across the CFB are comparable in their average temporal durations, unless the magnitude of shorter-term (fourth- and smaller-order) eustatic changes is larger than the rate of tectonic subsidence/uplift or sediment supply, these high-frequency sea-level changes will be modulated and have different preservation potentials in the stratigraphic record. Moreover, all high-frequency depositional sequences documented

by previous studies were mostly based on stratigraphic analysis conducted in a local or subbasinal area. The synchroneity of these high-frequency depositional sequences across the CFB has never been validated, due to the lack of chronostratigraphic constraints at such high temporal resolution—the temporal duration of fourth- to fifth-order sequences is smaller than the average duration of ammonite biozones in the Late Cretaceous WIS which is ~0.5 Ma. Therefore, simply attributing the observed stratigraphic stacking pattern (both long-term and short-term) in the stratigraphic record to dominant sea-level changes may lead to erroneous interpretations of the eustatic history during the geologic past, and the efforts of correlating these high-frequency depositional sequences based on their assumed synchroneity across the CFB or even the globe might simply be fortuitous.

Failure to consider the complex spatial variability in the combined effects of tectonics (both crustal and subcrustal processes), eustasy, and sediment supply is probably why the Late Cretaceous eustatic history reconstructed from different regions are not always consistent (Fig. 7). For instance, despite the general agreement of the timing of the highest global sea level during the earliest Turonian, the magnitude of sea-level rise remains controversial, ranging from ~40 m to ~300 m above the current sea level (Sahagian et al., 1996; Kominz et al., 2008; Haq, 2014). The disparate estimations of eustatic changes are probably caused by the fact that the magnitude of eustatic changes were all calculated based on the assumption that the study areas were tectonically quiescent. In many cases, the effects of dynamic topography are not considered in areas that were once considered to be quiescent, thereby affecting sea-level estimations. Moreover, various eustatic reconstructions tend to disagree on the trend of higher-order (i.e., third- to higher-order) eustatic changes on the resolution of ammonite biozones (Fig. 7). This highlights the challenge to isolate the eustatic signals from the stratigraphic record, which is essentially a product of various allogenic controls. In order to reconstruct the most reliable eustatic history, the effects of all other allogenic factors (e.g., tectonics, sediment supply) need to be ruled out, which can be achieved through careful correlations of stratigraphic stacking patterns based on robust time markers (e.g., biozone, geochronological data) across different regions.

5.4. Implication for future work

A high-resolution reconstruction of the paleogeographic evolution and shoreline history is critical to further our understanding of the complex interactions of various allogenic factors across space and through time. The main objective of this synthesis is to comprehensively document how tectonics, eustasy, and sediment supply had collectively produced the stratigraphic architecture of the Upper Cretaceous strata within the CFB. Based on all paleogeographic maps reconstructed in this synthesis, the roles of tectonics, sea level, sediment supply can be inferred (at least qualitatively). To quantify the relative role of different allogenic factors remains a challenging task and would still require future studies conducted through a holistic approach.

For example, future geodynamic models of the CFB and other retroarc foreland basins need to incorporate both flexural subsidence and dynamic topography associated with subcrustal processes, such as mantle flows. New geodynamic models also need to incorporate temporal and spatial variability in the flexural subsidence and dynamic topography. The magnitude and scale of flexural subsidence depend on the location and scale of active thrust sheets and the rigidity of the loaded lithosphere. The wavelength and locations of dynamic subsidence and uplift are dependent upon changes in the location, subduction angle and depth, and buoyancy of the subducting oceanic plateau (Dávila and Lithgow-Bertelloni, 2015; Humphreys et al., 2015; Li and Aschoff, 2022). More importantly, different subsidence mechanisms can interact with each other, and the effect of one certain subsidence mechanism may overprint or even obliterate the signature of other subsidence mechanisms in the stratigraphic record.

To develop a better understanding of the history of the CFB from the stratigraphic record, accurate ages of different rock units and a more refined Cretaceous time scale are required to allow accurate stratigraphic correlation and produce isopach maps dividing the Late Cretaceous into smaller intervals. The paleogeographic maps presented herein can certainly be further refined with more detrital zircon age and provenance data. These high-resolution paleogeographic maps can provide critical boundary conditions for forward modeling, such as sediment flux modeling (along-strike variability), landscape modeling, and paleobathemetric reconstructions, to better understand the evolution of paleogeography and shoreline under the combined influence various allogenic processes. Insights from these forward modeling, accompanied with high-resolution reconstruction of the geohistory from the stratigraphic analysis, are critical to understanding the landscape and tectonic evolutions of the CFB.

The complex interaction of tectonics, eustasy, and sediment supply revealed from this study, especially their variability along strike also applies for other retroarc foreland basin or sedimentary basins subject to similar subsidence mechanisms. Local variability in tectonics and sediment supply will likely produce laterally variable stratigraphic architecture. Eustatic reconstructions requires detailed correlation of the stratigraphic stacking patterns of different regions based on robust chronostratigraphic markers to rule out of effects of tectonics and sediment supply to achieve the most reliable eustatic history. Future analysis of the stratigraphic architecture in sedimentary basins (interpreting ancient stratigraphic record and modeling the development of stratigraphy) need to exercise extra cautions and always consider the complex interaction of tectonics, eustasy, and sediment supply across time and space.

6. Conclusions

Based on a range of stratigraphic, sedimentologic, and geochronological datasets, the third-order shoreline history (including location and migration trend) and paleogeographic evolution in the central part of the CFB through the Late Cretaceous were reconstructed in the form of 25 paleogeographic maps that emphasize shoreline development. The main conclusions drawn from this synthesis are as follows:

(1) The stratigraphic stacking pattern and shoreline migration trend along the coeval western shoreline in the Cordilleran Foreland Basin (CFB) were not synchronous during most of the Late Cretaceous, indicating the stratigraphic architecture of the CFB is the result of complex spatio-temporal interactions of tectonics (including crustal and subcrustal processes), eustasy, and sediment supply.

(2) Crustal and subcrustal tectonic subsidence mechanisms and their effects on the central part of the CFB through the Late Cretaceous were discriminated by integrating observations of shoreline migration and sediment dispersal patterns, paleocurrent data, and isopach patterns for well-constrained age-intervals. Specifically, flexural subsidence generated by loading of the Sevier fold-thrust belt was dominantly responsible for the subsidence in the CFB during the Cenomanian to the middle Campanian (100–80 Ma). Mantle-induced dynamic subsidence, possibly associated with the subduction of the conjugate Shatsky Rise, started to influence the topography in the Four Corners area during the late Santonian (~ 85 Ma) and became the dominant subsidence mechanism in the CFB during the middle to late Campanian (80–75 Ma). Subsidence in the study area during 75 to 66 Ma was controlled by the combined effects of dynamic subsidence and flexural subsidence induced by local Laramide-style uplifts.

(3) The regional spatial variability in the shoreline migration trend, as well as changes in the sediment dispersal pattern, helps constrain the effects of different subsidence mechanisms. The distinctly different shoreline migration distance between Wyoming and the southern study area during the Greenhorn transgression, the Greenhorn regression, and the Niobrara transgression strongly point to a more rigid lithosphere under Wyoming. Local tectonic subsidence in areas adjacent to the Sevier fold-thrust belt, inferred from the decoupled shoreline migration

trend at a given time, can help constrain the timing of pulses of flexural subsidence generation (timing of thrusting events). In additional to flexural subsidence, dynamic topography is another important mechanism able to influence the topography and paleogeography in the CFB. For instance, the southeastward migration of the shoreline protrusion from central Wyoming to the Wyoming-Colorado boundary during 81–76 Ma is in line with the increased dynamic subsidence (and deepening) in northcentral Colorado in front of the conjugate Shatsky rise. Combined dynamic subsidence and flexural subsidence generated by loading of Laramide-style uplifts were responsible for the last major transgression of the WIS in southern Wyoming and influenced the withdrawal of the seaway from the western US.

(4) The along-strike variation in shoreline migration trend along the coeval shoreline (i.e., concurrent progradation and retrogradation in different areas along the same shoreline) is the norm, rather than the exception, due to the along-strike variation in subsidence and sediment supply. The spatial variation in topographic load, lithospheric strength, mantle-induced dynamic topography, and sediment supply would result in subregional to regional, asynchronous shoreline migration trends and stratigraphic stacking patterns along the shoreline (i.e., along depositional strike). To reconstruct the most reliable eustatic history, the effects of all other allogenic factors (e.g., tectonics, sediment supply) need to be ruled out, which requires careful correlations of the stratigraphic architecture based on robust time markers (e.g., biozone, geochronological data) across different regions.

(5) Quantifying the relative roles of different allogenic factors on the architecture of the CFB strata remains a challenging task and still requires studies with more holistic approaches. Future geodynamic models of CFB and other retroarc foreland basins need to incorporate both flexural subsidence and mantle-induced dynamic topography, especially the complex spatially varying effects of these two mechanisms (e.g., the location, extent, and magnitude of subsidence/uplift). The compiled chronostratigraphic framework and paleogeographic maps that record the relationship between tectonics, sea level, and sedimentation need to be refined with more detailed stratigraphic, sedimentologic, and geochronological data. The high-resolution reconstruction of the geohistory of the CFB will allow resolving the complex link between tectonic subsidence, stratigraphic architecture, and sediment dispersal through landscape modeling and paleobathemetric reconstructions. A better understanding of the complex interactions between different allogenic factors and their effects on sediment basin fills will enable us to better use the stratigraphic record as important archives of paleoenvironmental evolutions and the linkage between surficial and deep-earth processes.

Declaration of Competing Interest

The authors declare that they have no known competing financial interests or personal relationships that could have appeared to influence the work reported in this paper.

Acknowledgements

We are grateful for the constructive review and editorial comments of Drs. Chris Fielding, Shaofeng Liu, Lijun Liu, and Ron Blakey. This research was partially supported by NSF grant EAR-1824550. Additionally, we wish to thank a host of graduate students at Colorado School of Mines and U. Alaska Anchorage who contributed much of the stratigraphic groundwork and data used in the regional database: Nick Danielle, Sarah Edwards, Jared Rountree, Brock Rust, Raju Sitaula (ABD), Parker Valora and Michelle Wiechman.

Appendix A. Supplementary data

Supplementary data to this article can be found online at https://doi.org/10.1016/j.earscirev.2022.103947.

References

Antia, J., Fielding, C.R., 2011. Sequence stratigraphy of a condensed low-accommodation succession: lower Upper Cretaceous Dakota Sandstone, Henry Mountains, southeastern Utah. AAPG Bull. 95 (3), 413–447.
Armstrong, R.L., 1968. Sevier orogenic belt in Nevada and Utah. GSA Bull. 79 (4), 429–458.
Aschoff, J.L., 2010. Preliminary regional sequence stratigraphic framework and characterization of potential fluvial reservoirs of the upper Mesaverde Group, Uinta Basin, Utah. Open-File Report 569, Utah Geological Survey.
Aschoff, J., Steel, R., 2011. Anomalous clastic wedge development during the Sevier-Laramide transition, North American Cordilleran foreland basin, USA. GSA Bull. 123 (9–10), 1822–1835.
Barron, E.J., 1989. Severe storms during Earth history. Geol. Soc. Am. Bull. 101 (5), 601–612.
Bartschi, N.C., Saylor, J.E., Lapen, T.J., Blum, M.D., Pettit, B.S., Andrea, R.A., 2018. Tectonic controls on Late Cretaceous sediment provenance and stratigraphic architecture in the Book Cliffs, Utah. GSA Bulletin 130 (11−12), 1763–1781.
Bhattacharya, J.P., Willis, B.J., 2001. Lowstand deltas in the frontier formation, powder river basin, wyoming: implications for sequence stratigraphic models. AAPG Bull. 85 (2), 261–294.
Bilodeau, W.L., 1986. The Mesozoic Mogollon Highlands, Arizona: an Early Cretaceous rift shoulder. The Journal of Geology 94 (5), 724–735.
Blakey, R.C., 2014. Paleogeography and paleotectonics of the western interior seaway, Jurassic-Cretaceous of North America. AAPG Search and Discovery Article #30392, 1–72.
Bond, G., 1976. Evidence for continental subsidence in North America during the Late Cretaceous global submergence. Geology 4 (9), 557–560.
Burgess, P.M., Moresi, L., 1999. Modelling rates and distribution of subsidence due to dynamic topography over subducting slabs: is it possible to identify dynamic topography from ancient strata? Basin Res. 11 (4), 305–314.
Bush, M.A., Horton, B.K., Murphy, M.A., Stockli, D.F., 2016. Detrital record of initial basement exhumation along the Laramide deformation front, southern Rocky Mountains. Tectonics 35 (9), 2117–2130.
Carvajal, C., Steel, R., 2011. Source-to-sink sediment volumes within a tectono-stratigraphic model for a laramide shelf-to-deep-water basin: methods and results. In: Busby, C., Azor, A. (Eds.), Tectonics of Sedimentary Basins: Recent Advances, pp. 131–151.
Cather, S.M., 2004. Laramide orogeny in central and northern New Mexico and southern Colorado. In: Mack, G.H., Giles, K.A. (Eds.), The Geology of New Mexico, A Geologic History. New Mexico Geological Society Special Publication 11, pp. 203–248.
Catuneanu, O., Beaumont, C., Waschbusch, P., 1997. Interplay of static loads and subduction dynamics in foreland basins: reciprocal stratigraphies and the "missing" peripheral bulge. Geology 25 (12), 1087–1090.
Chang, C., Liu, L., 2019. Distinct responses of intraplate sedimentation to different subsidence mechanisms: insights from forward landscape evolution simulations. Journal of Geophysical Research: Earth Surface 124 (5), 1139–1159.
Chang, C., Liu, L., 2020. Investigating the formation of the Cretaceous Western Interior Seaway using landscape evolution simulations. GSA Bull. 133 (1–2), 347–361.
Cobban, W.A., Merewether, E.A., Fouch, T.D., Obradovich, J.D., 1994. Some Cretaceous shorelines in the western interior of the United States. In: Caputo, M.V., Peterson, J. A., Franczyk, K.J. (Eds.), Mesozoic Systems of the Rocky Mountain Region. U.S.A. Rocky Mountain Section SEPM, Denver, Colorado, pp. 393–414.
Cobban, W.A., Walaszczyk, I., Obradovich, J.D., McKinney, K.C., 2006. A USGS Zonal Table for the Upper Cretaceous Middle Cenomanian-Maastrichtian of the Western Interior of the United States Based on Ammonites, Inoceramids, and Radiometric Ages. U.S. Geological Survey Open-File Report 2006–1250.
Coney, P.J., Reynolds, S.J., 1977. Cordilleran Benioff zones. Nature 270 (5636), 403–406.
Copeland, P., Currie, C.A., Lawton, T.F., Murphy, M.A., 2017. Location, location, location: the variable lifespan of the Laramide orogeny. Geology 45 (3), 223–226.
Cross, T.A., 1986. Tectonic controls of foreland basin subsidence and laramide style deformation, Western United States. In: Allen, P.A., Homewood, P. (Eds.), Foreland Basins, 8. International Association of Sedimentologists Special Publication, pp. 15–39.
Cross, T.A., Pilger, R.H., 1978. Tectonic controls of late Cretaceous sedimentation, western interior, USA. Nature 274 (5672), 653–657.
Dávila, F.M., Lithgow-Bertelloni, C., 2015. Dynamic uplift during slab flattening. Earth Planet. Sci. Lett. 425, 34–43.
Dean, C.D., Collins, D.S., van Cappelle, M., Avdis, A., Hampson, G.J., 2019. Regional-scale paleobathymetry controlled location, but not magnitude, of tidal dynamics in the Late Cretaceous Western Interior Seaway, USA. Geology 47 (11), 1083–1087.
DeCelles, P.G., 1988. Lithologic provenance modeling applied to the Late Cretaceous synorogenic Echo Canyon Conglomerate, Utah: a case of multiple source areas. Geology 16 (11), 1039–1043.
DeCelles, P.G., 1994. Late Cretaceous-Paleocene synorogenic sedimentation and kinematic history of the Sevier thrust belt, Northeast Utah and southwest Wyoming. GSA Bull. 106 (1), 32–56.
DeCelles, P.G., 2004. Late Jurassic to Eocene evolution of the Cordilleran thrust belt and foreland basin system, western U.S.a. Am. J. Sci. 304 (2), 105–168.
DeCelles, P.G., 2012. Foreland basin systems revisited: variations in response to tectonic settings. In: Busby, C., Azor, A. (Eds.), Tectonics of Sedimentary Basins, pp. 405–426.
DeCelles, P.G., Coogan, J.C., 2006. Regional structure and kinematic history of the Sevier fold-and-thrust belt, Central Utah. Geol. Soc. Am. Bull. 118 (7–8), 841–864.
DeCelles, P.G., Giles, K.A., 1996. Foreland basin systems. Basin Res. 8 (2), 105–123.

DeCelles, P.G., Lawton, T.F., Mitra, G., 1995. Thrust timing, growth of structural culminations, and synorogenic sedimentation in the type Sevier orogenic belt, western United States. Geology 23 (8), 699–702.
Devlin, W.J., Rudolph, K.W., Shaw, C.A., Ehman, K.D., 1993. The effect of tectonic and eustatic cycles on accommodation and sequence-stratigraphic framework in the Upper Cretaceous foreland basin of southwestern Wyoming. In: Posamentier, H.W., Summerhayes, C.P., Haq, B.U., Allen, G.P. (Eds.), Sequence Stratigraphy and Facies Associations, 18. International Association of Sedimentologists Special Publication, pp. 501–520.
Dickinson, W.R., Gehrels, G.E., 2008. Sediment delivery to the Cordilleran foreland basin: insights from U-Pb ages of detrital zircons in Upper Jurassic and Cretaceous strata of the Colorado Plateau. Am. J. Sci. 308 (10), 1041–1082.
Dickinson, W.R., Klute, M.A., Hayes, M.J., Janecke, S.U., Lundin, E.R., McKittrick, M.A., Olivares, M.D., 1988. Paleogeographic and paleotectonic setting of Laramide sedimentary basins in the central Rocky Mountain region. GSA Bull. 100 (7), 1023–1039.
Dickinson, W.R., Lawton, T.F., Pecha, M., Davis, S.J., Gehrels, G.E., Young, R.A., 2012. Provenance of the Paleogene Colton Formation (Uinta Basin) and Cretaceous–Paleogene provenance evolution in the Utah foreland: Evidence from U-Pb ages of detrital zircons, paleocurrent trends, and sandstone petrofacies. Geosphere 8 (4), 854–880.
Dyman, T., Merewether, E., Molenaar, C., Cobban, W., Obradovich, J., Weimer, R., Bryant, W., 1994. Stratigraphic transects for Cretaceous rocks, rocky mountains and great plains regions. In: Caputo, M.V., Peterson, J.A., Franczyk, K.J. (Eds.), Mesozoic Systems of the Rocky Mountain Region, USA. SEPM Rocky Mountain Section, pp. 365–391.
Edwards, C.M., Howell, J.A., Flint, S.S., 2005. Depositional and stratigraphic architecture of the Santonian Emery Sandstone of the Mancos Shale: implications for Late Cretaceous Evolution of the Western Interior Foreland Basin of Central Utah, U.S.a. J. Sediment. Res. 75 (2), 280–299.
Elder, W.P., Kirkland, J.I., 1994. Cretaceous paleogeography of the southern Western Interior region. In: Peterson, J.A., Franczyk, K.J. (Eds.), Mesozoic Systems of the Rocky Mountain Region. SEPM Special Publication, United States, pp. 415–440.
Elder, W.P., Gustason, E.R., Sageman, B.B., 1994. Correlation of basinal carbonate cycles to nearshore parasequences in the Late Cretaceous Greenhorn seaway, Western Interior U.S.a. Geol. Soc. Am. Bull. 106 (7), 892–902.
Eldrett, J.S., Ma, C., Bergman, S.C., Ozkan, A., Minisini, D., Lutz, B., Jackett, S.-J., Macaulay, C., Kelly, A.E., 2015. Origin of limestone–marlstone cycles: astronomic forcing of organic-rich sedimentary rocks from the Cenomanian to early Coniacian of the Cretaceous Western Interior Seaway, USA. Earth Planet. Sci. Lett. 423 (Supplement C), 98–113.
Ericksen, M.C., Slingerland, R.L., 1990. Numerical simulations of tidal and wind-driven circulation in the Cretaceous interior seaway of North America. Geol. Soc. Am. Bull. 102 (11), 1499–1516.
Fan, M., Carrapa, B., 2014. Late Cretaceous–early Eocene Laramide uplift, exhumation, and basin subsidence in Wyoming: crustal responses to flat slab subduction. Tectonics 33 (4), 509–529.
Ferron, C., 2019. Detrital Zircon Signal Inversion in the Cretaceous Southwestern U.S. Interior Seaway - A Case Study from the Gallup System New Mexico. Master's Thesis. McMaster University, 81 pp.
Fielding, C.R., 2011. Foreland basin structural growth recorded in the Turonian Ferron Sandstone of the Western Interior Seaway Basin, USA. Geology 39 (12), 1107–1110.
Fouch, T.D., Lawton, T.F., Nichols, D.J., Cashion, W.B., Cobban, W.A., 1983. Patterns and timing of synorogenic sedimentation in Upper Cretaceous rocks of central and Northeast Utah. In: Reynolds, M.W., Dolly, E.D. (Eds.), Mesozoic Paleogeography of the West-Central United States. SEPM Rocky Mountain Section, Second Rocky Mountain Patengeography Symposium, pp. 305–336.
Franczyk, K.J., Fouch, T.D., Johnson, R.C., Molenaar, C.M., Cobban, W.A., 1992. Cretaceous and Tertiary paleogeographic reconstructions for the Uinta-Piceance Basin Study Area, Colorado and Utah. U.S. Geological Survey Bulletin 1787Q.
Gallin, W.N., Johnson, C.L., Allen, J.L., 2010. Fluvial and marginal marine architecture of the John Henry Member, Straight Cliffs Formation, Kelly Grade of the Kaiparowits Plateau, south-Central Utah. In: Carney, S., Tabet, D., Johnson, C.L. (Eds.), Geology of South-Central Utah, Utah Geological Association Guidebook, 39, pp. 248–275.
Gani, M.R., Ranson, A., Cross, D.B., Hampson, G.J., Gani, N.D., Sahoo, H., 2015. Along-strike sequence stratigraphy across the Cretaceous shallow marine to coastal-plain transition, Wasatch Plateau, Utah, U.S.A. Sediment. Geol. 325, 59–70.
Gardner, M.H., 1995. Tectonic and eustatic controls on the stratal architecture of mid-Cretaceous stratigraphic sequences, central western interior foreland basin of North America. In: Dorobek, S.L., Ross, G.M. (Eds.), Stratigraphic Evolution of Foreland Basins, Stratigraphic Evolution of Foreland Basins. SEPM Special Publication, 52, pp. 243–282.
Goldstrand, P.M., 1990. Stratigraphy and paleogeography of Late Cretaceous and Paleogene rocks of Southwest Utah. In: Miscellaneous Publication 90–2. Survey, Utah Geological and Mineral.
Goldstrand, P.M., 1992. Evolution of Late Cretaceous and early Tertiary basins of Southwest Utah based on clastic petrology. J. Sediment. Res. 62 (3), 495–507.
Goldstrand, P.M., 1994. Tectonic development of Upper Cretaceous to Eocene strata of southwestern Utah. GSA Bull. 106 (1), 145–154.
Gooley, J.T., Johnson, C.L., Pettinga, L., 2016. Spatial and temporal variation of fluvial architecture in a prograding clastic wedge of the Late Cretaceous Western Interior Basin (Kaiparowits Plateau), U.S.a. J. Sediment. Res. 86 (3), 125–147.
Gradstein, F.M., Ogg, J.G., Schmitz, M.D., Ogg, G.M., 2012. The geologic time scale 2012. Elsevier.
Gurnis, M., 1992. Rapid continental subsidence following the initiation and evolution of subduction. Science 255 (5051), 1556.
Gustason, E.R., 1989. Stratigraphy and Sedimentology of the Middle Cretaceous (Albian-Cenomanian) Dakota Formation, Southwestern Utah. Ph.D. Thesis. University of Colorado, Boulder, 402 pp.
Hale, L.A., Van De Graaff, F.R., 1964. Cretaceous stratigraphy and facies patterns—northeastern Utah and adjacent areas. Inter mountain Association of Petroleum Geologists 13th Annual Field Conference, Guidebook to the Geology and Mineral Resources of the Uinta Basin—Utah's Hydrocarbon Storehouse, pp. 115–138.
Hampson, G.J., 2010. Sediment dispersal and quantitative stratigraphic architecture across an ancient shelf. Sedimentology 57 (1), 96–141.
Haq, B.U., 2014. Cretaceous eustasy revisited. Glob. Planet. Chang. 113, 44–58.
Haq, B.U., Hardenbol, J., Vail, P.R., 1987. Chronology of fluctuating sea levels since the Triassic. Science 235 (4793), 1156–1167.
Haque, Z., Geissman, J.W., DeCelles, P.G., Carrapa, B., 2020. A magnetostratigraphic age constraint for the proximal synorogenic conglomerates of the Late Cretaceous Cordilleran foreland basin, northeast Utah, USA. GSA Bulletin 133 (9–10), 1795–1814.
Heinzel, C.E., 2000. Stratigraphic, Petrographic, and Sedimentologic Analysis of Upper Cretaceous Deltaic Sedimentation of the Adaville Formation, Kemmerer Coal Mine Area, Southwestern Wyoming. Master's Thesis. University of Minnesota, Duluth, 101 pp.
Heller, P.L., Liu, L., 2016. Dynamic topography and vertical motion of the U.S. Rocky Mountain region prior to and during the Laramide orogeny. GSA Bull. 128 (5–6), 973–988.
Heller, P.L., Mathers, G., Dueker, K., Foreman, B., 2013. Far-traveled latest Cretaceous–Paleocene conglomerates of the Southern Rocky Mountains, USA: record of transient Laramide tectonism. GSA Bull. 125 (3–4), 490–498.
Horton, B.K., Constenius, K.N., DeCelles, P.G., 2004. Tectonic control on coarse-grained foreland-basin sequences: an example from the Cordilleran foreland basin. Utah Geol. 32 (7), 637–640.
Humphreys, E.D., Schmandt, B., Bezada, M.J., Perry-Houts, J., 2015. Recent craton growth by slab stacking beneath Wyoming. Earth Planet. Sci. Lett. 429, 170–180.
Hurd, T.J., Fielding, C.R., Hutsky, A.J., 2014. Variability in sedimentological and ichnological signatures across a river-dominated delta deposit: Peay Sandstone Member (Cenomanian) of the Northern Bighorn Basin, Wyoming, U.S.A. J. Sediment. Res. 84 (1), 1–18.
Hutsky, A.J., Fielding, C.R., Hurd, T.J., Clark, C.K., 2012. Sedimentology and stratigraphy of the Upper Cretaceous (Cenomanian) Frontier Formation, Northeast Bighorn Basin, Wyoming, U.S.A. The Mountain Geologist 49 (3), 77–98.
Jinnah, Z.A., Roberts, E.M., Deino, A.L., Larsen, J.S., Link, P.K., Fanning, C.M., 2009. New 40Ar-39Ar and detrital zircon U-Pb ages for the Upper Cretaceous Wahweap and Kaiparowits formations on the Kaiparowits Plateau, Utah: implications for regional correlation, provenance, and biostratigraphy. Cretac. Res. 30 (2), 287–299.
Johnson, R.C., Flores, R.M., 2003. History of the Piceance Basin from latest Cretaceous through early Eocene and the chracterization of lower Tertiary sandstone reservoirs. In: Peterson, K.M., Olson, T.M., Anderson, D.S. (Eds.), Piceance Basin 2003 Guidebook. Rocky Mountain Association of Geologists, pp. 21–62.
Jones, C.H., Farmer, G.L., Sageman, B., Zhong, S., 2011. Hydrodynamic mechanism for the Laramide orogeny. Geosphere 7 (1), 183–201.
Joo, Y.J., Sageman, B.B., 2014. Cenomanian to Campanian carbon isotope chemostratigraphy from the Western Interior Basin, U.S.A. J. Sediment. Res. 84 (7), 529–542.
Joo, Y.J., Sageman, B.B., Hurtgen, M.T., 2020. Data-model comparison reveals key environmental changes leading to Cenomanian-Turonian Oceanic Anoxic Event 2. Earth Sci. Rev. 203, 103123.
Jordan, T.E., 1981. Thrust loads and foreland basin evolution, Cretaceous, western United States. AAPG Bull. 65 (12), 2506–2520.
Kauffman, E.G., 1977. Geological and biological overview: Western Interior Cretaceous Basin. Mt. Geol. 14 (3–4), 75–99.
Kauffman, E.G., 1985. Cretaceous evolution of the Western Interior Basin of the United States. SEPM Guidebook 4 iv-xiii.
Kauffman, E.G., Caldwell, W.G.E., 1993. The Western Interior Basin in Space and Time. Special Paper - Geological Association of Canada, 39, pp. 1–30.
Kelley, S.A., 2002. Unroofing of the southern Front Range, Colorado: a view from the Denver Basin. Rocky Mountain Geology 37 (2), 189–200.
Kirschbaum, M.A., Mercier, T.J., 2013. Controls on the deposition and preservation of the Cretaceous Mowry Shale and Frontier Formation and equivalents, Rocky Mountain region, Colorado, Utah, and Wyoming. AAPG Bull. 97 (6), 899–921.
Kiteley, L.W., 1983. Facies analysis of the lower cycles of the Mesaverde Group (Upper Cretaceous) in northwestern Colorado. U.S. Geological Survey Open-File Report 83–820.
Kluth, C.F., 1997. Comparison of the location and structure of the Late Paleozoic and Late Cretaceous-Early Tertiary Front Range uplift. In: Bolyard, D.W., Sonnenberg, S. A. (Eds.), Geologic History of the Front Range. Rocky Mountain Association of Geologists, Denver, Colorado, pp. 31–42.
Koch, A.R., Johnson, C.L., Stright, L., 2019. Does fluvial channel-belt clustering predict net sand to gross rock volume? Architectural metrics and point-pattern analysis of a digital outcrop model. J. Sediment. Res. 89 (11), 1109–1126.
Kominz, M.A., Browning, J.V., Miller, K.G., Sugarman, P.J., Mizintseva, S., Scotese, C.R., 2008. Late Cretaceous to Miocene sea-level estimates from the New Jersey and Delaware coastal plain coreholes: an error analysis. Basin Res. 20 (2), 211–226.
Krystinik, L.F., DeJarnett, B.B., 1995. Lateral variability of sequence stratigraphic framework in the Campanian and Lower Maastrichtian of the Western Interior Seaway. In: Van Wagoner, J.C., Bertram, G.T. (Eds.), Sequence Stratigraphy of Foreland Basin Deposits—Outcrop and Subsurface Examples from the Cretaceous of North America. AAPG Memoir, pp. 11–26.

Laferriere, A.P., Hattin, D.E., Archer, A.W., 1987. Effects of climate, tectonics, and sea-level changes on rhythmic bedding patterns in the Niobrara Formation (Upper Cretaceous), U.S. Western Interior. Geology 15 (3), 233–236.
Larsen, J.S., Link, P.K., Roberts, E.M., Tapanila, L., Fanning, C.M., 2010. Cyclic stratigraphy of the Paleogene Pine Hollow Formation and detrital zircon provenance of Campanian to Eocene sandstones of the Kaiparowits and Table Cliffs basins, south-central Utah. In: Carney, S.M., Tabet, D.E., Johnson, C.L. (Eds.), Geology of South-Central Utah, Utah Geological Association Publication, 39, pp. 194–224.
Laskowski, A.K., DeCelles, P.G., Gehrels, G.E., 2013. Detrital zircon geochronology of Cordilleran retroarc foreland basin strata, western North America. Tectonics 32 (5), 1027–1048.
Laurin, J., Sageman, B.B., 2007. Cenomanian–Turonian coastal record in SW Utah, U.S.A.: orbital-scale transgressive–regressive events during oceanic anoxic event II. J. Sediment. Res. 77 (9), 731.
Lawton, T.F., 2008. Chapter 12 Laramide sedimentary basins. In: Miall, A.D. (Ed.), Sedimentary Basins of the World. Elsevier, pp. 429–450.
Lawton, T.F., Bradford, B.A., 2011. Correlation and provenance of Upper Cretaceous (Campanian) Fluvial Strata, Utah, U.S.A., from Zircon U-Pb geochronology and petrography. J. Sediment. Res. 81 (7), 495–512.
Lawton, T.F., Homewood, P., Allen, P.A., 1986. Compositional trends within a clastic wedge adjacent to a fold-thrust belt: Indianola Group, Central Utah, USA. In: Allen, P.A., Homewood, P. (Eds.), Foreland Basins, 8. International Association of Sedimentologists Special Publication, pp. 411–423.
Lawton, T.F., Pollock, S.L., Robinson, R.A.J., 2003. Integrating sandstone petrology and nonmarine sequence stratigraphy: application to the Late Cretaceous Fluvial Systems of Southwestern Utah, U.S.A. J. Sediment. Res. 73 (3), 389–406.
Lawton, T.F., Schellenbach, W.L., Nugent, A.E., 2014. Late Cretaceous fluvial-megafan and axial-river systems in the Southern Cordilleran Foreland Basin: drip tank member of straight cliffs formation and Adjacent Strata, Southern Utah, U.S.A. J. Sediment. Res. 84 (5), 407–434.
Lawton, T.F., Amato, J.M., Machin, S.E.K., Gilbert, J.C., Lucas, S.G., 2020. Transition from Late Jurassic rifting to middle Cretaceous dynamic foreland, southwestern U.S. and northwestern Mexico. GSA Bull. 132 (11–12), 2489–2516.
Leary, R., DeCelles, P., Gehrels, G., Morriss, M., 2015. Fluvial deposition during transition from flexural to dynamic subsidence in the Cordilleran foreland basin: Ericson Formation, Western Wyoming, USA. Basin Res. 27 (4), 495–516.
Leithold, E.L., 1994. Stratigraphical architecture at the muddy margin of the Cretaceous Western Interior Seaway, southern Utah. Sedimentology 41 (3), 521–542.
Li, Z., Aschoff, J., 2022. Constraining the effects of dynamic topography on the development of Late Cretaceous Cordilleran foreland basin, western United States. GSA Bull. 134, 446–462.
Li, Z., Schieber, J., 2018. Detailed facies analysis of the Upper Cretaceous Tununk Shale Member, Henry Mountains Region, Utah: Implications for mudstone depositional models in epicontinental seas. Sediment. Geol. 364, 141–159.
Li, Z., Schieber, J., 2020. Application of sequence stratigraphic concepts to the Upper Cretaceous Tununk Shale Member of the Mancos Shale Formation, south-central Utah: Parasequence styles in shelfal mudstone strata. Sedimentology 67 (1), 118–151.
Lin, W., Bhattacharya, J.P., Stockford, A., 2019. High-resolution sequence stratigraphy and implications for Cretaceous glacioeustasy of the Late Cretaceous Gallup System, New Mexico, U.S.A. J. Sediment. Res. 89 (6), 552–575.
Liu, S., Currie, C.A., 2016. Farallon plate dynamics prior to the Laramide orogeny: Numerical models of flat subduction. Tectonophysics 666, 33–47.
Liu, S., Nummedal, D., 2004. Late Cretaceous subsidence in Wyoming: quantifying the dynamic component. Geology 32 (5), 397–400.
Liu, S., Nummedal, D., Yin, P., Luo, H., 2005. Linkage of Sevier thrusting episodes and Late Cretaceous foreland basin megasequences across southern Wyoming (USA). Basin Res. 17 (4), 487–506.
Liu, L., Spasojević, S., Gurnis, M., 2008. Reconstructing Farallon plate subduction beneath North America back to the Late Cretaceous. Science 322 (5903), 934–938.
Liu, L., Gurnis, M., Seton, M., Saleeby, J., Müller, R.D., Jackson, J.M., 2010. The role of oceanic plateau subduction in the Laramide orogeny. Nat. Geosci. 3, 353.
Liu, S., Nummedal, D., Liu, L., 2011. Migration of dynamic subsidence across the Late Cretaceous United States Western Interior Basin in response to Farallon plate subduction. Geology 39 (6), 555–558.
Liu, S., Nummedal, D., Gurnis, M., 2014. Dynamic versus flexural controls of Late Cretaceous Western Interior Basin, USA. Earth Planet. Sci. Lett. 389, 221–229.
Livaccari, R.F., 1991. Role of crustal thickening and extensional collapse in the tectonic evolution of the Sevier-Laramide orogeny, western United States. Geology 19 (11), 1104–1107.
Livaccari, R.F., Burke, K., Şengör, A.M.C., 1981. Was the Laramide orogeny related to subduction of an oceanic plateau? Nature 289 (5795), 276–278.
López, J.L., Steel, R.J., 2015. Laramide signals and architecture of a widespread fluvial sand sheet: Canyon Creek Member, Southern Wyoming, U.S.A. J. Sediment. Res. 85 (9), 1102–1122.
Lorenz, J.C., Cooper, S.P., 2003. Tectonic setting and characteristics of natural fractures in Mesaverde and Dakota reservoirs of the San Juan Basin. N. M. Geol. 25, 3–14.
Luo, H., Nummedal, D., 2012. Forebulge migration: a three-dimensional flexural numerical modeling and subsurface study of southwestern Wyoming. In: Gao, D. (Ed.), Tectonics and Sedimentation: Implications for Petroleum Systems: AAPG Memoir 100, pp. 377–395.
Lynds, R.M., Xie, X., 2019. Detrital zircon geochronology of Upper Cretaceous to Paleocene sandstones from South-Central Wyoming: evidence for Middle Campanian Laramide Deformation. Tectonics 38 (12), 4077–4098.
Ma, C., Meyers, S.R., Sageman, B.B., 2017. Theory of chaotic orbital variations confirmed by Cretaceous geological evidence. Nature 542, 468.
Martinsen, O.J., Martinsen, R.S., Steidtmann, J.R., 1993. Mesaverde Group (Upper Cretaceous), Southeastern Wyoming: allostratigraphy versus sequence stratigraphy in a tectonically active Area1. AAPG Bull. 77 (8), 1351–1373.
Martinson, V.S., Heller, P.L., Frerichs, W.E., 1998. Distinguishing middle Late Cretaceous tectonic events from regional sea-level change using foraminiferal data from the U.S. Western Interior. GSA Bull. 110 (2), 259–268.
McGookey, D.P., Haun, J.D., Hale, L.A., Goodell, H.G., McCubbin, D.G., Weimer, R.J., Wulf, G.R., 1972. Cretaceous system. In: Mallory, W.W. (Ed.), Geologic Atlas of the Rocky Mountain Region. Rocky Mountain Association of Geologists, pp. 190–228.
Mederos, S., Tikoff, B., Bankey, V., 2005. Geometry, timing, and continuity of the Rock Springs uplift, Wyoming, and Douglas Creek arch, Colorado: implications for uplift mechanisms in the Rocky Mountain foreland, U.S.A. Rocky Mountain. Geology 40 (2), 167–191.
Melick, J.J., 2013. Subsurface description and modeling of geologic heterogeneity in large subsurface datasets: Using temporal and scalar hierarchies, Powder River Basin, WY and MT, U.S.A. Ph.D. Thesis. Montana State University, Bozeman, 237 pp.
Merewether, E.A., 1996. Stratigraphy and tectonic implications of Upper Cretaceous rocks in the Powder River basin, northeastern Wyoming and southeastern Montana. USGS Bulletin 1917T.
Merewether, E.A., Cobban, W.A., 1986. Biostratigraphic units and tectonism in the mid-Cretaceous foreland of Wyoming, Colorado, and adjoining areas. In: Peterson, S.A. (Ed.), Paleotectonics and Sedimentation in the Rocky Mountain Region, United States, Part III, Middle Rocky Mountains. American Association of Petroleum Geologists Memoir, 41, pp. 443–468.
Merewether, E.A., Cobban, W.A., Cavanaugh, E.T., 1979. Frontier Formation and equivalent rocks in eastern Wyoming. The Mountain Geologist 16, 67–101.
Merletti, G.D., Steel, R.J., Olariu, C., Melick, J.J., Armitage, P.J., Shabro, V., 2018. The last big marine transgression of the Western Interior Seaway: Almond Formation development from barrier spits across South Wyoming. Mar. Pet. Geol. 98, 763–782.
Miall, A.D., Catuneanu, O., Vakarelov, B.K., Post, R., 2008. Chapter 9 the Western Interior Basin. In: Miall, A.D. (Ed.), Sedimentary Basins of the World. Elsevier, pp. 329–362.
Miller, K.G., Wright, J.D., Browning, J.V., 2005. Visions of ice sheets in a greenhouse world. Mar. Geol. 217 (3–4), 215–231.
Minor, K.P., Steel, R.J., Olariu, C., 2021. Tectonic and eustatic control of Mesaverde Group (Campanian−Maastrichtian) architecture, Wyoming-Utah-Colorado region, USA. GSA Bulletin 134 (1–2), 419–445.
Mitchum, R.M., Van Wagoner, J.C., 1991. High-frequency sequences and their stacking patterns: sequence-stratigraphic evidence of high-frequency eustatic cycles. Sediment. Geol. 70 (2), 131–160.
Mitrovica, J.X., Beaumont, C., Jarvis, G.T., 1989. Tilting of continental interiors by the dynamical effects of subduction. Tectonics 8 (5), 1079–1094.
Molenaar, C.M., Rice, D.D., Sloss, L.L., 1988. Cretaceous rocks of the Western Interior basin. In: Sloss, L.L. (Ed.), The Geology of North America. Geological Society of America, Boulder, CO, pp. 77–82.
Molenaar, C.M., Cobban, W.A., Merewether, E.A., Pillmore, C.L., Wolfe, D.G., Holbrook, J.M., 2002. Regional stratigraphic cross sections of Cretaceous rocks from east-central Arizona to the Oklahoma Panhandle. USGS Misc. Field Studies Map 2382.
Muto, T., Steel, R.J., 1997. Principles of regression and transgression; the nature of the interplay between accommodation and sediment supply. J. Sediment. Res. 67 (6), 994–1000.
Obradovich, J.D., 1993. A Cretaceous time scale. In: Caldwell, W.G.E., Kauffman, E.G. (Eds.), Evolution of the Western Interior Basin, pp. 379–396.
Ogg, J.G., Hinnov, L.A., Huang, C., 2012. Chapter 27 - Cretaceous. In: Gradstein, F.M., Ogg, J.G., Schmitz, M.D., Ogg, G.M. (Eds.), The Geologic Time Scale. Elsevier, Boston, pp. 793–853.
Painter, C.S., Carrapa, B., 2013. Flexural versus dynamic processes of subsidence in the north American Cordillera foreland basin. Geophys. Res. Lett. 40 (16), 4249–4253.
Painter, C.S., Carrapa, B., DeCelles, P.G., Gehrels, G.E., Thomson, S.N., 2014. Exhumation of the North American Cordillera revealed by multi-dating of Upper Jurassic–Upper Cretaceous foreland basin deposits. GSA Bull. 126 (11–12), 1439–1464.
Pang, M., Nummedal, D., 1995. Flexural subsidence and basement tectonics of the Cretaceous Western Interior basin, United States. Geology 23 (2), 173–176.
Paola, C., Ganti, V., Mohrig, D., Runkel, A.C., Straub, K.M., 2018. Time not our time: physical controls on the preservation and measurement of geologic time. Annu. Rev. Earth Planet. Sci. 46 (1), 409–438.
Pecha, M.E., Gehrels, G.E., Karlstrom, K.E., Dickinson, W.R., Donahue, M.S., Gonzales, D. A., Blum, M.D., 2018. Provenance of Cretaceous through Eocene strata of the Four Corners region: insights from detrital zircons in the San Juan Basin, New Mexico and Colorado. Geosphere 14 (2), 785–811.
Peterson, F., Ryder, R.T., Law, B.E., 1980. Stratigraphy, sedimentology, and regional relationships of the Cretaceous System in the Henry Mountains region, Utah. In: Picard, M.D. (Ed.), Henry Mountains Symposium. Utah Geological Association Publication 8, United States, pp. 151–170.
Plink-Bjorklund, P., Kiteley, L., 2013. Denver Basin isolated sandbodies: signature of dynamic subsidence, Laramide uplifts and shoreline transitions. AAPG Search and Discovery Article #90163, 1–19.
Plint, A.G., Kreitner, M.A., 2007. Extensive thin sequences spanning Cretaceous foredeep suggest high-frequency eustatic control: Late Cenomanian, Western Canada foreland basin. Geology 35 (8), 735–738.
Primm, J.W., Johnson, C.L., Stearns, M., 2018. Basin-axial progradation of a sediment supply driven distributive fluvial system in the Late Cretaceous southern Utah foreland. Basin Res. 30 (2), 249–278.

Quinn, G.M., Hubbard, S.M., van Drecht, R., Guest, B., Matthews, W.A., Hadlari, T., 2016. Record of orogenic cyclicity in the Alberta foreland basin, Canadian Cordillera. Lithosphere 8 (3), 317–332.
Ray, D.C., van Buchem, F.S.P., Baines, G., Davies, A., Gréselle, B., Simmons, M.D., Robson, C., 2019. The magnitude and cause of short-term eustatic Cretaceous sea-level change: a synthesis. Earth Sci. Rev. 197, 102901.
Roberts, E.M., 2007. Facies architecture and depositional environments of the Upper Cretaceous Kaiparowits Formation, southern Utah. Sediment. Geol. 197 (3), 207–233.
Roberts, L.N.R., Kirschbaum, M.A., 1995. Paleogeography and the Late Cretaceous of the Western Interior of Middle North America; Coal Distribution and Sediment Accumulation. U.S. Geological Survey Professional Paper, p. 1561.
Robinson, R.A.J., Slingerland, R.L., 1998. Grain-size trends, basin subsidence and sediment supply in the Campanian Castlegate Sandstone and equivalent conglomerates of Central Utah. Basin Res. 10 (1), 109–127.
Rudolph, K.W., Devlin, W.J., Crabaugh, J.P., 2015. Upper Cretaceous sequence stratigraphy of the Rock Springs Uplift, Wyoming. The Mountain Geologist 52, 13–157.
Ryer, T.A., Lovekin, J.R., 1986. The Upper Cretaceous Vernal Delta of Utah; depositional or paleotectonic feature? In: Peterson, J.A. (Ed.), Paleotectonics and Sedimentation in the Rocky Mountain Region, United States, American Association of Petroleum Geologists Memoir, 41, pp. 497–510.
Sageman, B.B., Arthur, M.A., 1994. Early Turonian paleogeographic/paleobathymetric map, western interior, US. In: Caputo, M.V., Peterson, J.A., Franczyk, K.J. (Eds.), Mesozoic Systems of the Rocky Mountain Region, USA. SEPM Rocky Mountain Section, Denver, Colorado, pp. 457–470.
Sageman, B., Johnson, C., 1985. Stratigraphy and paleobiology of the Lincoln Limestone Member, Greenhorn Limestone, Rock Canyon Anticline, Colorado. In: Pratt, L.M., Kauffman, E.G., Zelt, F.B. (Eds.), Fine-Grained Deposits and Biofacies of the Cretaceous Western Interior Seaway: Evidence of Cyclic Sedimentary Processes. Society of Economic Paleontologists and Mineralogists, Tulsa, Tulsa, OK, pp. 100–109.
Sageman, B.B., Rich, J., Arthur, M.A., Birchfield, G.E., Dean, W.E., 1997. Evidence for Milankovitch periodicities in Cenomanian-Turonian lithologic and geochemical cycles, Western Interior U.S.A. J. Sediment. Res. 67 (2), 286–302.
Sahagian, D., Pinous, O., Olferiev, A., Zakharov, V., 1996. Eustatic Curve for the Middle Jurassic—Cretaceous based on Russian Platform and Siberian Stratigraphy: Zonal Resolution1. AAPG Bull. 80 (9), 1433–1458.
Saleeby, J., 2003. Segmentation of the Laramide Slab—evidence from the southern Sierra Nevada region. GSA Bull. 115 (6), 655–668.
Schlager, W., 1993. Accommodation and supply—a dual control on stratigraphic sequences. Sediment. Geol. 86 (1), 111–136.
Schmitt, J.G., Jones, D.A., Goldstrand, P.M., 1991. Braided stream deposition and provenance of the Upper Cretaceous-Paleocene(?) Canaan Peak Formation, Sevier foreland basin, southwestern Utah. In: Nations, J.D., Eaton, J.G. (Eds.), Stratigraphy, Depositional Environments; and Sedimentary Tectonics of the Western Margin, Cretaceous Western Interior Seaway. Geological Society of America Special Paper, 260, pp. 27–46.
Schröder-Adams, C., 2014. The Cretaceous Polar and Western Interior seas: paleoenvironmental history and paleoceanographic linkages. Sediment. Geol. 301, 26–40.
Schultz, S.K., MacEachern, J.A., Catuneanu, O., Dashtgard, S.E., 2020. Coeval deposition of transgressive and normal regressive stratal packages in a structurally controlled area of the Viking Formation, Central Alberta, Canada. Sedimentology 67 (6), 2974–3002.
Sethi, P.S., Leithold, E.L., 1994. Climatic cyclicity and terrigenous sediment influx to the early Turonian Greenhorn Sea, southern Utah. J. Sediment. Res. 64 (1b), 26–39.
Slingerland, R., Keen, T.R., 1999. Sediment transport in the Western Interior Seaway of North America; predictions from a climate-ocean-sediment model. In: Bergman, K. M., Snedden, J.W. (Eds.), Isolated Shallow Marine Sand Bodies. SEPM Special Publication, pp. 179–190.
Sonnenberg, S.A., Bolyard, D.W., 1997. Tectonic history of the Front Range in Colorado. In: Bolyard, D.W., Sonnenberg, S.A. (Eds.), Geologic History of the Colorado Front Range. Rocky Alounrain Association of Geologists, Denver, Colorado, pp. 125–133.
Spasojevic, S., Liu, L., Gurnis, M., 2009. Adjoint models of mantle convection with seismic, plate motion, and stratigraphic constraints: North America since the Late Cretaceous. Geochem. Geophys. Geosyst. 10 (5).
Szwarc, T.S., Johnson, C.L., Stright, L.E., McFarlane, C.M., 2015. Interactions between axial and transverse drainage systems in the Late Cretaceous Cordilleran foreland basin: evidence from detrital zircons in the Straight Cliffs Formation, southern Utah, USA. GSA Bull. 127 (3–4), 372–392.
Tindall, S.E., Storm, L.P., Jenesky, T.A., Simpson, E.L., 2010. Growth faults in the Kaiparowits Basin, Utah, pinpoint initial Laramide deformation in the western Colorado Plateau. Lithosphere 2 (4), 221–231.
Tufano, B.C., Pietras, J.T., 2017. Coupled flexural-dynamic subsidence modeling approach for retro-foreland basins: example from the Western Canada Sedimentary Basin. GSA Bull. 129 (11–12), 1622–1635.
Uličný, D., 1999. Sequence stratigraphy of the Dakota Formation (Cenomanian), southern Utah: interplay of eustasy and tectonics in a foreland basin. Sedimentology 46 (5), 807–836.
Vail, P.R., Mitchum Jr., R.M., Thompson III, S., 1977. Seismic stratigraphy and global changes of sea level, part four: global cycles of relative changes of sea level. In: Payton, C.E. (Ed.), Seismic Stratigraphy - Applications to Hydrocarbon Eploration, American Association of Petroleum Geologists Memoir, 26, pp. 83–97.
Van Cappelle, M., Hampson, G.J., Johnson, H.D., 2018. Spatial and temporal evolution of coastal depositional systems and regional depositional process regimes: Campanian Western Interior Seaway, USA. J. Sediment. Res. 88 (8), 873–897.
Van Wagoner, J.C., Van Mitchum, R.M., Campion, K.M., Rahmanian, V.D., 1990. Siliciclastic Sequence Stratigraphy in Well Logs, Cores, and Outcrops. Concepts for High-Resolution Correlation of Time and Facies. American Association of Petroleum Geologists, 74 pp.
Varban, B.L., Guy Plint, A., 2008. Sequence stacking patterns in the Western Canada foredeep: influence of tectonics, sediment loading and eustasy on deposition of the Upper Cretaceous Kaskapau and Cardium Formations. Sedimentology 55 (2), 395–421.
Weimer, R.J., 1984. Relation of unconformities, tectonics, and sea-level changes, Cretaceous of Western Interior, USA. In: Sehlee, J.S. (Ed.), Interregional Unconformities and Hydrocarbon Accumulation, pp. 7–35.
White, T., Furlong, K., Arthur, M., 2002. Forebulge migration in the Cretaceous Western Interior basin of the central United States. Basin Res. 14 (1), 43–54.
Wolfe, D.G., 1989. The stratigraphy and paleoenvironments of Middle Cretaceous strata along the central Arizona-New Mexico border. Master's Thesis. University of Colorado, Boulder, 222 pp.
Wroblewski, A.F.-J., 2003. Tectonic redirection of Paleocene fluvial drainage systems and lacustrine flooding in the Hanna Basin area, south-central Wyoming. In: R.R. G. and F.R. M. (Editors) (Ed.), Cenozoic Systems of the Rocky Mountain Region. Rocky Mountain Section (SEPM), Denver, pp. 227–252.
Yonkee, W.A., Weil, A.B., 2015. Tectonic evolution of the Sevier and Laramide belts within the north American Cordillera orogenic system. Earth Sci. Rev. 150, 531–593.
Zhu, Y., Bhattacharya, J.P., Li, W., Lapen, T.J., Jicha, B.R., Singer, B.S., 2012. Milankovitch-Scale Sequence Stratigraphy and Stepped Forced Regressions of the Turonian Ferron Notom Deltaic Complex, South-Central Utah, U.S.A. J. Sediment. Res. 82 (9), 723–746.